Calhoun: The NPS Institutional Archive

DSpace Repository

Theses and Dissertations | 1. Thesis and Dissertation Collection, all items

1969

On a multi-layer analysis of atmospheric diabatic processes and the generation of available potential energy.

Lawniczak, George Edward

University of Michigan

http://hdl.handle.net/10945/24788

Downloaded from NPS Archive: Calhoun

http://www.nps.edu/library

Calhoun is the Naval Postgraduate School's public access digital repository for research materials and institutional publications created by the NPS community. Calhoun is named for Professor of Mathematics Guy K. Calhoun, NPS's first appointed -- and published -- scholarly author.

Dudley Knox Library / Naval Postgraduate School
411 Dyer Road / 1 University Circle
Monterey, California USA 93943

NPS ARCHIVE
1969
LAWNICZAK, G.

LIBRARY
NAVAL POSTGRADUATE SCHOOL
MONTEREY, CALIF. 93940

DUDLEY KNOX LIBRARY
NAVAL POSTGRADUATE SCHOOL
MONTEREY, CA 93943-5101

ON A MULTI-LAYER ANALYSIS OF ATMOSPHERIC DIABATIC PROCESSES AND THE GENERATION OF AVAILABLE POTENTIAL ENERGY

by
George Edward Lawniczak, Jr.

A dissertation submitted in partial fulfillment
of the requirements for the degree of
Doctor of Philosophy in
The University of Michigan
1969

Doctoral Committee:

Professor Aksel C. Wiin-Nielsen, Chairman
Professor Edward S. Epstein
Professor Leslie M. Jones
Doctor Warren M. Washington, National Center for Atmospheric Research

JPS ARCHIVE
969
AWNICZAK, G.
Thesis
L319

LIBRARY
NAVAL POSTGRADUATE SCHOOL
MONTEREY, CALIF. 93940

DUDLEY KNOX LIBRARY
NAVAL POSTGRADUATE SCHOOL
MONTEREY, CA 93943-5101

[illegible]

ACKNOWLEDGMENTS

I would like to use these far too few lines to thank those persons responsible for my accomplishments. The list of individuals who have affected my life through their uniqueness is extremely long. But it starts with wonderful parents who laid the keel and provided the hull. They also furnished the first sail, the spanker. Masts were erected and with time the sails were added and unfurled, particularly by the science teacher at Bellevue High School, Mr. Ray, Professor George Haltiner, Capt. Paul Wolff, USN, and Professor Aksel Wiin-Nielsen. Special thanks also are extended to the U. S. Navy for granting me the time and port-calls required.

As for this dissertation, the assistance of Messrs. Roy Jenne and Dennis Joseph at NCAR and Capt. Wolff and his staff at FNWC, particularly Mr. Leo Clarke and Lt. Pete Kesel, USN, are greatly appreciated. The Office of Research Administration made the tasks of preparation and publication much simpler through the use of the skills of its personnel.

The association with the members of my committee, including an honorary member, Assistant Professor William R. Kuhn, was very rewarding and enjoyable. I am deeply indebted to the chairman of my doctoral committee, Professor Wiin-Nielsen, for his guidance and friendship. I also wish to thank the other members, Professors Epstein and Jones and my black mentor, Dr. Washington, for their critical review and helpful suggestions.

And finally, very special gratitude goes to my wife, Joni, and Mary Lucretia, Gregory Jude, and George Edward III who all wondered at times why daddy just didn't go sailing.

TABLE OF CONTENTS

	Page
LIST OF TABLES	v
LIST OF FIGURES	vii
LIST OF SYMBOLS	x
Chapter	
1. ENERGETICS AND AVAILABLE POTENTIAL ENERGY	1
1.1. Introduction	1
1.2. Previous Calculations	7
1.3. The Purpose of this Study	10
2. DEVELOPMENT OF THE EQUATIONS	12
2.1. The Basic Equation for Diabatic Processes	12
2.2. Calculation of Frictional Effects	14
2.3. Diabatic Processes at the Lower Boundary	17
2.4. The Generation of Available Potential Energy	18
3. THE DATA AND THEIR USE	21
3.1. Source and Type	21
3.2. Static Stability	21
3.3. Results of the Static Stability Checks	25
3.4. Computations of H_p, B, H_o, and G(A)	27
4. RESULTS OF THE COMPUTATIONS	30
4.1. Static Stability Check	30
4.2. Mean Diabatic Processes for March 1963	31
4.3. Monthly Average for the Various Levels	34
4.4. The Generation of Available Potential Energy	59
4.5. The Generation of APE as a Function of Latitude for the layer from 100 to 30 cb	60
4.6. Generation of APE Within Pressure Layers	67
4.7. Generation of Eddy APE by Wave Number	73
4.8. The Net Results of the Generation of APE	80
4.9. Calculations for January 1969	81
5. SUMMARY AND SUGGESTIONS	90
5.1. Conclusions	90
5.2. Suggestions for Future Research	94

TABLE OF CONTENTS (Concluded)

		Page
APPENDIX - FINITE DIFFERENCE FORMS OF THE EQUATIONS		98
A.1.	Basic Information	98
A.2.	Geostrophic Potential Vorticity, (2.6)	100
A.3.	Local Time Derivative of Geostrophic Potential Vorticity	100
A.4.	Stream Function, (4.1)	101
A.5.	Horizontal Advection	101
A.6.	Departure Value at the Terrain Height	102
A.7.	Pressure at Terrain Height	103
A.8.	Temperature at Terrain Height	103
A.9.	Geostrophic Surface Wind	104
A.10.	Geostrophic Surface Vorticity	104
A.11.	Friction Effects, (2.15)	104
A.12.	Omega in the Lower Boundary, (2.19), (2.20)	105
A.13.	Heating at the Lower Boundary, (2.17)	105
BIBLIOGRAPHY		106

LIST OF TABLES

Table		Page
1.	Upper Limit on the Static Stability Values	25
2.	Number of Grid-Point Failures as a Result of Static Stability Tests on the Analyses for 1200 GMT 1 March 1963	26
3.	Latitudinal Variation of the Generation of Zonal and Eddy Available Potential Energy in the Layer 100-30 cb Computed for the Ring Centered at the Indicated Latitude in Units 10^{-4} kj m^{-2} sec^{-1} for March 1963	65
4.	Layer Variation of the Generation of Zonal and Eddy Available Potential Energy for the Region from 28.75N to 88.75N in the Units 10^{-6} kj m^{-2} sec^{-1} cb^{-1} for March 1963	70
5.	Individual Wave Contributions to the Generation of Eddy Available Potential Energy in the Layer from 50 to 30 cb in the Units 10^{-4} kj m^{-2} sec^{-1} for the Indicated Times	71
6.	Harmonic Analysis of the Generation of Eddy Available Potential Energy in the Layer 100-30 cb for the Region 28.75N to 88.75N in the Units 10^{-4} kj m^{-2} sec^{-1} for March 1963	75
7.	Comparisons of the Generation of Available Potential Energy Based on Different Analysis Sets for 0000 GMT 5 March 1963 for the Region 18.75N to 88.75N in the Units 10^{-4} kj m^{-2} sec^{-1}	80
8.	Monthly Averages of the Diabatic Processes in the Layer from 100 to 30 cb as a Function of Latitude in the Units 10^{-2} kj sec^{-1} ton^{-1} for January 1969	83
9.	Latitudinal Variation of the Generation of Zonal Available Potential Energy in the Layer 100-30 cb Computed for the Ring Centered at the Indicated Latitude in Units 10^{-4} kj m^{-2} sec^{-1} for January 1969	84
10.	Latitudinal Variation of the Generation of Eddy Available Potential Energy in the Layer 100-30 cb Computed for the Ring Centered at the Indicated Latitude in Units 10^{-4} kj m^{-2} sec^{-1} for January 1969	86

LIST OF TABLES (Concluded)

Table		Page
11.	Layer Variation of the Generation of Zonal and Eddy Available Potential Energy for the Indicated Regions in the Units 10^{-6} kj m^{-2} sec^{-1} cb^{-1} for January 1969	87
12.	Harmonic Analysis of the Generation of Eddy Available Potential Energy in the Layer 100-30 cb for the Indicated Regions in the Units 10^{-4} kj m^{-2} sec^{-1} for January 1969	88
13.	Monthly Average of the Generation of Zonal and Eddy Available Potential Energy for the Layer 100-30 cb Bounded by the Indicated Latitude Circles in the Units 10^{-4} kj m^{-2} sec^{-1} for January 1969	89

LIST OF FIGURES

Figure		Page
1.	Flow diagrams of energy for an atmosphere in hydrostatic equilibrium.	4
2.	Area of the Northern Hemisphere contained within the NNC octagon used in numerical analysis.	22
3.	The separation of the atmospheric column from 100 to 10 cb into layers for use in the static stability check.	24
4.	The levels at which the integrand of (2.8), B, and the diabatic processes, H, are calculated.	28
5.	A comparison of the monthly average of static stability based on data as indicated by the dashed line and the analytic representation as shown by the solid line for March 1963.	32
6.	Zonal average of the diabatic processes for March 1963, as a function of latitude and pressure in the units 10^{-2} kj sec^{-1} ton^{-1}.	33
7.	Zonal average of the diabatic processes for January 1963, as a function of latitude and pressure in the units 10^{-2} kj sec^{-1} ton^{-1}. (After Vernekar, 1967.)	35
8.	Area mean values for the diabatic processes as a function of pressure. The values are for the heating region and the cooling region as separated by the latitude circle at 51.25N.	36
9.	Monthly average of the diabatic processes at the lower boundary for March 1963, in the units 10^{-2} kj sec^{-1} ton^{-1}.	38
10.	Monthly average of the diabatic processes at 77.5 cb for March 1963, in the units 10^{-2} kj sec^{-1} ton^{-1}.	39
11.	Monthly average of the diabatic processes at 60 cb for March 1963, in the units 10^{-2} kj sec^{-1} ton^{-1}.	40
12.	Monthly average of the diabatic processes at 40 cb for March 1963, in the units 10^{-2} kj sec^{-1} ton^{-1}.	41
13.	Monthly average of the diabatic processes at 25 cb for March 1963, in the units 10^{-2} kj sec^{-1} ton^{-1}.	42

Figure		Page
14.	Monthly average of the diabatic processes at 17.5 cb for March 1963, in the units 10^{-2} kj sec^{-1} ton^{-1}.	43
15.	Monthly average of the diabatic processes at 12.5 cb for March 1963, in the units 10^{-2} kj sec^{-1} ton^{-1}.	44
16.	Mean 70-cb height contours for March 1963.	47
17.	Mean diabatic processes in the layer from 100 to 30 cb for March 1963. Horizontal lines are the interpolated values from Davis (1963).	52
18.	Resultant differences when the NMC analysis is subtracted from the FNWC analysis for 50 cb. The map time is 0000 GMT 5 March 1963, and unit is meters.	54
19.	Mean values of the diabatic processes in the layer from 100 to 30 cb using the three analysis sets as indicated.	56
20.	Zonal average of the geostrophic wind for March 1963, in m sec^{-1}.	58
21.	Monthly average of the generation of zonal APE as a function of latitude for layer from 100 to 30 cb for March 1963.	61
22.	Monthly average of the generation of eddy APE as a function of latitude for the layer from 100 to 30 cb for March 1963.	63
23.	Monthly average of the generation of zonal APE as a function of pressure layers for March 1963.	68
24.	Monthly average of the generation of eddy APE as a function of pressure layers for March 1963.	69
25.	Monthly average of the individual wave contributions to the generation of eddy APE for the layer from 100 to 30 cb for March 1963.	74
26.	Monthly averages of the latitudinal variation and the individual wave contributions for the layer from 100 to 85 cb for March 1963.	76
27.	Same as Fig. 26 but for the layer from 85 to 70 cb.	77

LIST OF FIGURES (Concluded)

Figure		Page
28.	Same as Fig. 26 but for the layer from 70 to 50 cb.	78
29.	Same as Fig. 26 but for the layer from 50 to 30 cb.	79
30.	Vertical and horizontal finite differencing grids.	99

LIST OF SYMBOLS

a = mean radius of the earth

c_p = specific heat of air at constant pressure

d = distance between horizontal grid points

e = eddy parameter when used as a subscript

f = Coriolis parameter, $2\Omega\sin\varphi$

$\bar{f}$ = value of the Coriolis parameter at 45N

g = acceleration of gravity

i = pressure layer counter in (2.30), (2.31), (2.22)

i = grid-point counter in the x-direction in Appendix

$\vec{i}$ = unit horizontal vector pointing toward the east

j = latitude band counter in (2.30), (2.31)

j = grid-point counter in the y-direction in Appendix

$\vec{j}$ = unit horizontal vector pointing toward the north

k = number of latitude bands in (2.30), (2.31)

$\vec{k}$ = unit vertical vector pointing upward

m = meters when used in units specifications

m = number of pressure layers in (2.30), (2.31)

m = map factor in Appendix, $(\frac{1.86603}{1 + \sin\varphi})$

n = wave number when used as a subscript

o = lower boundary parameter when used as a subscript

p = pressure

$\bar{p}$ = 100 cb

t = time

u = component of speed along the x axis

v = component of speed along the y axis

x = distance coordinate increasing toward the east

y = distance coordinate increasing toward the north

y = Fourier coefficient in (2.30), (2.31)

z = height above mean sea level

z = a zonal parameter when used as a subscript

z = Fourier coefficient in (2.30), (2.31)

A = available potential energy

APE = available potential energy

B = integrand of (2.8)

C_D = drag coefficient

D = departure value

E = eddy parameter when used as a subscript

F_x = horizontal component of friction force per unit mass in the x-direction

F_y = horizontal component of friction force per unit mass in the y-direction

G = generation of available potential energy

H = diabatic processes per unit mass and unit time

I = internal energy

K = kinetic energy

L = characteristic horizontal scale

N = total number of harmonic components considered in (2.31)

P = potential energy

R = gas constant for air

R_o = Rossby number

R_i = Richardson number

S = surface area

ST = specific temperature anomaly in Appendix

T = temperature

U = characteristic zonal wind speed

$\vec{V}_o$ = geostrophic surface wind vector

$\vec{V}$ = horizontal nondivergent wind vector

Y = Fourier coefficient in (2.30), (2.31)

Z = Fourier coefficient in (2.30), (2.31)

Z_p = standard height of a given pressure level

α = specific volume

ζ = vertical component of relative vorticity

θ = potential temperature

λ = longitude

ξ = geostrophic potential vorticity

ρ = density

σ = a measure of static stability

τ_x = horizontal component of frictional stress acting in the x-direction

τ_y = horizontal component of frictional stress acting in the y-direction

φ = latitude

ψ = rescaled stream function

ω = dp/dt

Δ = a difference operator

Φ = gz, the geopotential

Ψ = stream function

$\nabla = \partial/\partial x\ \vec{i} + \partial/\partial y\ \vec{j}$

$\nabla^2 = \partial^2/\partial x^2 + \partial^2/\partial y^2$

' = deviation from area mean value

ABSTRACT

Presently, little is known about the intensity of the general circulation of the atmosphere. If an accurate measure of the generation of available potential energy (APE) could be made then this intensity would be known. Using Lorenz' (1955) definitions, the volume integration of the covariance between the deviations of the diabatic processes and temperature from their isobaric area mean values is used to calculate this generation.

A seven-layer quasi-nondivergent model is used to compute the net effect of the diabatic processes within each layer. The data are the daily objective height analyses for the Northern Hemisphere from the National Meteorological Center for March 1963. The surface area contained within the analyses extends from about 20N to the pole.

Utilizing the simplified vorticity and the full thermodynamic equations, the lower boundary processes and the accumulated vertical changes in the total derivative (horizontal) of the geostrophic potential vorticity are used to calculate the diabatic effects. Effects of variable terrain height and surface friction are included. Static stability is assumed to be pressure dependent.

Analysis errors apparently cause erroneous values to be calculated south of 30N. Also, the values above 40 cb are unusable. This is due to the failure of the quasi-nondivergent theory in this region. Therefore, only the results in 18% of the earth's atmosphere are available for analysis.

Monthly mean averages of the diabatic processes in the layer from 100 to 30 cb indicate that the transition of the surface cover to permanent snow-cover

is felt throughout the troposphere. Extensive heating areas at the 40-cb level imply that average high cloudiness is required in order to trap the long wave emission.

Using the daily values of the diabatic effects, daily computations for the generation of zonal and eddy APE are made. In the troposphere in March 1963, the average generation of zonal APE was 45×10^{-4} kj m^{-2} sec^{-1} and eddy APE was destroyed at the rate of -22×10^{-4} kj m^{-2} sec^{-1}. Therefore, on the average, heating (cooling) occurred in the low (high) latitudes and the warm (cold) eddies were cooled (heated) for this month. If the remaining half of the hemisphere is included in future calculations, most likely the zonal generation value will be larger and the destruction of eddy APE will be smaller.

For the region examined, most of the generation and destruction occurs in the lowest 30 cb of the atmosphere. There is a near balance between the zonal and eddy components in the lowest 15 cb which suggests that most of the net generation of APE occurs above the boundary layer.

Harmonic analysis reveals that waves 2 through 8 are responsible for the majority of the destruction of eddy APE. Waves 2 and 3 are the dominant modes which suggests that the land-sea distribution and thermal contrasts are quite important during March 1963.

CHAPTER 1

ENERGETICS AND AVAILABLE POTENTIAL ENERGY

1.1. INTRODUCTION

The concept of energy describes the ability of an object or a system to do work, i.e., to exert a force through a distance. Studies of the energetics of the earth's atmosphere are intended to show how the atmosphere works by determining the energy flows among the various energetical forms. Energy forms which are significant within the atmosphere consist of three distinct types: (1) kinetic energy, (2) potential energy, and (3) internal energy.

Kinetic energy is the measure of work that a moving object can perform in being slowed to a state of rest. An example is the energy the wind expends as it propels a sailboat. Obviously the faster a particle moves the more kinetic energy it has.

Potential energy defines the capability of doing work by virtue of an object's position in an external force field. A mass at a greater distance from the center of the force field has more potential energy. Matter falling due to the force of a gravitational field is an example of a body losing this form of energy.

Internal energy may be defined as the sum of the electromagnetic potential energy of electrons, nuclei, and the molecules of matter and the kinetic energy due to the molecular motions. This energy is closely associated with the average energy of the thermal motions of molecules, i.e., the temperature of an object. When two identical objects with different temperatures are placed in

contact, the warmer mass transfers internal energy to the cooler body through molecular collisions until both objects have the same temperature or internal energy.

Energy is important because all matter possesses it and because energy is a conserved property, i.e., it can be neither created nor destroyed but only transformed from one form to another or transferred to another system. Thus a system in isolation from the rest of the universe acts under the constraints of conservation of energy. Since the earth-atmosphere system shows no tendencies for velocity and temperature changes over a long time it can be considered to be an isolated system. This means that over a sufficiently long time the system must be in equilibrium with the environment. Since the system interacts with its environment only through radiational processes, insolational warming received from the sun must be balanced by a cooling loss through long wave emission. However these relationships are valid only over a long time. Substantial departures from equilibrium may exist for short periods.

Energy studies based on atmospheric observations must employ the hydrostatic assumption. This is true because the assumption is used in calculating these atmospheric data. The hydrostatic assumption states that the upward-directed component of the pressure gradient force is balanced by the downward-acting acceleration of gravity at all times throughout the atmosphere. A direct consequence of this assumption is that the vertical velocity of the system is not a free variable but must be determined from the other state parameters. Since the resulting vertical velocities required to maintain the balance are small the flow within the atmosphere can be considered to be basically horizontal.

Within an hydrostatic atmosphere, Haurwitz (1941) has shown that the potential and internal energy of a column are proportional. That is, an increase of one requires an increase in the other. Therefore it is convenient to combine potential and internal energy into one form. Total potential energy is the name given to the sum of these components in an hydrostatic atmosphere. Wiin-Nielsen (1968) shows that the energy flow for an atmosphere exhibiting this equilibrium can be displayed as in the upper diagram of Fig. 1. Here G(I) represents the generation of internal energy; $C(I,K_H)$ signifies the conversion of internal energy into the kinetic energy of the horizontal flow; C(I,P) portrays the relationship between internal and potential energy; $D(K_H)$ denotes the dissipation by friction of the kinetic energy of the horizontal flow. The direction of the arrows is determined by noting that over a sufficient time period the generation and conversion terms must off-set the removal of kinetic energy since the winds do not ultimately cease to blow.

Another useful approximation available to the investigator is the quasi-geostrophic theory. Charney (1948) provided a system by which the magnitudes of the terms in the hydrodynamical equations could be compared through the use of nondimensional analysis. He formulated the results for the synoptic weather scale while Burger (1958) extended this concept to the planetary waves. The approximation consists of keeping only the terms of largest comparable magnitude. It gets its name because the geostrophic wind relationship is the resultant when the horizontal accelerations are neglected in the first two equations of motion. Use of the theory is made when the vorticity equation is formed by cross-differentiating the first two equations of motion and subtracting. The

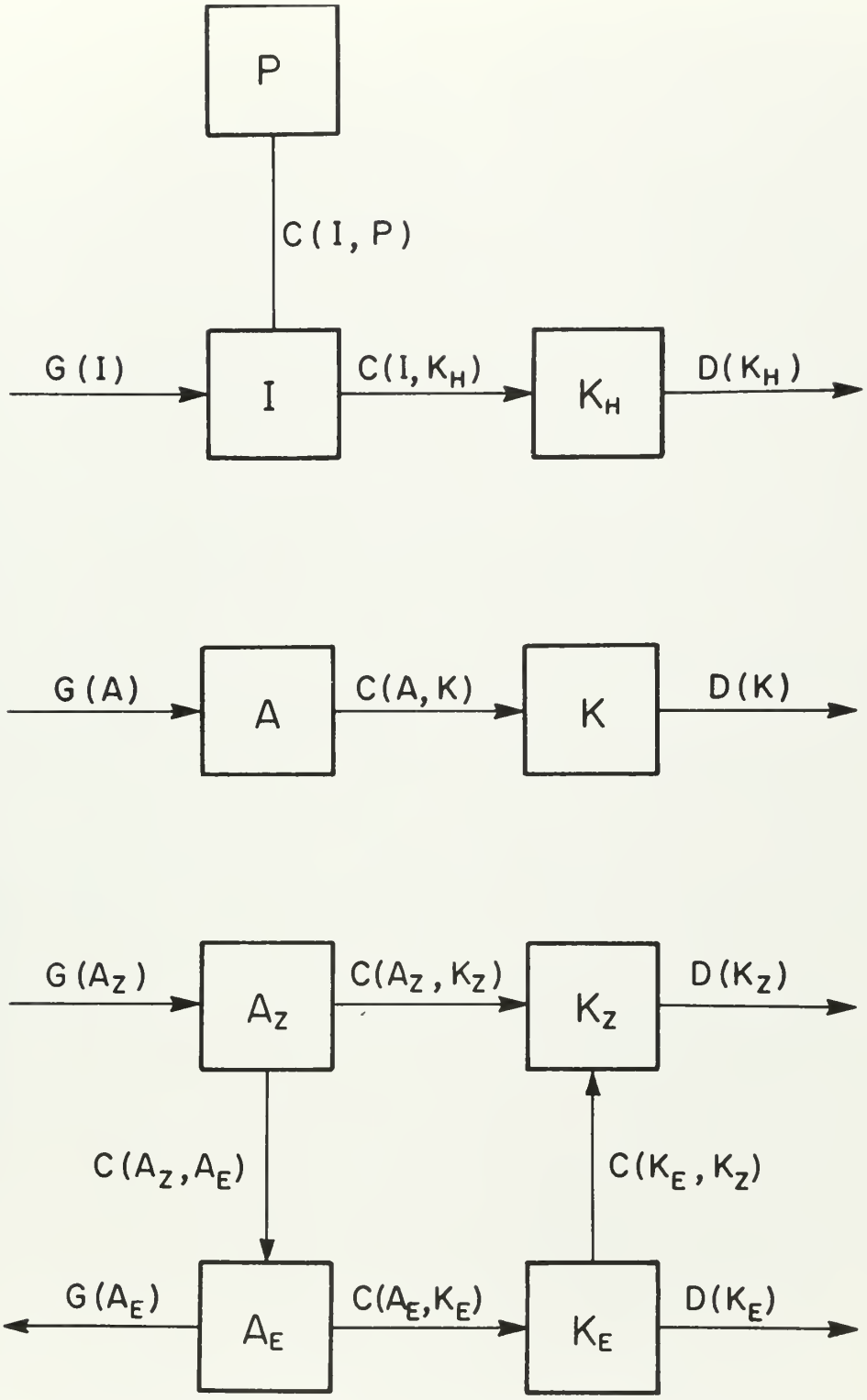

Fig. 1. Flow diagrams of energy for an atmosphere in hydrostatic equilibrium.

geostrophic wind is not used in the divergence term in the vorticity equation and hence the "quasi" portion of the name. Results of numerical forecasts using the theory led to the problem of spurious anticyclogenesis. This is due to the divergent nature of the geostrophic wind where southerly flow is convergent and northerly flow is divergent. This pattern does not resemble the observed picture presented by observations. A stream wind obtained from a stream function was introduced in place of the geostrophic wind to correct this defect. Since the calculated stream wind is a horizontally nondivergent wind, the assumption will be referred to as the quasi-nondivergent theory in this paper. Further, the H subscript on the symbols involving the horizontal wind is dropped in the remainder of the text.

Lorenz (1955) introduced the concept of available potential energy (APE). He defined it as that energy which would be available for conversion to kinetic energy if the atmosphere were brought hydrostatically to a state of minimum total potential energy through isentropic readjustment. The minimum state is characterized by horizontal stratification of the potential temperature surfaces. An energy flow picture using this definition is displayed as the middle diagram in Fig. 1. The letter "A" represents the portion of the sum of potential and internal energy which can be transformed; G(A) represents the generation of APE; C(A,K) is the conversion of APE to kinetic energy; D(K) denotes the frictional dissipation of kinetic energy. It is clear from this figure that in an hydrostatic, adiabatic, and frictionless atmosphere, the sum of available potential energy and kinetic energy is conserved. A decrease in one must be accompanied by an increase in the other. However APE is exactly zero

when potential temperature surfaces are horizontally stratified. The kinetic energy of the geostrophic wind would likewise be zero in such a case because the pressure surfaces coincide with the potential temperature surfaces. Since the actual wind tends to be largely geostrophic in nature, large values of kinetic energy must therefore correspond to large values of APE. Thus when there is a simultaneous increase of both energy forms, diabatic processes must be responsible. Using Lorenz' (1955) sample calculations, the average amount of total potential energy which is available for conversion to kinetic energy is about one percent. Oort (1964) indicates that the average kinetic energy is smaller than average APE by a factor of three-fourths while Wiin-Nielsen (1967) shows the factor to be one-half. It appears that there is sufficient APE for conversion to kinetic energy.

Wiin-Nielsen (1967, 1968) has pointed out that knowledge of the intensity, i.e., the rate of energy transformation, of the atmospheric general circulation is limited. If thorough measurements of G(A), C(A,K), or D(K) were accessible then this intensity could be ascertained. However the assessment of any of these quantities is not available as a well-known value for the globe or either hemisphere. Generation of APE requires knowledge of the distribution of the diabatic heating and cooling. Conversion of APE to kinetic energy is dependent upon knowing the vertical velocity. Dissipation of kinetic energy is based on frictional effects both in the boundary layer and in the remainder of the atmosphere.

Lacking adequate knowledge about the horizontal components of the frictional force, D(K) could be evaluated as a residual term in the manner of Kung (1966,

1967). Wiin-Nielsen (1968) notes that such a procedure is difficult. He shows that the calculation involves tendencies toward a balance between numerically large quantities. Thus extreme accuracy in the observations of atmospheric data is needed in order to avoid errors. It is doubtful that such accuracy exists even in the dense data collection networks.

The choice of computing either G(A) or C(A,K) is one of selecting equally intricate options. Vertical velocities needed for the conversion term are the result of the divergent part of the horizontal wind. Forecast models employing the quasi-nondivergent and adiabatic assumptions have provided weather predictions for a little over a decade and the results indicate that these approximations yield useful prognoses over short time periods. Based on the resolvable scale of the models this implies that the effects of the divergent wind and the diabatic processes are small over these short time periods. If adequate information concerning the diabatic processes were available then the calculated vertical velocity fields using this knowledge would contain more useful information. This paper continues the examination of diabatic processes and the generation of available potential energy.

1.2. PREVIOUS CALCULATIONS

Many calculations for G(A) have used the approximate expression derived by Lorenz (1955). He first shows that the average APE depends on the variance of pressure relative to the isentropic surfaces. This is the result of keeping only the first term of a power series expansion for APE. He then approximates this variance as the variance of temperature on an isobaric level. Using the

isobaric form, G(A) is computed by: (1) determining the deviations from the isobaric area mean for both diabatic processes and temperature, and (2) calculating the volume integral of the covariance of these deviations. Dutton and Johnson (1967), in criticizing the results of investigators who used the simplified expression, argue that the approximation neglects the generation of of APE due to heating (cooling) on an isentropic surface at higher (lower) pressure. (Isentropic surfaces exhibit strong upward slopes in a poleward direction within the troposphere.) They also mention that the approximation does not retain dependence on total diabatic heating. However, Wiin-Nielsen (1968, Equations 51 and 56) shows that the approximation is energetically consistent with the quasi-nondivergent theory and must be used in studies where the theory is invoked.

Following what has become a common practice, the distribution of any parameter over the globe may be separated into a zonal or mean value and an eddy or remaining value. The eddies constitute the difference after the mean has been subtracted from the total. Oort (1964) compiled the results of many investigators and developed an annual picture of the atmospheric cycle in terms of zonal and eddy quantities. He gives a value of 31×10^{-4} kj m^{-2} sec^{-1} for the generation of zonal APE and -8×10^{-4} kj m^{-2} sec^{-1} for the generation of eddy APE in the space domain. (Values in the space domain are determined by performing calculations on each set of a time series and then averaging the results. Using the terminology of Lorenz (1967), the results in the space domain answer questions concerning the standing zonal and standing eddy circulations. Multiplication by 10^3 converts the units of 10^{-4} kj m^{-2} sec^{-1} to watts m^{-2}.)

Oort's cycle implies that on the average there is heating where it is warm and cooling where it is cold along a longitude circle and just the opposite along a latitude circle. The bottom diagram in Fig. 1 shows the energy flow using the separation of APE and kinetic energy into zonal and eddy components. Directions of the arrows are based on Oort's (1964) results for the space domain.

Smagorinsky, Manabe, and Holloway (1965) reported on the results of a numerical model which did not contain the effects of mountains, land and sea contrast or a hydrological cycle. They obtained a generation of 43×10^{-4} kj m^{-2} sec^{-1} for zonal APE and a destruction of -9×10^{-4} kj m^{-2} sec^{-1} for eddy APE. Manabe and Smagorinsky (1967) commented on a model with a hydrological cycle where the lower boundary consists of a wet and flat surface without heat capacity. They computed a generation of 5×10^{-4} kj m^{-2} sec^{-1} for eddy APE apparently due to the large release of latent heat in the tropics.

Dutton and Johnson (1967) applied the expression for the generation of zonal APE in isentropic coordinates to a somewhat arbitrary assignment of the components of Lettau's (1954) heat budget within a two-layer model to compute a generation of 56×10^{-4} kj m^{-2} sec^{-1}. Using the results of Kung's (1966) study of the dissipation of kinetic energy, they concluded that the generation of eddy APE was positive and equal to 8×10^{-4} kj m^{-2} sec^{-1}. Kung (1967) expanded his data to include 1200 GMT observations as well as 0000 GMT soundings over North America. A new computation revised the value of dissipation from 64×10^{-4} kj m^{-2} sec^{-1} downward to 41×10^{-4} kj m^{-2} sec^{-1}. This of course reverses the picture proposed by Dutton and Johnson (1967) since the generation of eddy APE becomes -15×10^{-4} kj m^{-2} sec^{-1} using Kung's newer estimate.

Wiin-Nielsen (1968) has commented on the results of Dutton and Johnson (1967) and Kung (1966, 1967). He points out that the method employed by Dutton and Johnson applies to the mixed space-time domain while Kung's results refer to the space domain. (The mixed domain gives results which apply to the sum of the time-mean and standing zonal motions and the sum of the transient and standing eddy circulations.) Oort (1964) displays the dangers involved in mixing such computations in that the generation of eddy APE has opposite signs in the two regimes. Wiin-Nielsen (1968) also mentions the limitations involved in using cross-sectional data along a particular meridian to create zonal averages.

1.3. THE PURPOSE OF THIS STUDY

Results of previous investigations of diabatic processes and the generation of APE, other than numerical simulation, are based on models with limited vertical resolution. These models use observational or climatological data and examples are Wiin-Nielsen and Brown (1960), Brown (1964), and Dutton and Johnson (1967). These investigations must confront the problems associated with sparse data coverage and analysis errors. Although the numerical simulation models do not suffer these defects they do impose certain artificialities due to ignorance of the real behavior of the atmosphere. To date they have not included a realistic treatment of the lower boundary effects.

The present observational system of upper-air soundings of heights and winds which assumes the hydrostatic balance will remain the primary source of atmospheric data for some time to come. Application of the simple quasi-nondivergent theory seems reasonable in light of the amount and geographic distri-

bution of data. Eventually numerical simulation will offer results based on a more realistic treatment of the atmosphere. Then the findings of simple theory based on observed data can be used to evaluate the calculations of simple theory based on the results of numerical simulation.

The purpose of this inquiry is to determine the feasibility of using a quasi-nondivergent model utilizing greater vertical resolution than previously used to compute the diabatic processes and the generation of APE. Results of a more realistic treatment of the lower boundary condition are also examined. Chapter 2 contains the development of the equations used to calculate diabatic heating and cooling and the zonal and eddy components of G(A). The data and a scheme for ensuring vertical consistency of the analyses are discussed in Chapter 3. Results of the computations are presented in Chapter 4 and the conclusions and a summary are provided in Chapter 5. The Appendix contains the finite difference forms for the equations used in the various calculations.

CHAPTER 2

DEVELOPMENT OF THE EQUATIONS

2.1. THE BASIC EQUATION FOR DIABATIC PROCESSES

Wiin-Nielsen and Brown (1960) used a two-level, quasi-nondivergent model to calculate diabatic heating and cooling from observational data. Using the same model, Brown (1964) extended the study to a larger data sample and introduced a more reasonable lower boundary condition involving the terrain and frictionally induced vertical velocities. However, frictional forces were neglected in the vorticity equation and as in the previous investigation static stability was made a constant for the layer 80-40 cb. This paper is a continuation of that work with the added refinements of greater resolution in the vertical and a more realistic treatment of the lower boundary. In addition, the static stability is allowed to vary with pressure.

The vorticity and thermodynamic equations for the quasi-nondivergent model including the effects of diabatic processes and friction have the form

$$\frac{\partial \zeta}{\partial t} + \vec{V}\cdot\nabla(\zeta+f) = \bar{f}\frac{\partial \omega}{\partial p} + \left(\frac{\partial F_y}{\partial x} - \frac{\partial F_x}{\partial y}\right) \tag{2.1}$$

and

$$\frac{\partial}{\partial t}\left(\frac{\partial \Phi}{\partial p}\right) + \vec{V}\cdot\nabla\left(\frac{\partial \Phi}{\partial p}\right) + \alpha\omega = -\frac{RH}{c_p p} \tag{2.2}$$

respectively.

In the above equations, $\vec{V}$ is the nondivergent part of the horizontal velocity vector which is computed from the stream function Ψ, i.e., $\vec{V} = \vec{k} \times \nabla\Psi$;

$\zeta = \frac{\partial v}{\partial x} - \frac{\partial u}{\partial y}$ is the relative vorticity; f is the Coriolis parameter where $\bar{f}$ is its value at 45N; ω is the vertical p-velocity, $\frac{dp}{dt}$, where p is pressure and t is time; g = 9.8 m sec^{-2} is the acceleration of gravity; $\nabla = \frac{\partial}{\partial x}\vec{i} + \frac{\partial}{\partial y}\vec{j}$ is the horizontal part of the gradient operator where $\vec{i}$ and $\vec{j}$ are unit vectors; $\Phi = gz$ where z is the height above mean sea level; $\sigma = -\alpha \frac{\partial(\ell n\theta)}{\partial p}$ is the static stability where α is the specific volume and θ is the potential temperature; R = 287 kj ton^{-1} deg^{-1} is the gas constant for air; c_p = 1004 kj ton^{-1} deg^{-1} is the specific heat at constant pressure; H is the time rate of diabatic heating or cooling per unit mass where a positive quantity means heating; F_x and F_y are the x and y components of the frictional force respectively.

In (2.1) the vertical advection of vorticity and the terms expressing the turning of the vortex tubes have been neglected. This is equivalent to neglecting the vertical advection of momentum in the first two equations of motion from which (2.1) is derived. In the first term on the right side of (2.1), $\bar{f}$ replaces $(f+\zeta)$. Wiin-Nielsen (1959a) has shown that these deletions and approximations are required in the simplified vorticity equation in order to satisfy and be consistent with certain properties which the complete vorticity equation exhibits.

Solving (2.2) for ω gives the result

$$\omega = -\left[\frac{\partial}{\partial t}\left(\frac{1}{\sigma}\frac{\partial \Phi}{\partial p}\right) + \vec{V}\cdot\nabla\left(\frac{1}{\sigma}\frac{\partial \Phi}{\partial p}\right) + \frac{RH}{c_p \sigma p}\right] . \qquad (2.3)$$

If (2.3) is differentiated with respect to pressure, the equation

$$\frac{\partial \omega}{\partial p} = -\left[\frac{\partial}{\partial t}\frac{\partial}{\partial p}\left(\frac{1}{\sigma}\frac{\partial \Phi}{\partial p}\right) + \vec{V}\cdot\nabla\frac{\partial}{\partial p}\left(\frac{1}{\sigma}\frac{\partial \Phi}{\partial p}\right) + \frac{R}{c_p}\frac{\partial}{\partial p}\left(\frac{H}{\sigma p}\right)\right] \qquad (2.4)$$

is obtained. Substituting (2.4) into (2.1) produces

$$\frac{\partial \zeta}{\partial t} + \vec{V}\cdot\nabla(\zeta+f) + \frac{\partial}{\partial t}\frac{\partial}{\partial p}\left(\frac{\bar{f}}{\sigma}\frac{\partial \Phi}{\partial p}\right) + \vec{V}\cdot\nabla\frac{\partial}{\partial p}\left(\frac{\bar{f}}{\sigma}\frac{\partial \Phi}{\partial p}\right) = -\frac{\bar{f}R}{c_p}\frac{\partial}{\partial p}\left(\frac{H}{\sigma p}\right) + \left(\frac{\partial F_y}{\partial x} - \frac{\partial F_x}{\partial y}\right) \quad . \quad (2.5)$$

Letting

$$\xi = \zeta + f + \frac{\partial}{\partial p}\left(\frac{\bar{f}}{\sigma}\frac{\partial \Phi}{\partial p}\right) \quad , \quad (2.6)$$

represent the geostrophic potential vorticity, (2.5) can be rewritten as

$$\frac{\partial}{\partial p}\left(\frac{H}{\sigma p}\right) = -\frac{c_p}{\bar{f}R}\left[\frac{\partial \xi}{\partial t} + \vec{V}\cdot\nabla\xi - \left(\frac{\partial F_y}{\partial x} - \frac{\partial F_x}{\partial y}\right)\right] \quad . \quad (2.7)$$

Integrating (2.7) with respect to pressure from $p = p_o$, where the subscript o indicates a lower boundary value, to some arbitrary pressure $p = p$, gives the basic equation for calculating diabatic processes,

$$\boxed{H = \frac{\sigma p}{\sigma_o p_o} H_o + \sigma p \int_{p=p_o}^{p=p} -\frac{c_p}{\bar{f}R}\left[\frac{\partial \xi}{\partial t} + \vec{V}\cdot\nabla\xi - \left(\frac{\partial F_y}{\partial x} - \frac{\partial F_x}{\partial y}\right)\right] dp} \quad . \quad (2.8)$$

The terms inside the brackets can be computed from observations on pressure levels. Thus the diabatic heating and cooling at any level can be calculated provided that H_o can be determined.

2.2. CALCULATION OF FRICTIONAL EFFECTS

Phillips (1963) explained that a necessary condition for geostrophic balance to be assumed is that frictional forces are small compared to the Coriolis acceleration. This assumption means that important frictional effects must be limited to the boundary layer. The average pressure at the earth's surface in

the Northern Hemisphere is about 97 cb in the winter for the surface area north of 20N. For convenience it will be assumed that the effective lower boundary of the atmosphere is 92.5 cb. Assuming also that the depth of the layer in which the frictional forces vanish at the top is 15 cb, then the 85-cb level is the middle of this layer. The effects of the frictional forces in the boundary layer are assigned to the 85-cb level calculations.

Let

$$F_x = g \frac{\partial \tau_x}{\partial p} \tag{2.9}$$

and

$$F_y = g \frac{\partial \tau_y}{\partial p} \tag{2.10}$$

where τ_x and τ_y are the surface stress components. Substituting (2.9) and (2.10) into the term representing the frictional effects in (2.8) leads to

$$\left(\frac{\partial F_y}{\partial x} - \frac{\partial F_x}{\partial y} \right) = g \frac{\partial}{\partial p} \left(\frac{\partial \tau_y}{\partial x} - \frac{\partial \tau_x}{\partial y} \right) . \tag{2.11}$$

Since the stress vanishes at the top of the friction layer by assumption, using finite differencing (2.11) becomes

$$g \frac{\partial}{\partial p} \left(\frac{\partial \tau_y}{\partial x} - \frac{\partial \tau_x}{\partial y} \right) = \frac{g}{\Delta p} \left(\frac{\partial \tau_y}{\partial x} - \frac{\partial \tau_x}{\partial y} \right)_o \tag{2.12}$$

where $\Delta p = 15$ cb.

If the terrain stress is further assumed to be proportional to the square of the surface geostrophic wind in the manner of Lettau (1959) and Cressman

(1960), these stress components can be approximated as

$$\tau_x = C_D \rho_o u_o V_o , \quad \tau_y = C_D \rho_o v_o V_o . \tag{2.13}$$

Using (2.13), (2.12) can be written as

$$\frac{g}{\Delta p}\left(\frac{\partial \tau_y}{\partial x} - \frac{\partial \tau_x}{\partial y}\right)_o = \frac{g p_o}{\Delta p R T_o}\left[\frac{\partial}{\partial x}(C_D v_o V_o) - \frac{\partial}{\partial y}(C_D u_o V_o)\right] . \tag{2.14}$$

The equation of state, $p = \rho RT$, has been used in (2.14) to eliminate density which was itself assumed to be constant with respect to local space differentiation. In (2.14), p_o is the pressure at the terrain height; C_D is the coefficient of drag based on Cressman's (1960) work; V_o is the resultant geostrophic surface wind and u_o and v_o are its components; T_o is the temperature at terrain height. The computation of pressure, temperature, and geostrophic surface wind at the lower boundary is performed using techniques developed by Clarke and Lawniczak (1962) which utilize the terrain data of Berkofsky and Bertoni (1955). The procedure is outlined in the Appendix.

In (2.14) a further assumption is made that the local space variations of $C_D V_o$ are negligible. The final form for calculating friction is therefore

$$\frac{g}{\Delta p}\left(\frac{\partial \tau_y}{\partial x} - \frac{\partial \tau_x}{\partial y}\right)_o = \frac{g p_o C_D V_o \zeta_o}{\Delta p R T_o} \tag{2.15}$$

where ζ_o is the surface relative vorticity.

2.3. DIABATIC PROCESSES AT THE LOWER BOUNDARY

Applying the hydrostatic equation, $\frac{\partial \Phi}{\partial p} = -\alpha$, and the state equation to (2.2) yields

$$\frac{\partial T_o}{\partial t} + \vec{V}_o \cdot \nabla T_o - \frac{p_o \sigma_o \omega_{\ell o}}{R} = \frac{H_o}{c_p} \tag{2.16}$$

or

$$\boxed{H_o = c_p \left(\frac{\partial T_o}{\partial t} + \vec{V}_o \cdot \nabla T_o \right) - \frac{c_p}{R} p_o \sigma_o \omega_{\ell o}} \tag{2.17}$$

where σ_o is the static stability at the terrain height and $\omega_{\ell o}$ is the vertical velocity in the lower boundary. Within quasi-nondivergent theory static stability can be at most a function of pressure and as such is modelled after Wiin-Nielsen (1959b) with the form

$$\sigma = \frac{\bar{\sigma} \bar{p}^2}{p^2} \tag{2.18}$$

where $\bar{\sigma} = 1 \text{ m}^2 \text{ sec}^{-2} \text{ cb}^{-2}$ and $\bar{p} = 100$ cb.

The omega in the lower boundary, $\omega_{\ell o}$, is calculated following the results of Cressman (1960) and Haltiner, Clarke, and Lawniczak (1963). Their results show that the vertical velocity induced by the terrain can be approximated as

$$\omega_o = \vec{V}_o \cdot \nabla p_o \tag{2.19}$$

and the frictionally induced omega can be computed from

$$\omega_{\ell f} = - \frac{g p_o C_D V_o \zeta_o}{f R T_o} \tag{2.20}$$

where ω_o is the terrain vertical velocity and $\omega_{\ell f}$ is the friction vertical velocity. Therefore

$$\omega_{\ell o} = \omega_o + \omega_{\ell f} \quad . \tag{2.21}$$

The integrand of (2.8) can be computed at the pressure levels for which data are available. Letting B equal the integrand and using the results of (2.17), the diabatic processes can be calculated at the required levels by using the following summation:

$$\boxed{H_p = \frac{\sigma p}{\sigma_o p_o} H_o + \sigma p \left[- \sum_{i=1}^{i=ip} B_i (\Delta p)_i \right]} \tag{2.22}$$

where H_p is the result at the top of the ip-th layer.

2.4. THE GENERATION OF AVAILABLE POTENTIAL ENERGY

It has been shown by Lorenz (1955) that the computation of the generation of APE, using pressure as the vertical coordinate, depends on the covariance of the deviations of temperature and diabatic processes from their areal averages. As shown by Wiin-Nielsen and Brown (1960), this generation or rate of energy conversion can be calculated from

$$G = - \frac{R}{c_p} \int_{p=o}^{p=p_o} \frac{1}{\sigma p} \int_S H' \left(\frac{\partial \Phi}{\partial p} \right)' \, dS dp \tag{2.23}$$

where G represents the generation of APE in the units kj sec^{-1}; S is the surface area and $dS = a^2 \cos\varphi \, d\lambda \, d\varphi$ where a is the radius of the earth, φ is the latitude, and $d\lambda$ and $d\varphi$ are the increments of latitude and longitude respectively; the prime indicates that the value is the deviation from the area mean value.

The area mean value is calculated from

$$(\overline{\ }) = \frac{a^2}{S} \int_{\varphi_1}^{\varphi_2} \int_{o}^{2\pi} (\ ) \cos\varphi d\lambda d\varphi \tag{2.24}$$

where the over-bar denotes the average of the parameter; $S = 2\pi a^2(\sin \varphi_2 - \sin \varphi_1)$ is the area of the region and φ_1 and φ_2 are the limiting latitudes.

Using techniques similar to those employed by Wiin-Nielsen, Brown, and Drake (1963), the generation term can be separated into wave-number domain such that

$$G = G_z + G_e \tag{2.25}$$

where G_z measures the contribution from the zonal or the north-south covariance and G_e measures the eddy portion or the east-west covariance. Letting the Fourier series

$$H' = Y_o(\varphi) + \sum_{n=1}^{\infty} [Y_n(\varphi) \cos n\lambda + Z_n(\varphi) \sin n\lambda] \tag{2.26}$$

represent the diabatic deviation field and

$$\left(\frac{\partial \Phi}{\partial p}\right)' = y_o(\varphi) + \sum_{n=1}^{\infty} [y_n(\varphi) \cos n\lambda + z_n(\varphi) \sin n\lambda] \tag{2.27}$$

represent the thickness deviation field, the contribution from the north-south covariance becomes

$$G_z = -\frac{2\pi Ra^2}{c_p} \int_{p=o}^{p=p_o} \frac{1}{\sigma p} \int_{\varphi_1}^{\varphi_2} Y_o y_o \cos\varphi d\varphi dp \ . \tag{2.28}$$

The calculation of the generation due to the eddies can be expressed as

$$G_e = -\frac{\pi Ra^2}{c_p}\int_{p=o}^{p=p_o}\frac{1}{\sigma p}\int_{\varphi_1}^{\varphi_2}\sum_{n=1}^{N}[Y_n y_n + Z_n z_n]\cos\varphi d\varphi dp \quad . \tag{2.29}$$

Using numerical approximation, (2.28) and (2.29) becomes

$$\boxed{G_z = -\frac{2\pi Ra^2\Delta\varphi}{c_p}\sum_{i=1}^{i=m}\frac{\Delta p_i}{\sigma_i p_i}\sum_{j=1}^{j=k} Y_o y_o \cos\varphi_j} \tag{2.30}$$

and

$$\boxed{G_e = -\frac{\pi Ra^2\Delta\varphi}{c_p}\sum_{i=1}^{i=m}\frac{\Delta p_i}{\sigma_i p_i}\sum_{j=1}^{j=k}\sum_{n=1}^{N}[Y_n y_n + Z_n z_n]\cos\varphi_j} \tag{2.31}$$

where m determines the vertical resolution; k determines the latitudinal resolution; N is the numerical limit on the harmonic components; and $\Delta\varphi$ is the latitude increment. Note that for a particular n, (2.31) becomes

$$G_{e,n} = -\frac{\pi Ra^2\Delta\varphi}{c_p}\sum_{i=1}^{i=m}\frac{\Delta p_i}{\sigma_i p_i}\sum_{j=1}^{j=k}[Y_n y_n + Z_n z_n]\cos\varphi_j \quad . \tag{2.32}$$

Dividing (2.30) and (2.31) by S will give the generation in units of kj m^{-2} sec^{-1}.

CHAPTER 3

THE DATA AND THEIR USE

3.1. SOURCE AND TYPE

Data used in this investigation are the National Meteorological Center (NMC) routine objective height analyses which consist of the 0000 GMT and 1200 GMT fields for the month of March 1963. They were obtained, along with the analyses from the Air Force Global Weather Central (GWC) for the same month, from the National Center for Atmospheric Research at Boulder, Colorado. For this particular month the NMC analyses at 100, 85, 70, 50, 30, 20, 15, and 10 cb and the GWC set for 85, 70, 50, 40, 30, 20, and 10 cb were provided.

The analyses consist of grid-point values from the NMC octagon containing 1977 points. This array covers the Northern Hemisphere using a polar stereographic projection true at 60N where the distance between grid points at this latitude is 381 km. The lowest latitude circle fully contained within the first two rows of boundary points is 20N. Fig. 2 shows the surface area covered by this octagon. The right side is slightly shortened by the map limits.

Wherever analyses were missing in the NMC set the analyses from the GWC set, if available, were used. Five fields out of 496 were absolutely missing and these five were formed by averaging the available analyses. Eight GWC fields were used to replace missing NMC fields.

3.2. STATIC STABILITY

Static stability is quite important for the calculations involving (2.8).

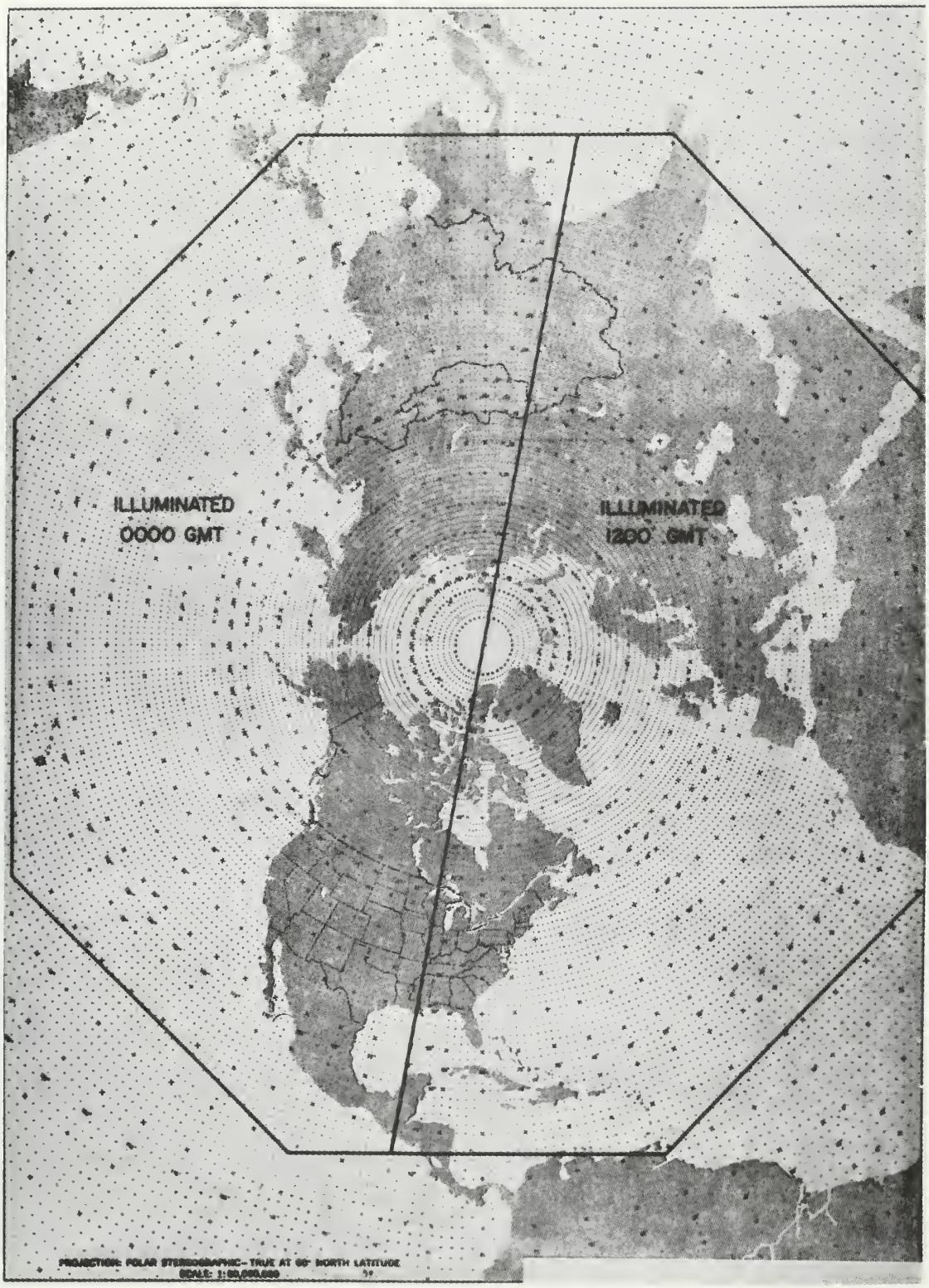

Fig. 2. Area of the Northern Hemisphere contained within the NMC octagon used in numerical analysis.

As pointed out by Holl, Bibbo, and Clark (1963), the analysis of the atmospheric structure, in addition to satisfying the equation of state and the hydrostatic equation, must also be statically stable everywhere. Although deviations from static stability and hydrostatic equilibrium exist in the atmosphere it is doubtful that these deviations can be accurately represented by the data or should be contained in large-scale analyses.

A 10-parameter version of the static stability model developed by Holl, Bibbo, and Clark (1964) in which temperature is linear in pressure to the R/c_p power, was used to ensure the vertical consistency of the NMC analyses. Static stability is computed using the form

$$\sigma^* = -Rp_o^{-R/c_p} p^{1+R/c_p} \frac{d\theta}{dp} \qquad (3.1)$$

where σ^* has the units of velocity squared and is equal to σp^2. This model partitions the column from 100 to 10 cb into 8 layers. A one-to-one transform is developed between the heights at 10 mandatory pressure levels and the 100-cb height, the thickness for the layer from 100 to 50 cb and the static stability parameters for 8 layers. An inverse transform is available so that given one set the other can be generated. Fig. 3 presents in detail how the column is subdivided. Within the model, the heights at 100 and 50 cb are unaltered by the check because these levels receive the greatest amount of attention in the analysis scheme. The 100-cb analysis is closely related to the surface analysis where the amount of surface data exceeds the available upper-air soundings by a factor of 8. Above 50 cb, there is less data generally available and the inaccuracies are larger. Also the 50-cb level incorporates as a first

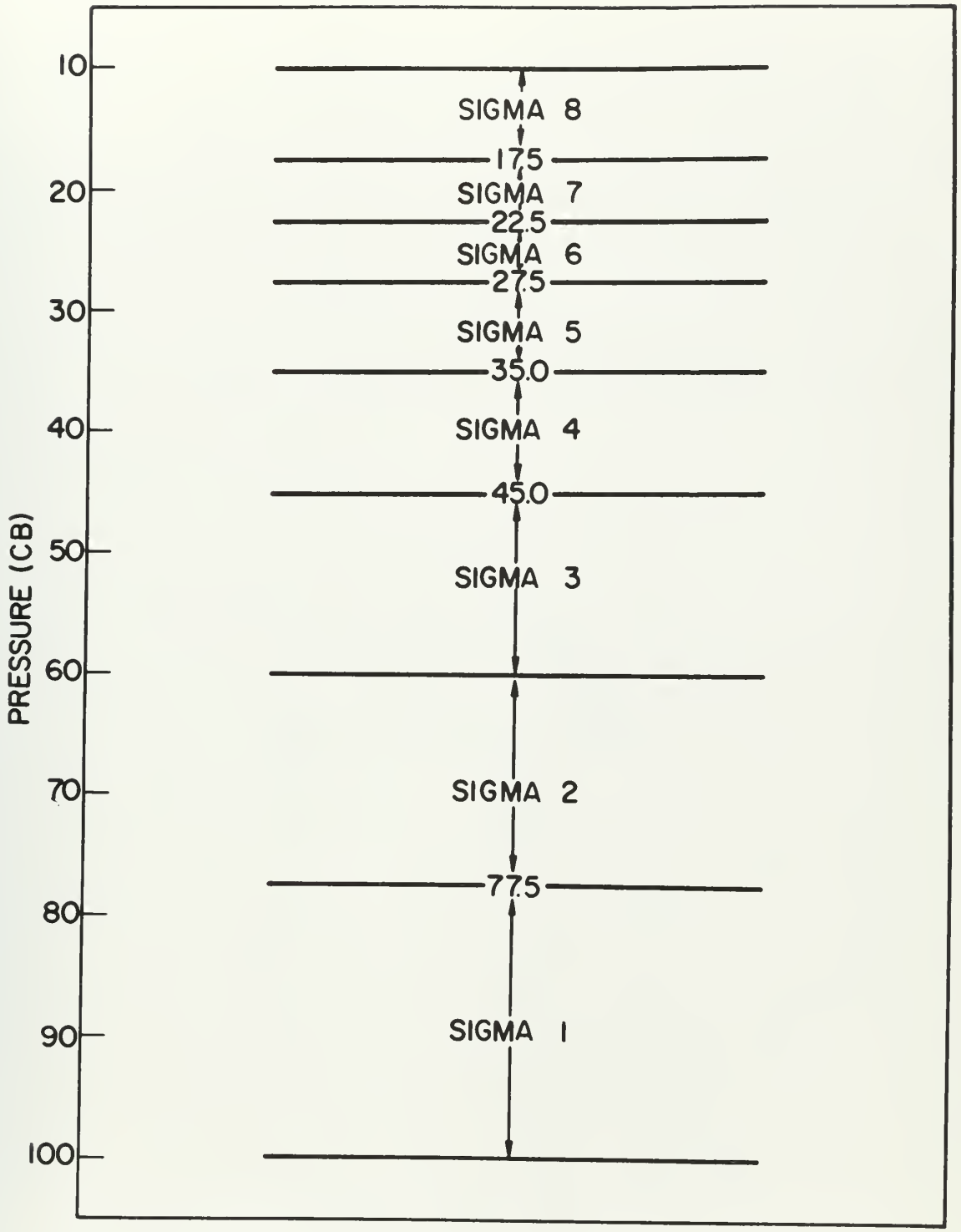

Fig. 3. The separation of the atmospheric column from 100 to 10 cb into layers for use in the static stability check.

approximation to the final analysis a short-range forecast which is the result of special emphasis in the forecast model. However, the remaining levels are changed to make the computed static stability lie within a prescribed range. Table 1 shows the upper limit placed on the computed value for each layer. Should this limit be exceeded, the limit minus 1000 m^2 sec^{-2} is substituted and the heights in the column are recomputed. Should the value be less than 100 m^2 sec^{-2}, it is replaced with a value of 200 m^2 sec^{-2} and the heights are likewise recomputed.

TABLE 1

UPPER LIMIT ON THE
STATIC STABILITY VALUES

Layer	Limit (m^2 sec^{-2})
Sigma 1	39000
Sigma 2	25000
Sigma 3	21000
Sigma 4	23000
Sigma 5	35000
Sigma 6	35000
Sigma 7	35000
Sigma 8	35000

3.3. RESULTS OF THE STATIC STABILITY CHECKS

The 10-level model requires the heights at 100, 85, 70, 50, 40, 30, 25, 20, 15, and 10 cb. Using the GWC 40-cb analysis and linear interpolation to

form the 25-cb heights, a test was run on the 1200 GMT fields for 1 March. Results are listed in Table 2 under the heading "Test A." The very high number of failures in the sigma 4 layer which contains the 40-cb level indicates that the GWC analysis is incompatible with the NMC fields. High failure rates in the sigma 3 and sigma 5 layers are the result of the dependence on the 40-cb heights. No further use was made of the GWC 40-cb analysis and no tests were made on the GWC fields.

TABLE 2

NUMBER OF GRID-POINT FAILURES AS A RESULT OF
STATIC STABILITY TESTS ON THE ANALYSES FOR 1200 GMT 1 March 1963

Test	Sigma 1	Sigma 2	Sigma 3	Sigma 4	Sigma 5	Sigma 6	Sigma 7	Sigma 8	Total
A	70	119	707	1143	733	--	--	--	1654
B	76	59	56	10	172	1141	12	0	1408
C	76	59	54	9	780	83	78	0	864
D	74	52	0	6	57	47	56	0	243

The next test involved using a Lagrangian three-point interpolation formula. The formula was applied to the heights at 70, 50, and 30 cb to obtain the 40-cb height and to the heights at 30, 20, and 10 cb to compute the 25-cb heights. Table 2 list the results under "Test B." Improvement is clearly evident around 40 cb but the sigma 6 layer which contains the 25-cb level has unacceptable results.

Next, a test using the Lagrangian scheme for the heights at 40 cb and a linear fit at 25 cb was made. "Test C" in Table 2 has the results and the

problem layer in this test is sigma 5 which contains the 30-cb level. In the calculation of sigma 5, the heights at 40, 30, and 25 cb are the dominant elements. Since the heights at 40 and 25 cb are computed, it appears that the check is too sensitive.

A tolerance limit was added to the check to lessen its sensitivity. The height value at 40 cb has the greatest effect on sigma 3 (excluding the layer containing the 40-cb height) and the height at 25 cb likewise has the greatest effect on sigma 5. Prior to checking the column, a calculation of sigma 3 and sigma 5 is made. Should either fail the check and a tolerance of ± 15 meters on the appropriate height, either 40 or 25 cb, allows the check to pass, a ± flag for that sigma is set. During the check of the column should a sigma fail the test, the precomputed tolerance for the heights at 40 and 25 cb is added to the failed value. If the test then passes, the "fail flag" is removed. In addition, a consecutive check was programmed. If the sigma values in two adjoining layers should fail a special flag is set. The rest of the sigmas are computed without regard to the pass or fail criterion. Pressure heights are then recomputed incorporating the effect of the corrected value in the lowest sigma layer which failed. A complete stability check is then performed on the new height set. The results are listed in Table 2 under "Test D" and this became the final version of the static stability test.

3.4. COMPUTATIONS OF H_p, B, H_o, AND G(A)

Fig. 4 shows the levels at which H_p and B can be calculated based on the available data. For convenience the lower boundary effects, represented by the

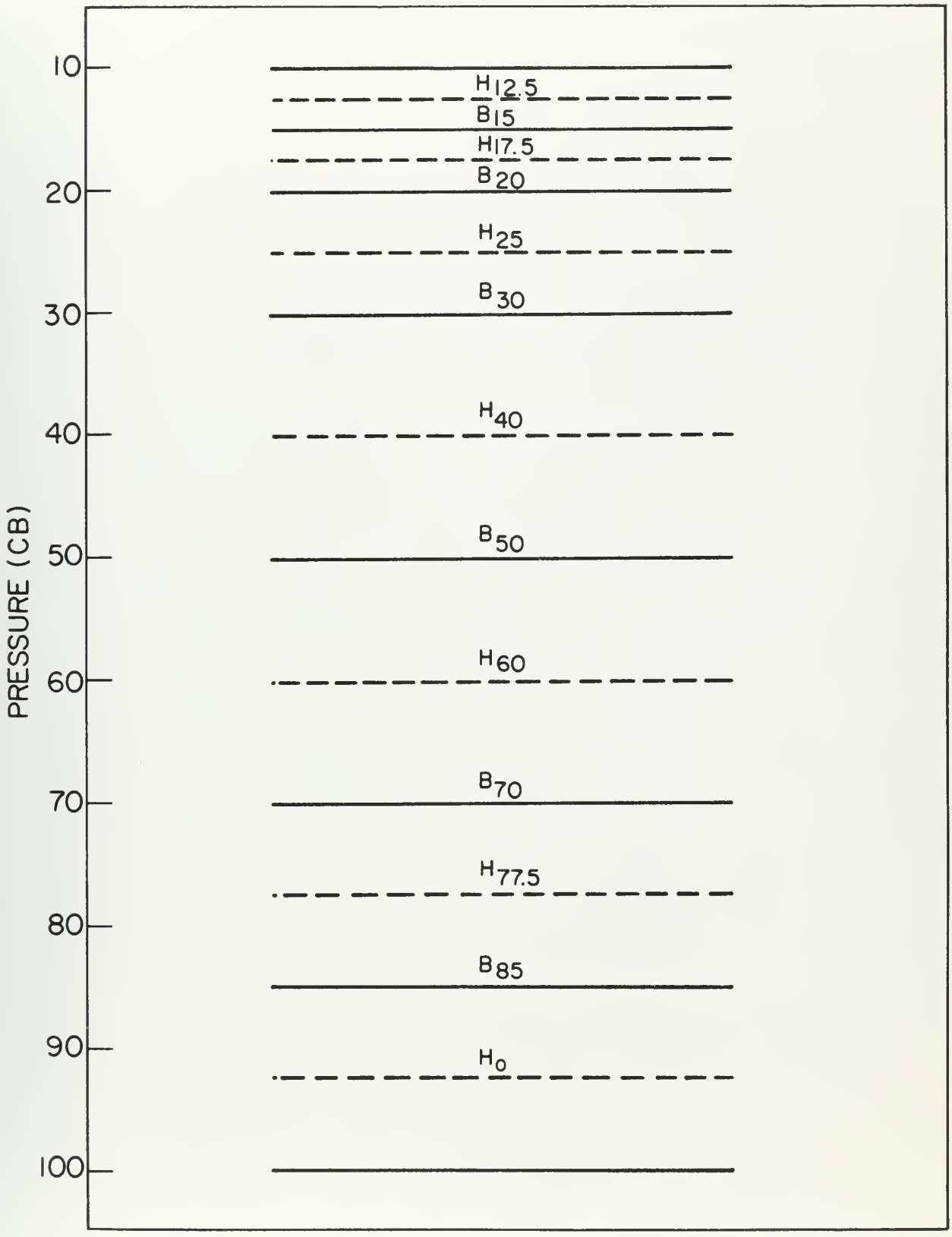

Fig. 4. The levels at which the integrand of (2.8), B, and the diabatic processes, H, are calculated.

diabatic term, H_o, have been assigned to the 92.5-cb level. The effects of the frictional forces are included in the calculation of B at the 85-cb level. Once H_p fields have been computed the generation of APE can be determined. Based on the available data the vertical resolution parameter, m, in (2.30) and (2.31) takes on the value 7. The latitude-longitude increment is taken as 2.5 deg and the region is set as that bounded by the latitude rings at 20N and 87.5N. Thus σ_1 = 18.75N and σ_2 = 88.75N while k takes on the value 28.

CHAPTER 4

RESULTS OF THE COMPUTATIONS

4.1. STATIC STABILITY CHECK

A static stability test discussed in Section 3.3 was performed on the data which consist of height analyses at 100, 85, 70, 50, 30, 20, 15, and 10 cb. The time period covered runs from 1200 GMT 1 March 1963, to 1200 GMT 31 March 1963. For these data the average number of grid points requiring a height correction in the vertical structure is 395. This number includes the effects of the combined NMC and GWC sets as well as the averaged fields which together involve four different analysis times. Height fields at 15 cb for 0000 GMT 6 and 7 March and 1200 GMT 19 March and the 100-cb heights for 0000 GMT 7 and 15 March were formed by averaging the available analyses from the adjoining times. All of the NMC analyses are missing for 0000 GMT 7 March and the GWC set was substituted. GWC fields at 85 and 70 cb for 0000 GMT 15 March are also required. A significantly greater number of stability failures are encountered for these four periods as would be expected. Excluding their effect, the average number of grid-point failures is 369. Most of the stability problems occur in the sigma 1 and sigma 7 layers. An average of 160 failures in the sigma 1 layer and 104 in the sigma 7 layer are computed. Again, the total number of grid points is 1977 so about 19% of these points present some stability problem in the vertical structure. Now it is quite likely that these failures are random. No tests were made to determine otherwise. If in fact they are random, then time averaging procedures should remove their effect.

However, since almost 20% of the vertical structure of the NMC analyses is questionable relative to their static stability, numerical calculations based on these unchecked data would seem to be also questionable.

Finally, Fig. 5 shows the comparison between the average of the computed static stability for the month, indicated by the dashed line, and the analytic representation as indicated by the solid line. For the region of the Northern Hemisphere involved in this study the analytic form is quite obviously acceptable.

4.2. MEAN DIABATIC PROCESSES FOR MARCH 1963

Calculations of H and B were made using the data as illustrated in Fig. 4. Computations were made using the finite difference equations given in the Appendix and the results are available at twelve-hourly intervals for the month. Fig. 6 depicts the zonally averaged values of the diabatic processes in the meridional plane as a function of latitude and pressure for March 1963. Values south of 30N are not shown as the same unrealistic picture presented by Wiin-Nielsen and Brown (1960) resulted, i.e., the values rapidly decrease and become negative. This is probably due to a lateral boundary problem associated with the analyses which will be discussed shortly. The units are 10^{-2} kj sec^{-1} ton^{-1} and multiplication by 0.864 converts them to deg day^{-1}.

The stratospheric rates in the layer from 30 to 12.5 cb do not correlate with any known computations involving observational data or model atmospheres. For example, based on the numerical results of Manabe, Smagorinsky, and Strickler (1965) and Manabe and Hunt (1968), the values in this layer should be near

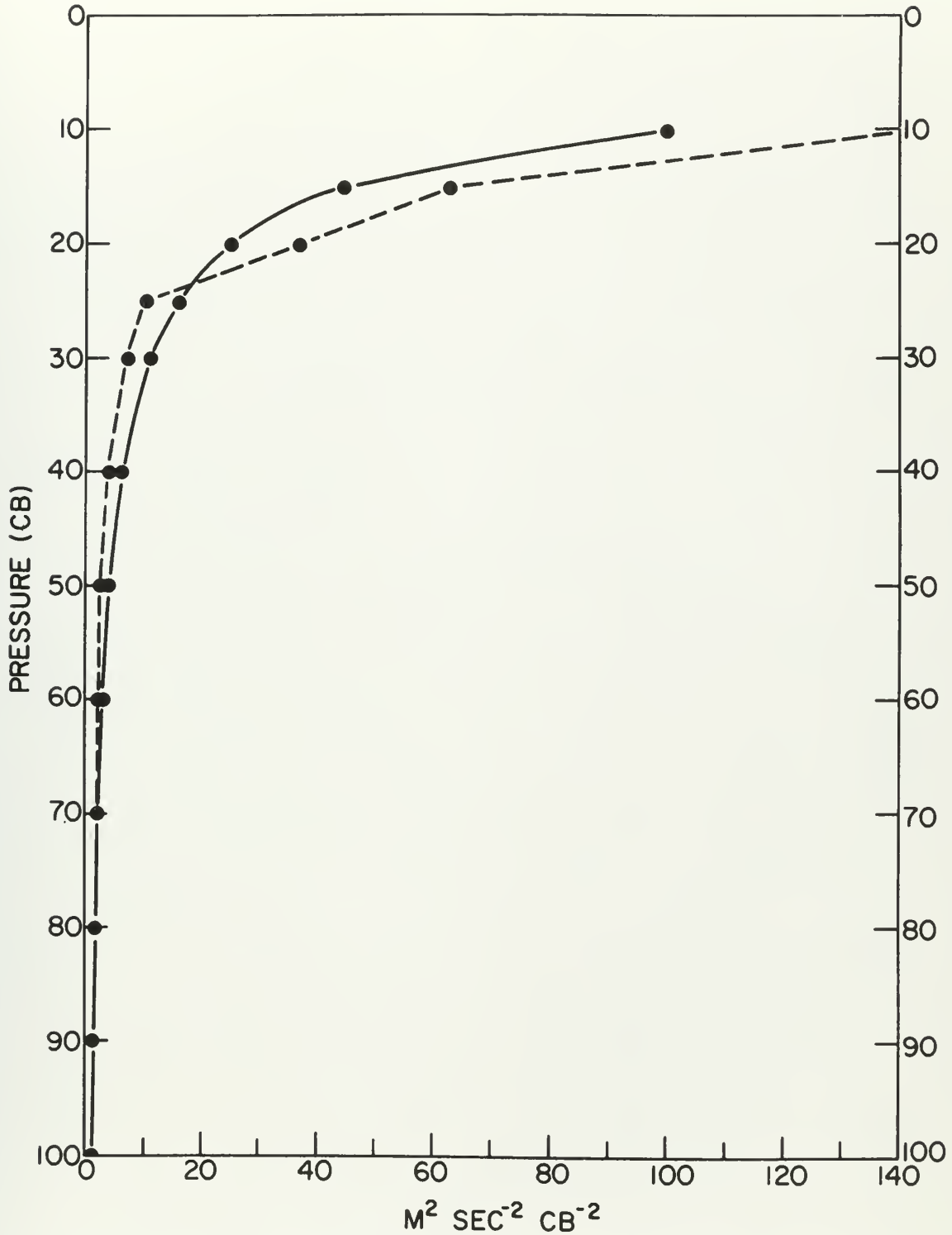

Fig. 5. A comparison of the monthly average of static stability based on data as indicated by the dashed line and the analytic representation as shown by the solid line for March 1963.

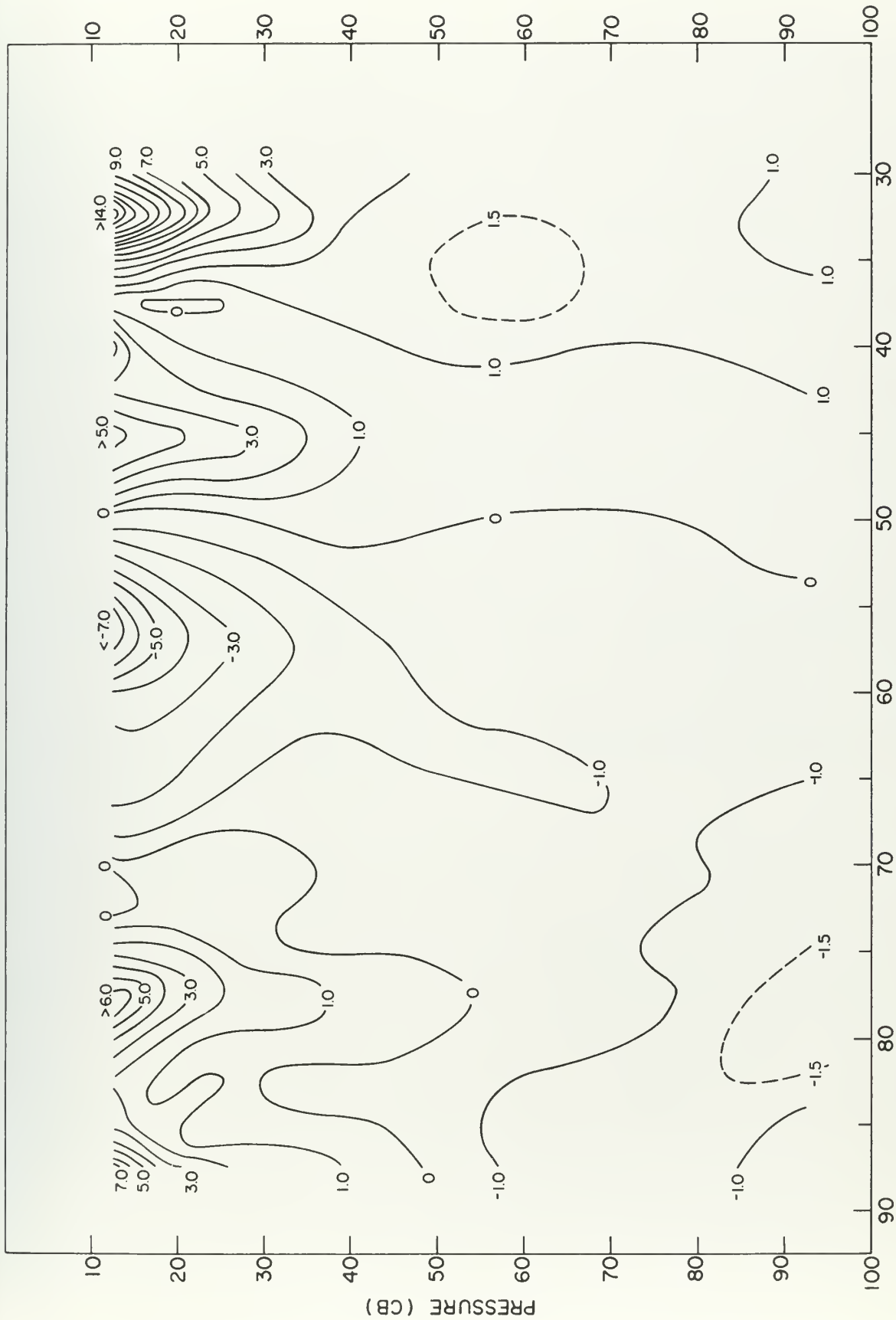

Fig. 6. Zonal average of the diabatic processes for March 1963, as a function of latitude and pressure in the units 10^{-2} kj sec^{-1} ton^{-1}.

$- 0.6 \times 10^{-2}$ kj sec^{-1} ton^{-1}.

In contrast, the tropospheric detail in the layer from 100 to 30 cb appears comparable to previous results. Vernekar (1967) for example calculated the mean values for diabatic processes for January 1963. He calculated them using a computed vertical velocity forced only by the vertical variation of the horizontal eddy transport of zonal momentum. His results are displayed as Fig. 7 and essentially show the same pattern from 100 to 30 cb.

Excluding the results above 30 cb and south of 30N, the area mean values for the layers from 100 to 30 cb are shown in Fig. 8. On the basis of the vertical nature of the zero line in Fig. 6, the latitude band centered at 50N was used to separate the heating and cooling areas. The computed values of H are plotted as values for their respective layers. Overall the results indicate that there is little difference with pressure in the troposphere. Otherwise the maximum cooling occurs in the layer from 85 to 70 cb and maximum heating in the layer from 50 to 30 cb.

4.3. MONTHLY AVERAGE FOR THE VARIOUS LEVELS

Within the troposphere and the lower stratosphere the important diabatic processes are the absorption of solar radiation, the emission of long wave radiation, the release of latent heat (provided that some condensate returns to the surface as precipitation) and the transfer of sensible heat across the earth-atmosphere interface. The method of computing the diabatic effect used here precludes the separation into contributions from the components. Some qualitative remarks can be made however.

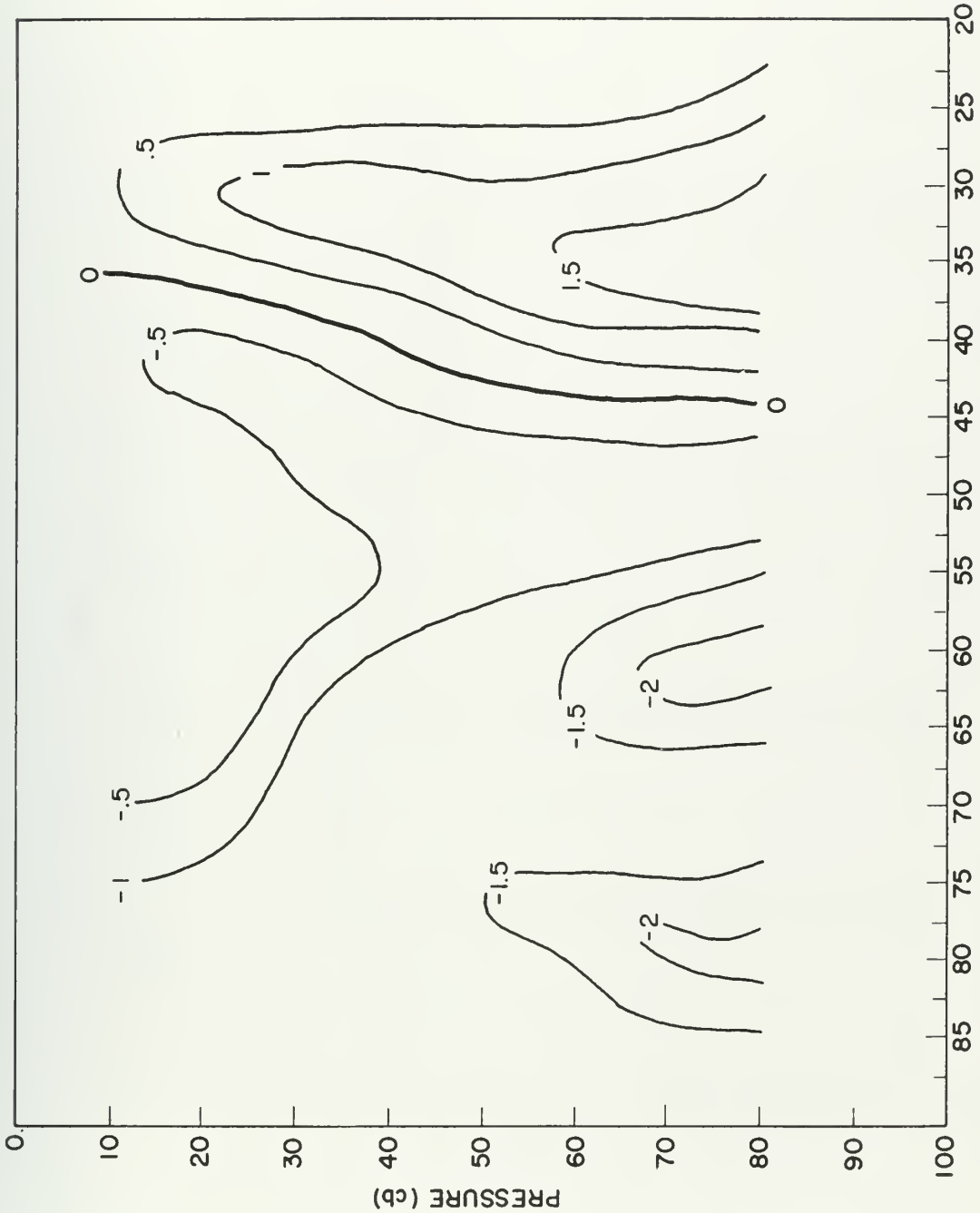

Fig. 7. Zonal average of the diabatic processes for January 1963, as a function of latitude and pressure in the units 10^{-2} kj sec^{-1} ton^{-1}. (After Vernekar, 1967.)

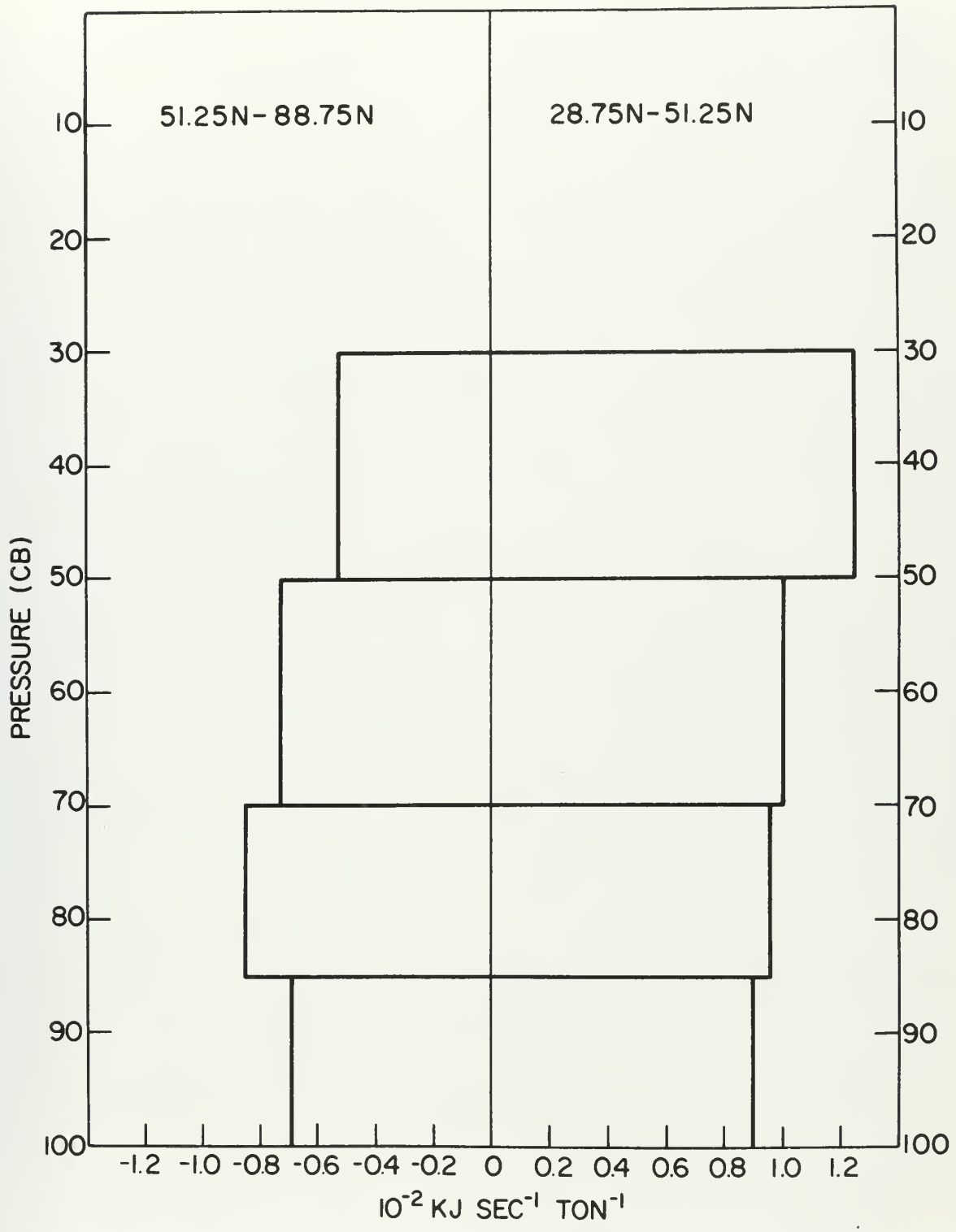

Fig. 8. Area mean values for the diabatic processes as a function of pressure. The values are for the heating region and the cooling region as separated by the latitude circle at 51.25N.

Within the total depth of the atmosphere the cooling effect of the divergence of long wave radiation flux is the dominant element. In the middle latitudes and the tropics, the contributions from the net gain of latent heat release, solar absorption and the boundary flux are important in the lower troposphere, i.e., the layer from 100 to 50 cb. Cooling effects of long wave radiation should dominate the layers above 50 cb in the high troposphere and low stratosphere and the polar atmosphere. However, in regions involving cloudiness, both radiational warming and cooling areas can be found as shown by Johnson and Shen (1968) for example.

Monthly averages for the lower boundary and the levels at 77.5, 60, 40, 25, 17.5, and 12.5 are presented in Fig. 9 through 15. The units are the same as in Fig. 6. Areas where average heating occurred during the month are cross-hatched. Values for maximum rates of heating and cooling are plotted in the appropriate regions. The latitude circle at 30N has been outlined to indicate the practical limit of this study. It also separates the hemisphere into halves relative to the surface area.

Monthly averages of the diabatic processes due to the presence of a lower boundary are displayed in Fig. 9. Phillips (1963) has shown that a maximum heating rate consistent with the geostrophic assumption is of the order 0.1 kj sec^{-1} ton^{-1}. Within quasi-nondivergent theory there are also limitations on the frictional and terrain induced vertical velocities. Since the vertical velocities are included in the computation of diabatic processes in the lower boundary and are not used elsewhere it is sufficient to limit the magnitude of the heating term. A limit was set at 0.7 kj sec^{-1} ton^{-1} and an average of two

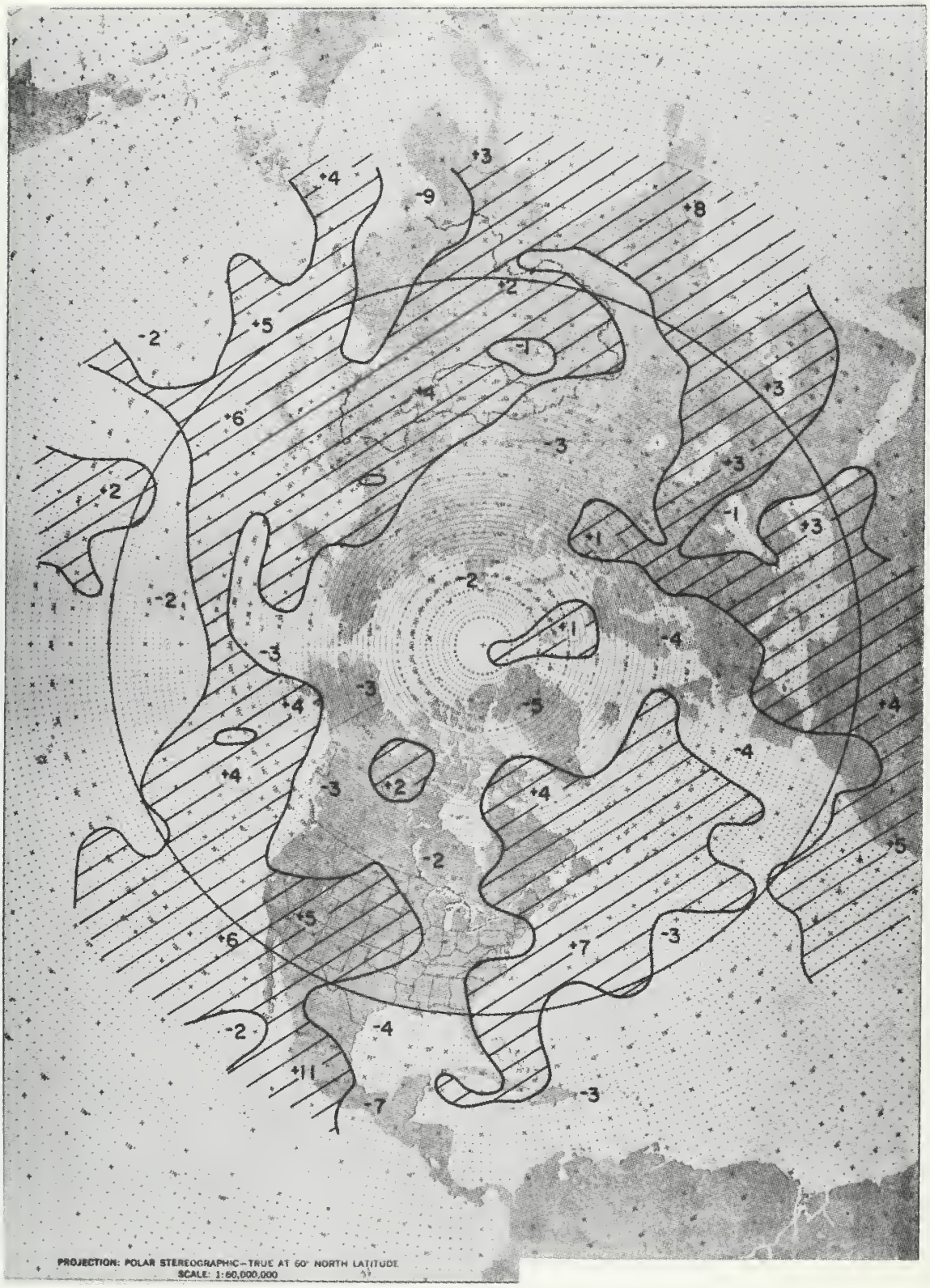

Fig. 9. Monthly average of the diabatic processes at the lower boundary for March 1963, in the units 10^{-2} kj sec^{-1} ton^{-1}.

Fig. 10. Monthly average of the diabatic processes at 77.5 cb for March 1963, in the units 10^{-2} kj sec^{-1} ton^{-1}.

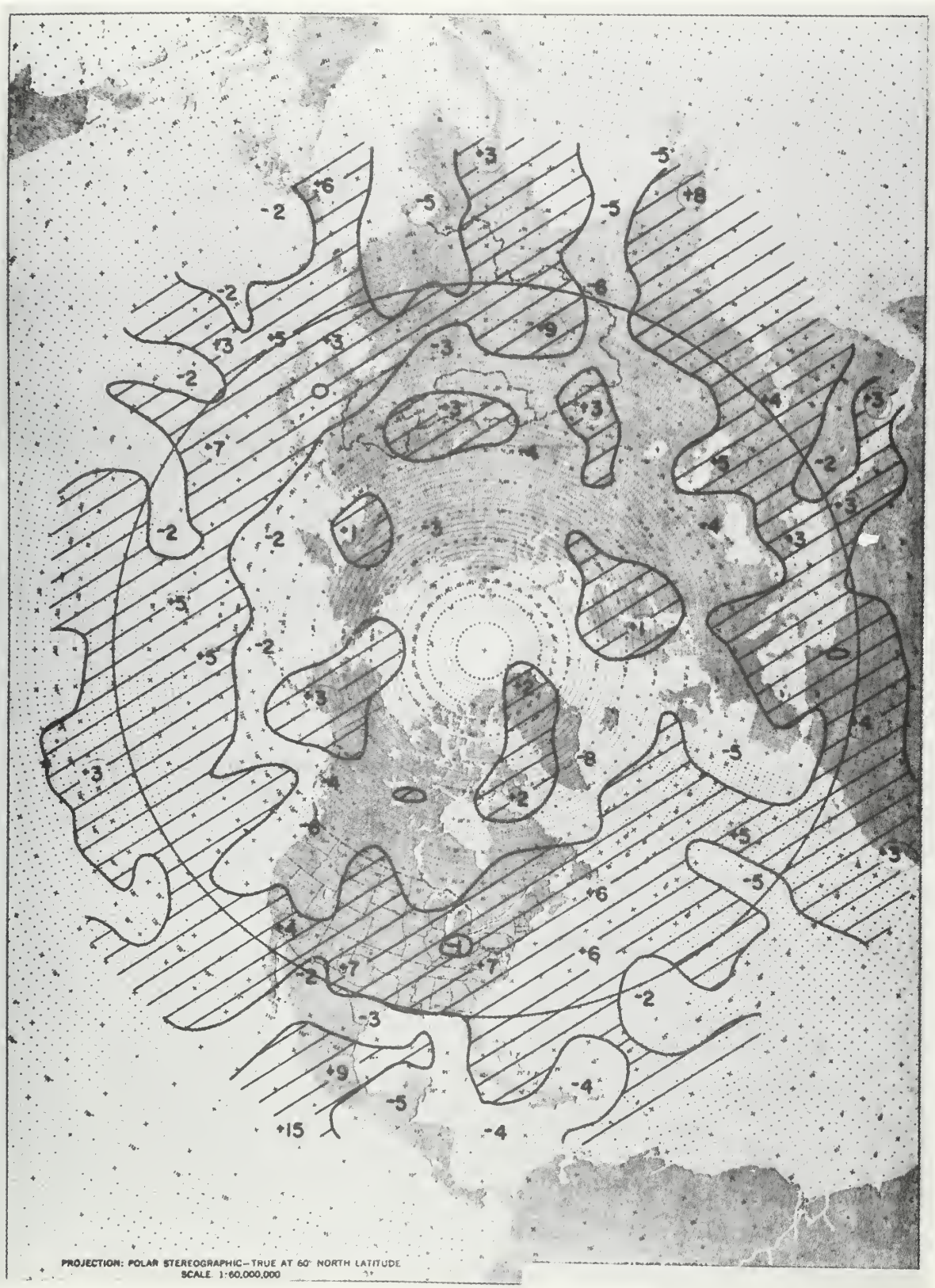

Fig. 11. Monthly average of the diabatic processes at 60 cb for March 1963, in the units 10^{-2} kj sec^{-1} ton^{-1}.

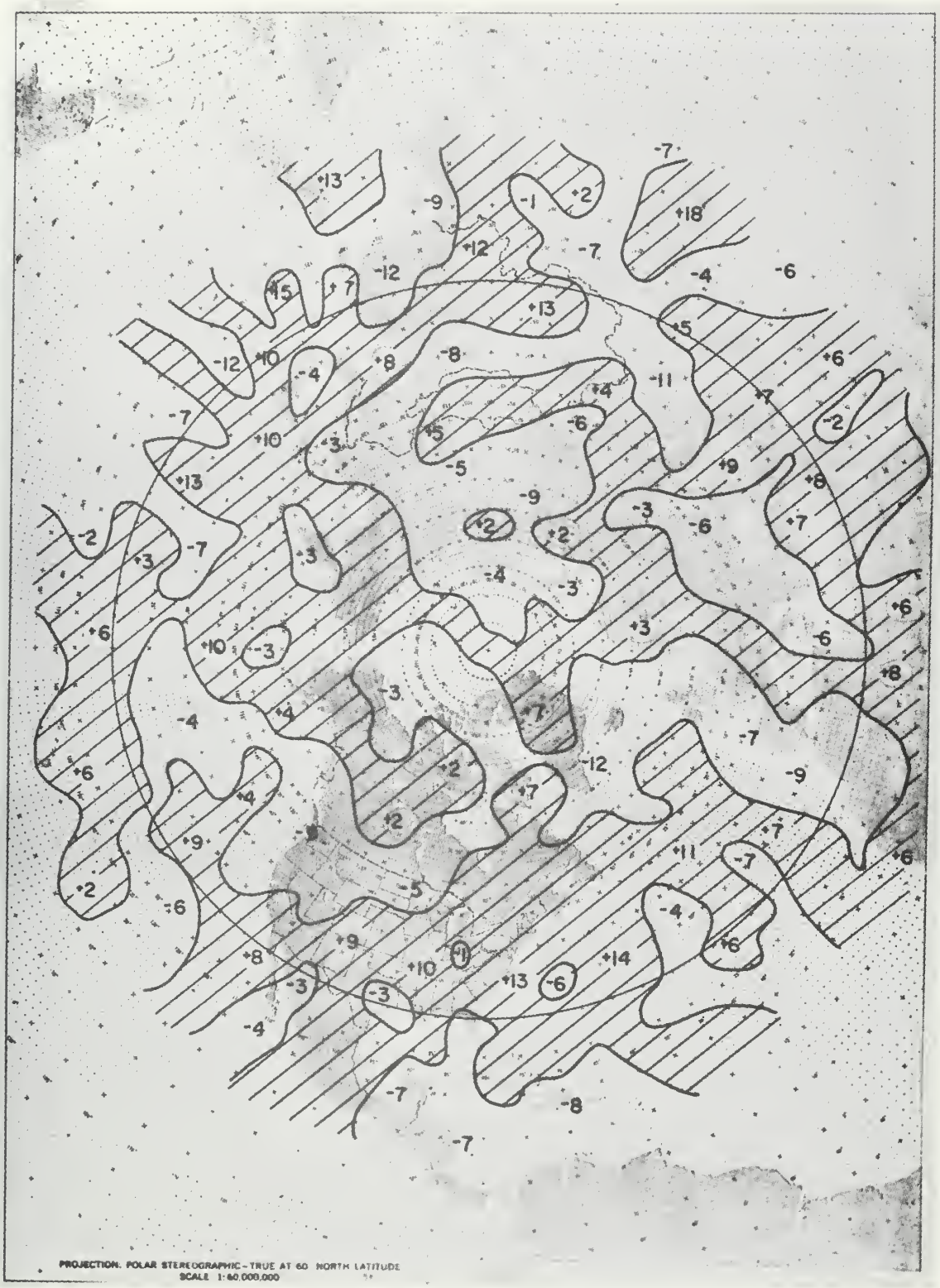

Fig. 12. Monthly average of the diabatic processes at 40 cb for March 1963, in the units 10^{-2} kj sec^{-1} ton^{-1}.

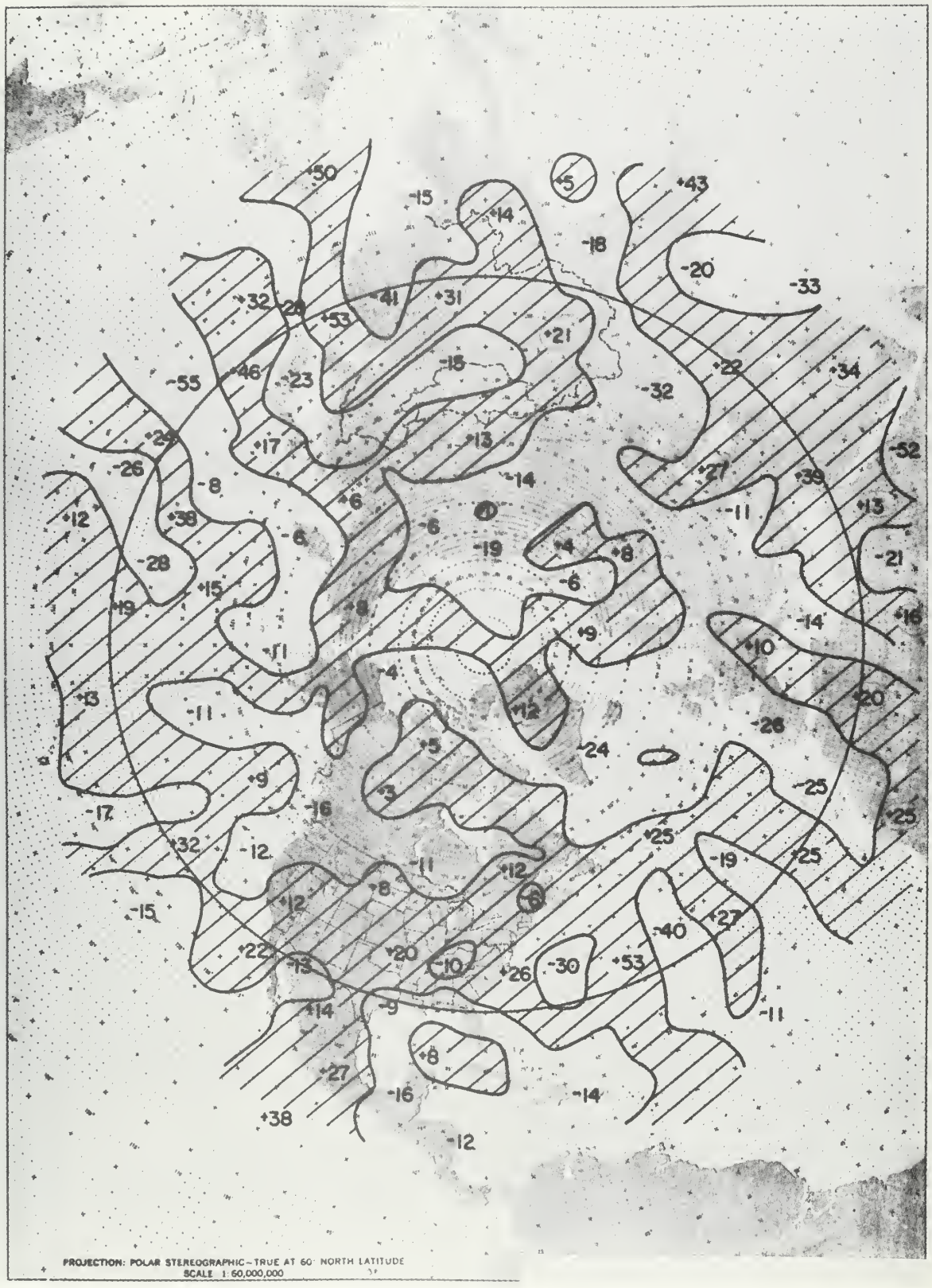

Fig. 13. Monthly average of the diabatic processes at 25 cb for March 1963, in the units 10^{-2} kj sec^{-1} ton^{-1}.

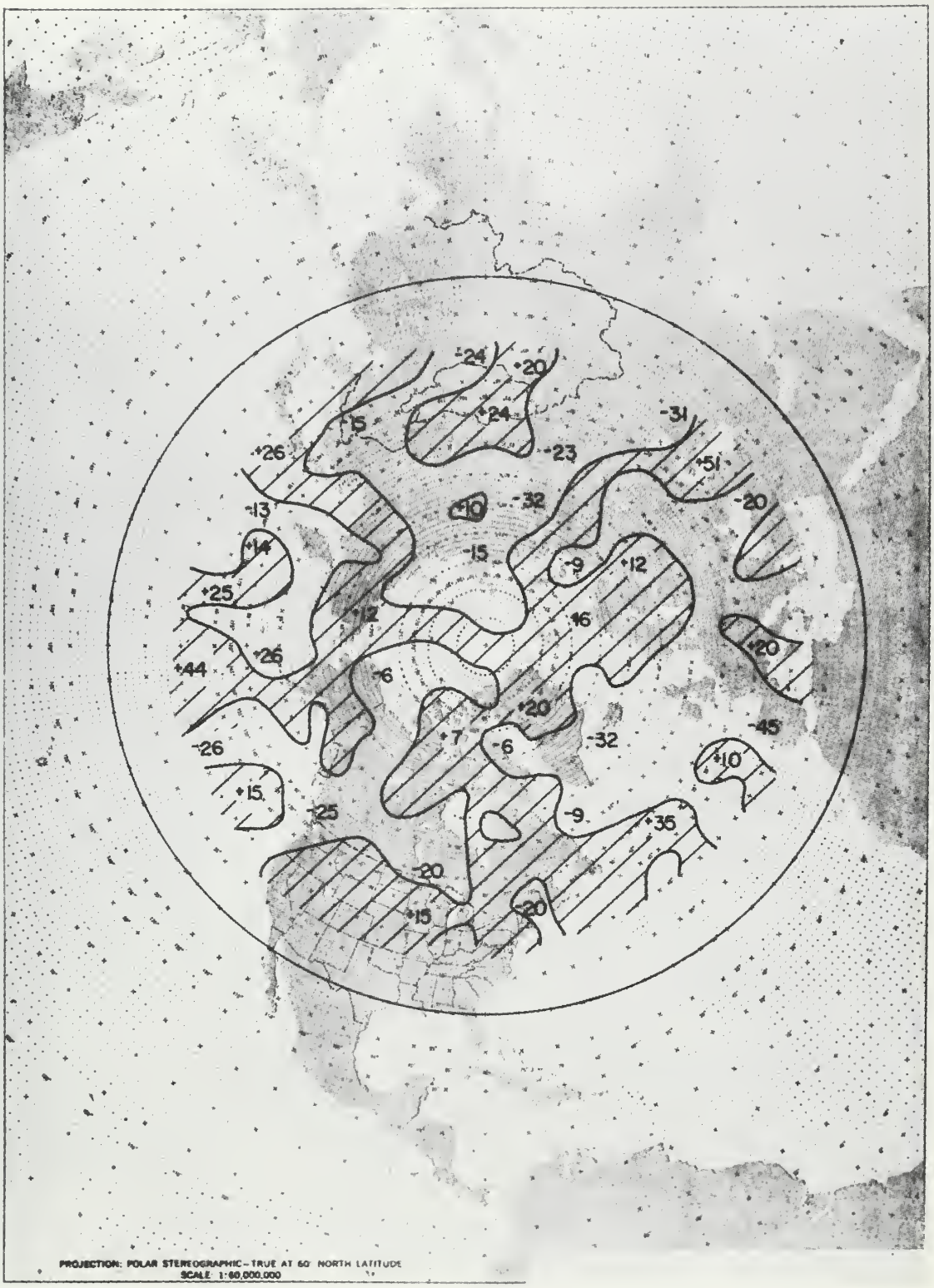

Fig. 14. Monthly average of the diabatic processes at 17.5 cb for March 1963, in the units 10^{-2} kj sec^{-1} ton^{-1}.

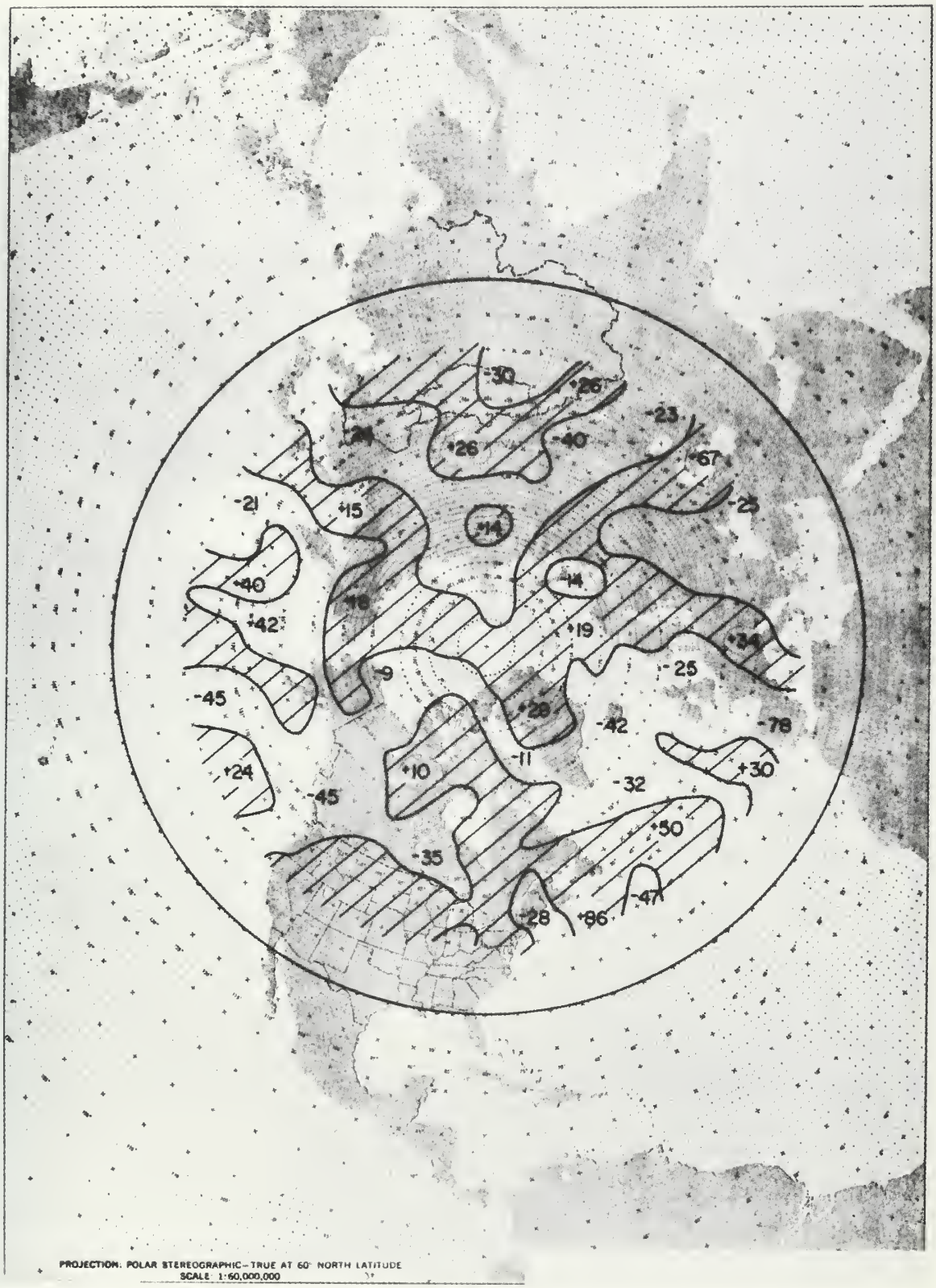

Fig. 15. Monthly average of the diabatic processes at 12.5 cb for March 1963, in the units 10^{-2} kj sec^{-1} ton^{-1}.

grid-point values per analysis time failed the check and were reset to the limit.

Patterns presented in Fig. 9 are based on calculations using (2.17). They are therefore the results of the averages of the local time change in and the horizontal advection of the temperature at terrain height and the vertical velocities induced by the surface. Effects of heat transport across the interface are probably wholly contained in this computation for the lower boundary. The general picture of cooling over the land masses and warming over the ocean bodies seems to support this. Heating patterns in the western oceanic regions are well correlated with the warm Gulf Stream and the Kuroshio Current.

The fact that this average for the lower boundary has a variable pressure base should not be forgotten. This base ranges from 104 cb over the oceans to 47 cb in the region of the Himalyas. Thus there are areas in which latent heat release and radiational warming due to low cloudiness are strong modifying influences in the lower boundary.

Dickson and Posey (1967) have prepared snow-cover probability charts for the Northern Hemisphere. Their charts indicate the probability of the cover being 1 in. or greater in depth. Continental areas north of 50N have a factor of 0.5 for the month of March. These same areas north of 55N have a factor of 1.0. Figure 6 shows that the change between the mean heating and cooling regions occurs at 53N in the lower boundary. Sellers (1965) has tabulated the distribution of various parameters in latitude bands of ten-degree width for the globe. Between 50N and 70N the oceans cover about 36% of the surface area. In March, the oceans north of 70N are either covered by ice or snow. Therefore the surface area north of 53N can be considered to be snow-covered for

this study. The vertical orientation of the zero line in Fig. 6 seemingly indicates that this effect is felt throughout the troposphere.

In order to compute the diabatic processes at higher levels in the atmosphere the effects of the variable lower boundary were assigned to the constant pressure level at 92.5 cb. Therefore the results in the other levels contain effects which are not really there. This is so because (2.22) is used to calculate the processes at all levels above the boundary layer. However, the number of grid points at which the pressure at terrain height is generally less than 85 cb is small. Primary areas where it does occur are the Rocky Mountains, the Himalyas, and the Greenland Plateau.

Mean monthly 70-cb height contours, taken from the June 1963, issue of Weatherwise, are depicted in Fig. 16. Long wave troughs are located along the western coast of North America, the eastern Asiatic coast, in western Russia and the eastern North Atlantic Ocean. The middle latitudes are dominated by three waves from the western United States westward to western Europe while the flow pattern exhibits strong zonal characteristics eastward from the middle of the United States to the middle of the Atlantic Ocean. Diabatic fields at 77.5 and 60 cb (Fig. 10 and 11) show that a good correlation exists between the extensions of the cooling regions into the lower latitudes and the trough positions. The effects of the minor trough near Hudson's Bay can be detected also. Andrews (1963) reports that record and near-record amounts of precipitation fell in the Ohio and Tennessee Valleys during the month. Changes from cooling to heating in this region in the layers above the lower boundary are most likely due to the release of latent heat and radiational warming below

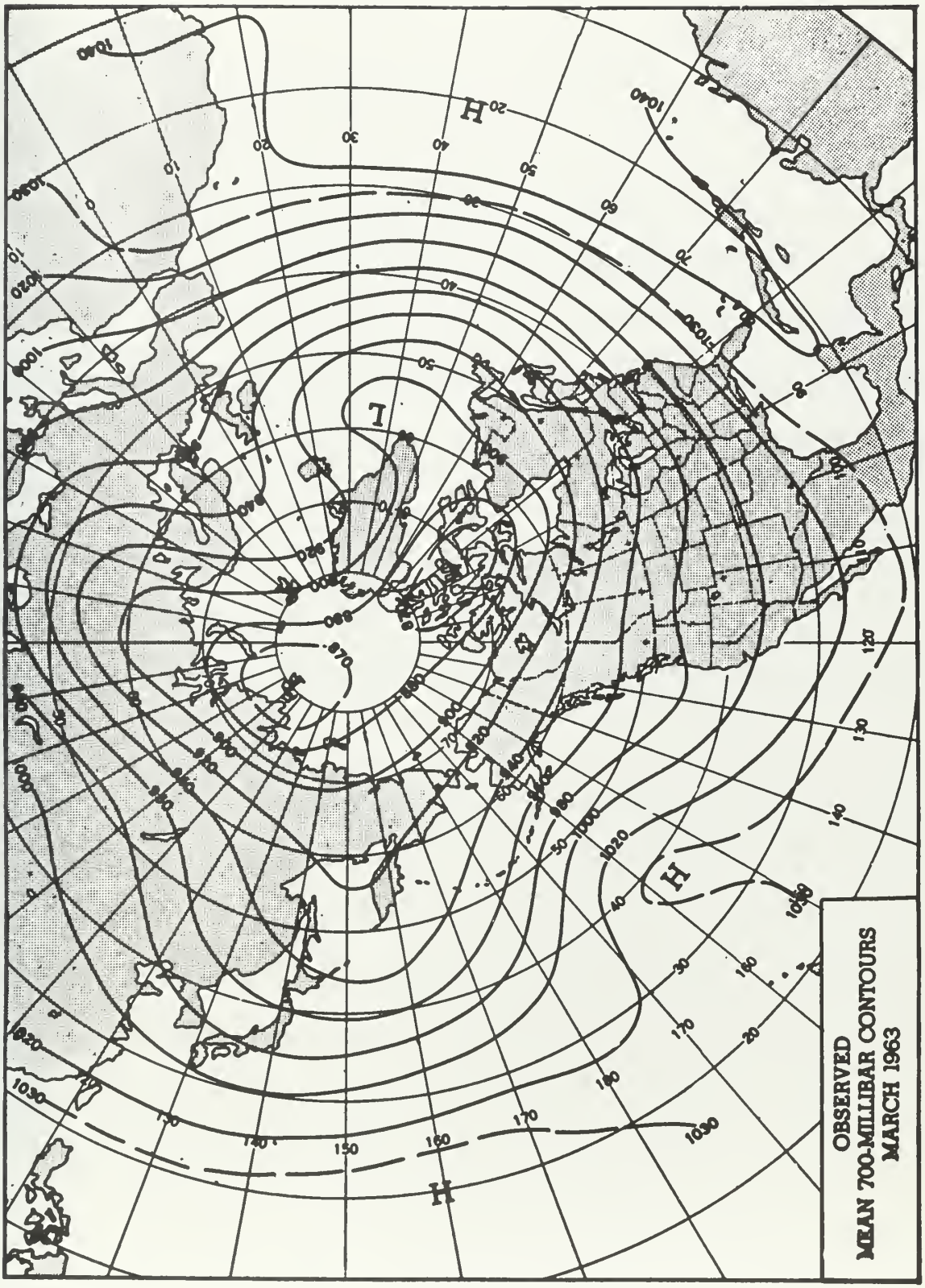

Fig. 16. Mean 70-cb height contours for March 1963.

cloud bases. Andrews (1963) also reports that portions of the Southern Plains and lower Mississippi Valley suffered a precipitation deficiency. This area, particularly at the lower boundary and the 77.5-cb level, shows strong diabatic cooling.

The remaining levels, Fig. 12 through 15, should contain mostly the effects of long wave radiation. London (1957) acknowledges that radiational warming beneath clouds and the base of the stratosphere does occur but probably is the exception rather than the rule. Extensive areas of diabatic heating in these figures imply that this is not true. However, an explanation requires the existence of multi-layer cloud decks and/or multiple tropopauses. But note that the large magnitudes of the heating and cooling rates, especially at the 12.5-cb level, indicate that something is wrong with these calculations. This of course is the same conclusion that was reached from the results presented in Fig. 6.

Results for the 40-cb level appear to be acceptable. Besides the effect of cloud decks, perhaps the effect of the release of latent heat above 50 cb is also required to explain these heating patterns. The answer cannot be resolved by this investigation. However, the amount of water vapor generally thought to be present above 50 cb would not appear to be significant enough to offer a substantial contribution toward latent heat release. Thus the logical conclusion seems to be that the clouds are the ultimate cause of the heating patterns. The presence of cirrus clouds would be quite effective in producing these warm areas as has been shown by Johnson and Shen (1968). At least the required cloud patterns needed to support the results in Fig. 12 would be

generally eastward of the trough positions shown in Fig. 16. Katayama (1966, 1967a, 1967b) has carried out extensive calculations for the radiation budget of the Northern Hemisphere. Although many assumptions are made, particularly with respect to cloud properties, favorable comparisions of the total solar radiation at the earth's surface with other studies appear to justify his calculation procedure. He states that the "existence of high-level clouds has an intense effect on decreasing" the net long wave radiation at 20 cb. Katayama (1967b) shows how low, middle, and high clouds can cause heating in various layers within the vertical structure through flux convergence of the long wave component.

What appears to be the answer to the problems with the calculation at the higher levels can be seen in the patterns of Fig. 12 through 15. At the 40-cb level the analysis is beginning to breakup into small irregularities south of 30N. This feature is much more obvious at 25 cb. The results become so unmanageable at the other levels that no contouring is shown south of 40N. Referring to (2.8) and (2.22), the term representing the frictional effects is included in the computation of B at 85 cb only. Ignoring H_o, which is of smaller order anyway, the remaining terms involved in computing the diabatic processes are the local time change in and the horizontal advection of potential vorticity. The computation at any level is the resultant of the vertical summation of these effects in the layers below.

As a consequence of quasi-nondivergent theory, the terms representing the local time change and the advection must be of comparable order or time scale. Sample calculations for B show that this is true at 50 cb for example. But

for 30, 20, and 15 cb the advective term is greater by at least one order of magnitude in much of the boundary areas and at scattered interior grid points. Since the local time change of potential vorticity at 50 and 15 cb are of the same order, the problem seeems to be with the horizontal advection term.

An analysis of the computed potential vorticity using (2.6) indicates that the patterns are of type 1 as defined by Phillips (1963). This means that geostrophic potential vorticity is characterized by "approximate uniformity." In other words, the values at any level do not exhibit a large range. This is true because of the quasi-horizontal nature of the isobaric surfaces. Therefore the wind used to advect the gradient of potential vorticity is suspect.

The horizontal nondivergent wind used for advection is computed using the linear balance equation introduced by Shuman (1957). It has the form

$$\nabla^2\Psi = \frac{\nabla^2\Phi}{f} - \frac{\nabla f \cdot \nabla\Phi}{f^2} \qquad (4.1)$$

Ellsaesser (1968) found this to be the best approximation to use in calculating a nondivergent wind. The linearized form is the result of excluding the other terms in the divergence equation. Their exclusion is based on the fact that they are of order Rossby number cr smaller. The nondimensional Rossby number, R_o, is the ratio of the characteristic wind or particle speed, U, to the product of the Coriolis parameter with a characteristic horizontal wave length for the motion, L. Within the atmosphere the patterns of interest are such that $U \leq 100$ m sec^{-1}, $L \geq 1000$ km and $f = 10^{-4}$ sec^{-1}. Therefore $R_o \leq 1$. The value 1 is associated with minimum L and maximum U. For a characteristic atmospheric wind speed of 15 m sec^{-1} and a characteristic wave-length of 10^6 m, $R_o \tilde{=} 0.15$.

One could argue perhaps that in the stratosphere the Rossby number is no longer a small quantity and that discarded terms of order R_o must be retained in the equations. It is an observed fact that both the characteristic wind speed and wavelength increase with height in the troposphere and low stratosphere. However, even allowing U to double and L to remain at 10^6 m, the Rossby number is only about 0.3. Thus the balance equation does not appear to be a bad assumption in the layer from 30 to 10 cb.

It should not be forgotten that much manipulation was involved in calculating and correcting the static stability of this region. The sensitivity of the check implies that care must be exercised. Discontinuities of the lapse rate of temperature in a sigma layer due to the tropopause are probably the main cause of the problems. However, a new version of the check was programmed which requires only the data levels which are available. Height fields corrected by the new stability test and the unaltered original analyses for a sample period were used to recalculate the diabatic processes. The same failures of the method were encountered above 30 cb with both sets.

Significant errors in the analyses which would damage the calculations could be present. Mean heating for the layer from 100 to 30 cb in the meridional plane as a function of latitude is shown in Fig. 17. The horizontal lines are the values based on an interpolation of the January and April tabulations of Davis (1963) for the 101 to 30-cb layer. Other comparisons can be made to the partial layer results of Wiin-Nielsen and Brown (1960) and Vernekar (1967) who includes the results of Brown (1964). These results essentially parallel the results presented here. Agreement in Fig. 17 seems reasonable

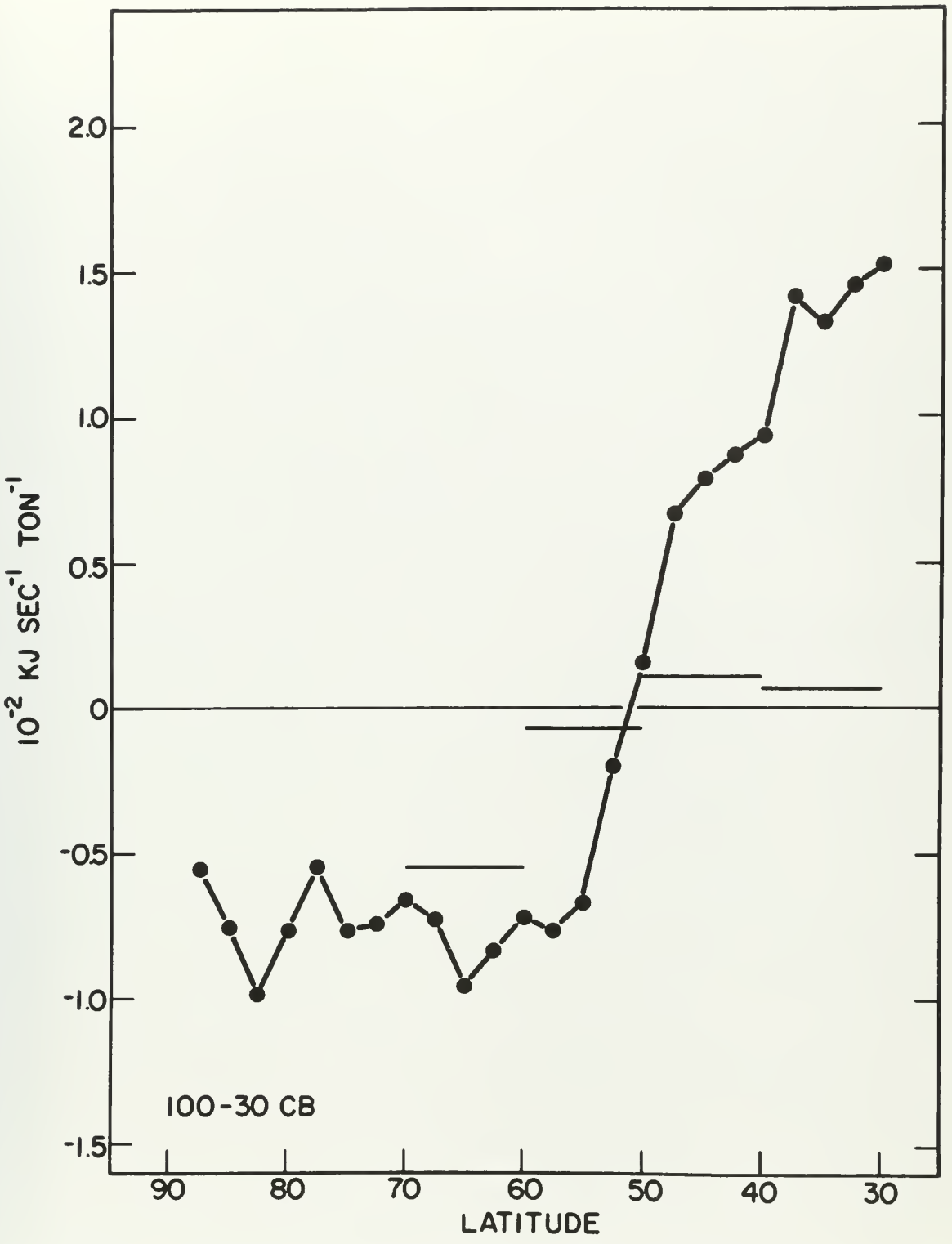

Fig. 17. Mean diabatic processes in the layer from 100 to 30 cb for March 1963. Horizontal lines are the interpolated values from Davis (1963).

north of 50N but south of 50N there is a substantial difference. Holopainen (1967) questions the scheme of objective analysis employed by NMC on the basis of the results of Wiin-Nielsen, Brown, and Drake (1963, 1964). The reason is the deviation of their computations of the mean poleward flux of angular momentum from other calculations he presents. Deviations are particularly pronounced south of 50N being larger by a factor of about 1.6 at 35N.

The Fleet Numerical Weather Central (FNWC), Monterey, California, provided data for a sample period during the month under investigation. Analysis at FNWC is performed on a square grid containing 3969 points in which the equator is an inscribed circle. The NMC octagon is a subset of the FNWC grid. Fig. 18 shows the difference when the NMC analysis is subtracted from the FNWC analysis. The level is 50 cb, map time is 0000 GMT 5 March 1963, and the unit is meters. Boundary problems apparently imposed by the limits of the octagon are readily observable. In general, the NMC analysis is significantly higher on the boundary and the difference extends to 30N. If the differences in Fig. 18 are characteristic of all NMC analyses, the poor results south of 30N may be explainable. Additionally, there are substantial differences in the top-half of the map. This is probably caused by a data sparsity in one analysis vs. the other. The dipole near the pole could be the result of a position difference for a system. It should be also mentioned that there are differences in the techniques of numerical analysis as outlined by Cressman (1959) and Carstensen and Lawniczak (1966).

Effects of analysis errors or uncertainties, whether caused by technique or lack of information, cannot be taken lightly. Zonal values for the diabatic

Fig. 18. Resultant differences when the NMC analysis is subtracted from the FNWC analysis for 50 cb. The map time is 0000 GMT 5 March 1963, and the unit is meters.

processes in the layer from 100 to 30 cb using three different analysis sets are shown in Fig. 19. The three sets are: (1) the original NMC analyses (NSS NMC), (2) the statically stable NMC fields (SS NMC), and (3) the fields provided by FNWC (NSS FNWC). (The FNWC data were not checked for static stability. FNWC began using the vertical consistency scheme in June 1963, so the data used here probably do contain some inconsistencies.) There appears to be little difference between the results using the different NMC sets. However, the results of the FNWC data show striking differences. The outstanding deviations are in the polar region and the area from 20N to 60N. A requirement for additional global data to eliminate analysis uncertainties could not be presented more clearly than in the preceding discussion.

As pointed out previously, the calculation of diabatic processes at lower pressure levels in the atmosphere depends on the vertical summation of the B computation in layers at higher pressure. Thus once the results at a particular level become erroneous they are propagated in the remaining levels at lower pressure. Phillips (1963) explains that for geostrophic motion of type 1, the product of the square of the Rossby number with the Richardson number must be of order 1 for the characteristic scale of motion. The Rossby number has already been defined as

$$R_o = \frac{U}{fL} . \qquad (4.2)$$

Wiin-Nielsen (1965, Eq. 2.10) shows that the Richardson number can be written as

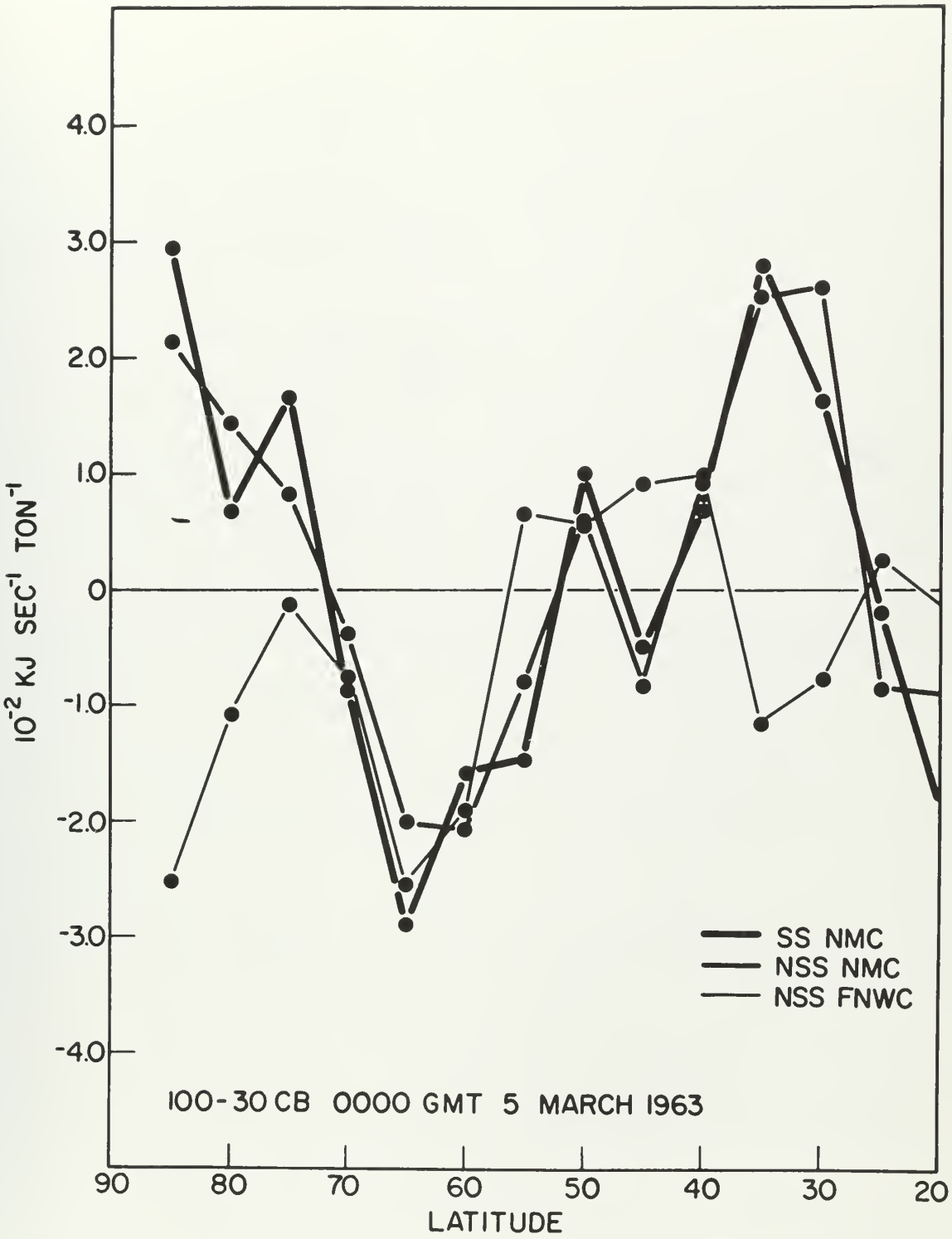

Fig. 19. Mean values of the diabatic processes in the layer from 100 to 30 cb using the three analysis sets as indicated.

$$R_i = \frac{\sigma}{\left(\frac{dU}{dp}\right)^2} \tag{4.3}$$

This is true in a model using quasi-nondivergent theory where the static stability is defined as stated in Chapter 2. Using (4.2) and (4.3), Phillips' criterion for geostrophic motion becomes

$$\frac{U^2}{f^2 L^2} \cdot \frac{\sigma}{\left(\frac{dU}{dp}\right)^2} \tilde{=} 1 \ . \tag{4.4}$$

One of the critical terms in (4.4) is the vertical wind shear. Obviously as the shear approaches zero from either side the relationship cannot be maintained. This means that the quasi-nondivergent theory must fail in regions where a maximum or a minimum in the vertical wind profile exists or where U is independent of the pressure coordinate. The mean zonal wind as a function of latitude and pressure for March 1963, is plotted in Fig. 20 with the units m sec^{-1}. Relationships between the maximum in the zonal wind and the diabatic patterns between 30 and 10 cb of Fig. 6 cannot be accidental. The greatest magnitude of diabatic heating in Fig. 6 is directly coupled with the jet stream in Fig. 20. Based on the discussion of the boundary problem around the sides of the octagon, it is reasonable to conclude that the magnitude of the zonal wind at and above 50 cb near the boundary is too large. But the shear characteristics associated with a jet still remain.

The results displayed in Fig. 5 shows that the static stability parameter undergoes a change of at least two orders of magnitude in the layer from 100 to 10 cb. In itself this is enough to invalidate (4.4) in the stratosphere. This range in the values for static stability is also included in the calcula-

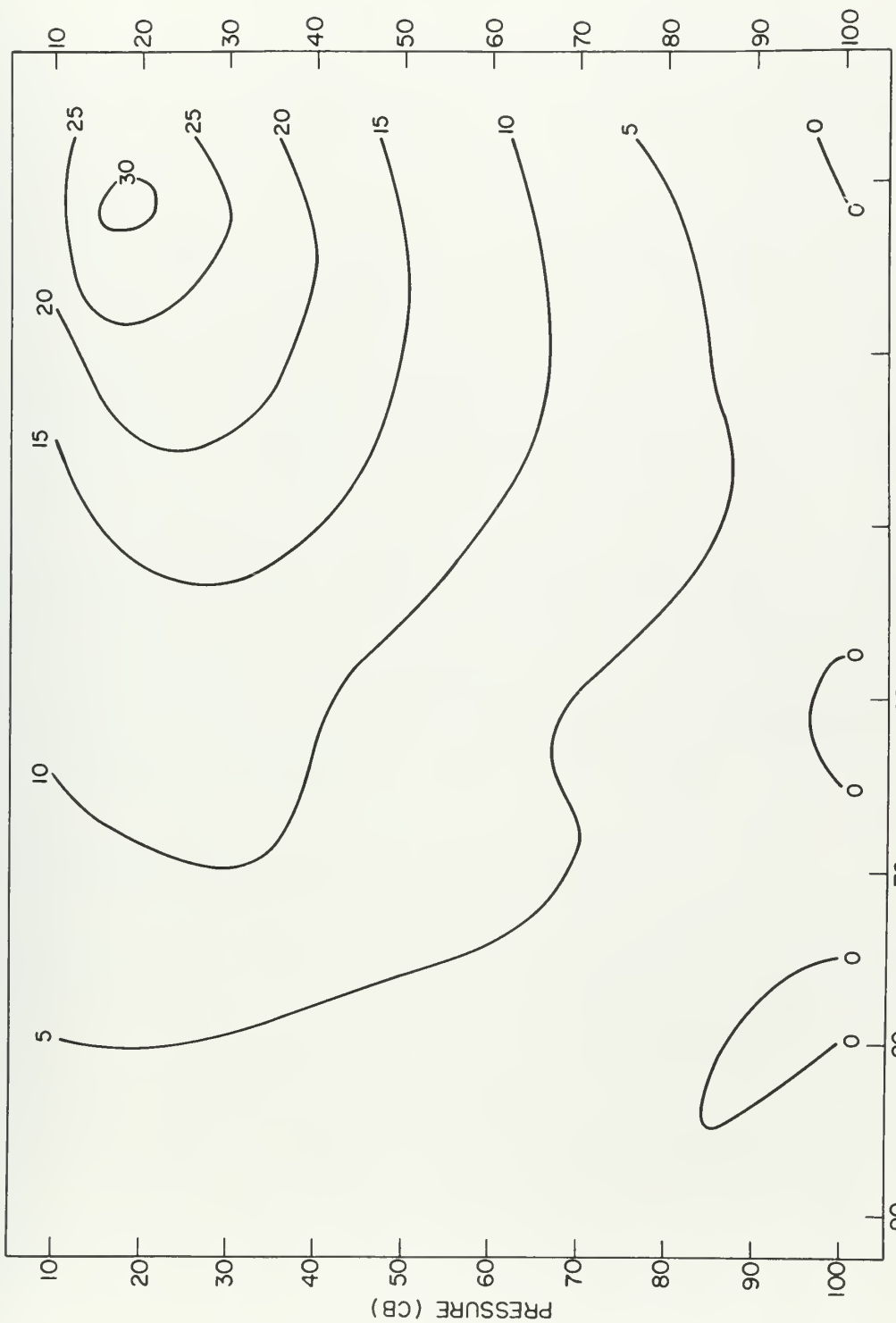

Fig. 20. Zonal average of the geostrophic wind for March 1963, in m sec^{-1}.

tion of diabatic processes as can be seen in (2.22). Note that the vertical summation of B and the diabatic processes at the lower boundary are multiplied by a factor which has a range of one order of magnitude in the same layer.

Phillips (1963) also shows that (4.4) is violated if the characteristic wavelength approaches the planetary scale. But there is a problem in assigning a value for the stability since his relationship is a function of density stratification. Increasing the static stability would tend to cancel the increasing wavelength in the denominator. Therefore, based on the preceding discussion, it can be expected that the quasi-nondivergent theory must fail where: (1) a level of maximum characteristic wind speed is encountered which causes the horizontal advection term to dominate the calculation, and (2) a region of substantial increase in the value of the static stability parameter exists. Both of these conditions exist in the high troposphere so unacceptable results in this region using the method of this study must follow.

4.4. THE GENERATION OF AVAILABLE POTENTIAL ENERGY

Since the computations of diabatic processes above 40 cb seem unreasonable the values were not used in calculating the generation of APE. Also the values south of 30N are questionable and they were not used. This means that the results of the computation represent only 70% of the atmosphere which covers the surface area from 28.75N to 88.75N. Although (2.23) requires the volume integration over the whole atmosphere, this is simply impossible at this time because of the lack of information over much of the globe. This inquiry therefore measures the contribution from about 18% of the atmosphere's volume. As

for the exclusion of the stratosphere, Oort (1964a), Smagorinsky, Manabe, and Holloway (1965), Manabe and Smagorinsky (1967), Perry (1967), and Manabe and Hunt (1968) all show that most of the generation of APE occurs in the troposphere. The reasonable results in the troposphere as shown in Fig. 6 justify making the generation calculations.

In the application of (2.30) and (2.31), because of the limitations just mentioned, the vertical resolution parameter, m, is equal to 4 and the latitudinal band count, k, is equal to 24. The diabatic fields at 92.5, 77.5, 60, and 40 cb are assumed to be representative for their respective layers in the same manner as in the calculation for H. Grid-point analyses for the diabatic processes and the layer thicknesses were transformed into latitude bands of 2.5 deg width containing 256 points using bi-linear interpolation. These bands were then separated into Fourier components using harmonic analysis and only the first fifteen wave components and the mean were used in the calculations of the generation of APE.

Diabatic and thickness values are available at twelve-hourly intervals from 0000 GMT 2 March through 0000 GMT 31 March. Likewise, the computations for the generation of APE cover the same period with the same interval. Individual results for each set were then averaged over the period in order to obtain the means.

4.5. THE GENERATION OF APE AS A FUNCTION OF LATITUDE FOR THE LAYER FROM 100 TO 30 cb

The monthly average of the generation of zonal APE as a function of latitude for the layer from 100 to 30 cb is plotted in Fig. 21 where the units

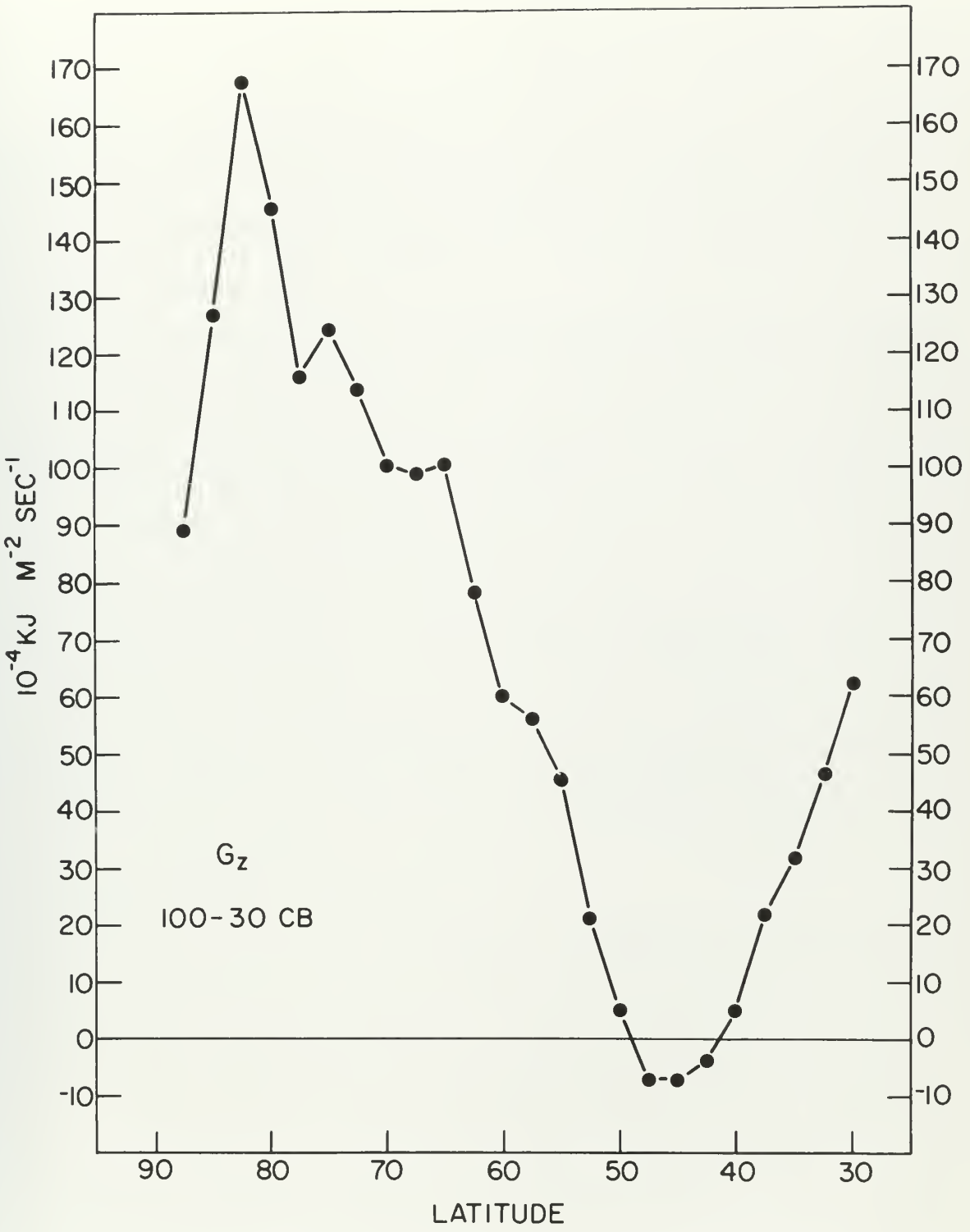

Fig. 21. Monthly average of the generation of zonal APE as a function of latitude for the layer from 100 to 30 cb for March 1963.

are 10^{-4} kj m^{-2} sec^{-1} and the values are related to the areas of their respective latitude bands. Each band's contribution involves an area weighting factor which obviously has a greater value in the lower latitudes. For example, the area for the band centered at 30N is larger than the area for the band at 60N by a factor of about 1.7.

An obvious result shown in Fig. 21 is that the plotted values are mostly positive. This means that on the average the zonal processes are positively correlated. Diabatic heating therefore takes place in the warm low latitudes and diabatic cooling occurs in the colder polar latitudes. A small negative region between 40N and 50N exists because the transition zones for the area deviations of the mean diabatic processes and the mean temperature field do not coincide. Based on the relationship between the values shown for the area from 30N to 60N, it would be easy to imagine a mirror image extending from 45N to about 7.5N. Considering the area factor this would mean a substantial addition to the generation of zonal APE.

Average monthly results for the generation of eddy APE are shown as Fig. 22. Here an obvious result is that the values are all negative which means that, on the average, warm eddies are cooled and the cold eddies are warmed everywhere. Maximum destruction of eddy APE occurs in the latitude band centered at 65N while a secondary maximum exists at 50N. Brown's (1964) results for April 1961 and 1962, also show peaks at 65N and 50N. He likewise computes minima in the destruction of eddy APE between 70N and 75N as well as near 57N and 45N. A probable explanation for the maximum destructive zones in Fig. 22 is that they represent average frontal positions and therefore the areas in

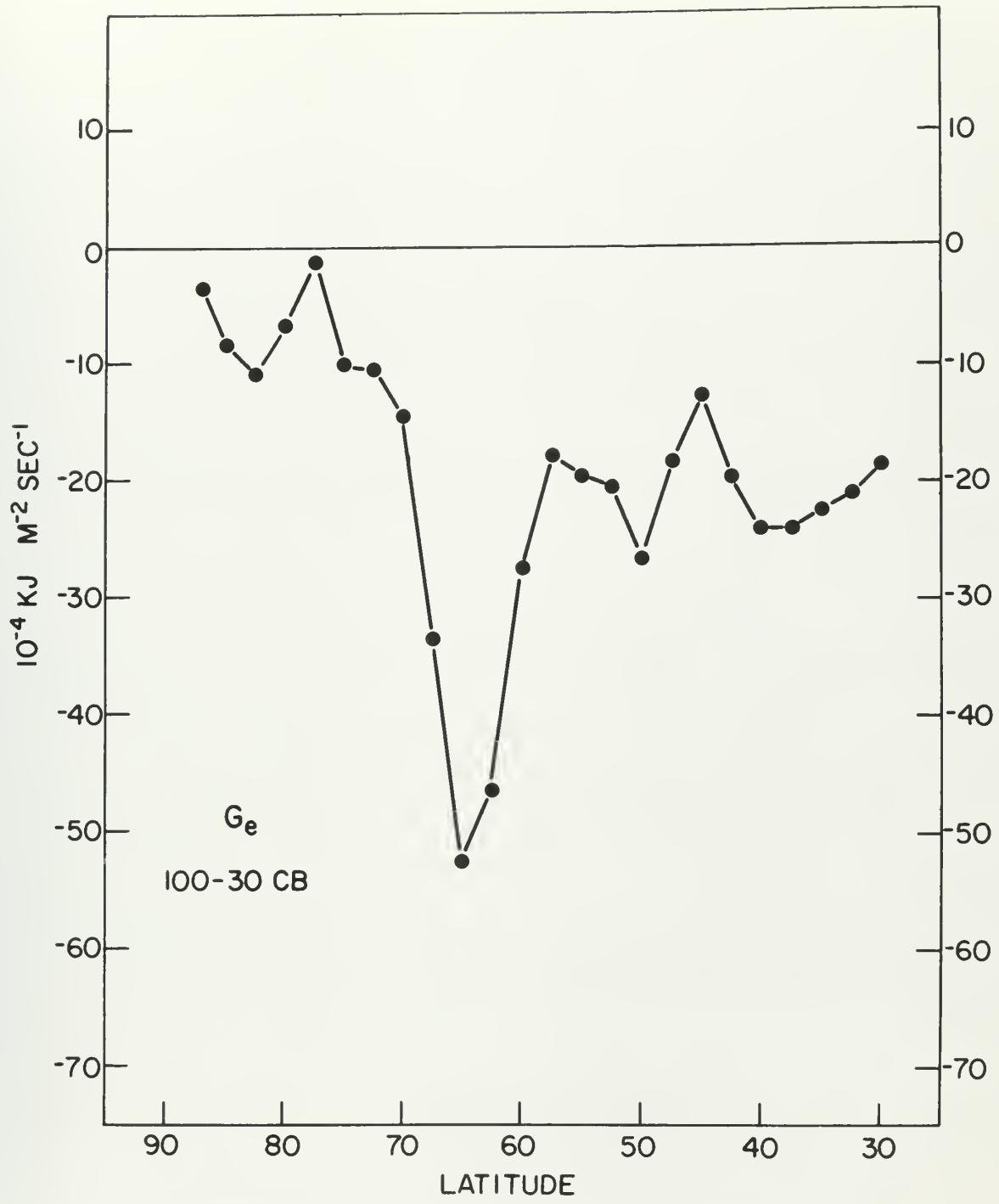

Fig. 22. Monthly average of the generation of eddy APE as a function of latitude for the layer from 100 to 30 cb for March 1963.

which maximum baroclinic activity occurs. Weather patterns associated with the arctic front are related to the area between 60N and 70N. Intense circulation features characterized this band throughout the month as indicated by the hemispheric surface analyses provided by FNWC. The most persistent feature was the low-pressure center near Greenland and Iceland. Long wave radiational and boundary cooling of the warm eddies would be quite effective in destroying eddy APE along this front. Air masses with temperatures lower than the freezing temperature would also contribute to the destruction if they moved over surfaces with temperatures closer to the freezing mark. Daily values indicate that destruction occurred 91% of the time in the rings centered at 62.5N and 65N. Significant periods of generation were calculated for the remaining rings which helps to account for the relative maximum of destruction at 65N. Polar front activity is responsible for the patterns in Fig. 22 between 30N and 50N. Precipitation processes and the resultant release of latent heat in the warm eddies coupled with the trapping effects of clouds are most likely the reason for the variability shown. These processes would of course reduce the net destructive effect.

Based on observations in the latitudes south of 30N, it is doubtful that destruction or generation of eddy APE could be substantial in that region. The familiar wave patterns of the middle and high latitudes simply do not exist there. Effects on the scale of short waves may be important in the tropics but the lack of adequate observations plus the present resolvability of the numerical grid prevent any meaningful calculations to be made.

Standard deviations for each latitude band are tabulated in Table 3 along

with the values plotted in Fig. 21 and 22. Variability about the mean on a day-to-day basis is of course indicated by the magnitude of the standard devi-

TABLE 3

LATITUDINAL VARIATION OF THE GENERATION OF ZONAL AND EDDY AVAILABLE POTENTIAL ENERGY IN THE LAYER 100-30 cb COMPUTED FOR THE RING CENTERED AT THE INDICATED LATITUDE IN UNITS 10^{-4} kj m^{-2} sec^{-1} FOR MARCH 1963

Latitude	G_z	Standard Deviation	G_e	Standard Deviation
30.0	62.39	63 06	-18.63	22.72
32.5	46.67	40.93	-20.90	23.54
35.0	31.88	29.77	-22.34	30.82
37.5	22.02	22.66	-23.98	34.83
40.0	5.14	7.93	-24.17	38.55
42.5	-3.67	12.48	-19.58	36.16
45.0	-7.20	18.02	-12.54	27.13
47.5	-7.17	26.60	-18.30	36.90
50.0	5.16	28.12	-26.61	41.87
52.5	21.33	33.53	-20.49	39.57
55.0	45.40	45.82	-19.48	30.33
57.5	56.27	68.13	-17.86	31.28
60.0	60.20	72.12	-27.46	31.79
62.5	78.50	80.87	-46.32	37.12
65.0	100.78	107.47	-52.39	49.33
67.5	99.11	99.73	-33.50	36.73
70.0	100.50	94.55	-14.52	42.06
72.5	113.77	123.86	-10.45	63.11
75.0	124.37	192.28	-10.10	75.05
77.5	116.06	237.39	- 1.22	66.12
80.0	145.72	261.12	- 6.69	53.99
82.5	167.86	266.44	-10.93	41.34
85.0	127.11	312.26	- 8.34	31.06
87.5	89.14	426.73	- 3.51	13.66

ation. Weather phenomena are quite changeable about the globe and must necessarily produce such variations on a daily basis as recorded in Table 3. Assuming normal distribution, generation of zonal APE occurred most of the

time between 30N and 40N and from 55N to 72.5N. Between 40N and 50N the transition zone is quite variable. North of 70N the standard deviations indicate that substantial changes occur over the period examined. Changes in the weather within the small area of the polar cap certainly contribute to this variability. Because of the small area and the characteristic scale of weather patterns, most of the generation of APE is confined to the zonal component. Daily values for the generation of zonal APE reveal that north of 70N significant periods of destruction are encountered throughout the month. The length of these periods increases in the bands closer to the pole. Since centers of low pressure and high pressure exchange positions around and at the pole several times throughout the month, the wide range of values per area in this small region is not surprising. Now it might seem rational to fault the numerical analysis in this area and blame the large standard deviations on the lack of data. While it is true that significant data coverage probably terminates near 75N, the very nature of numerical analysis prevents the area north of that latitude from exhibiting a random character. The first approximation for the analysis is generally a short-range forecast in which persistence of the existing pattern is most easily recognized. If the area were completely devoid of information then this persistence of the first approximation would control the final version of the analysis. Variability about the mean would be small as a result. However, the analysis about this region would have to be essentially unchanging in order for that to happen. Examination of the results at 87.5N shows that the average length of either a period of destruction or generation of zonal APE is about 54 hr. Therefore the conclusion is that the variability

is in fact real.

4.6. GENERATION OF APE WITHIN PRESSURE LAYERS

A comparison of the average generation of zonal and eddy APE for the month as a function of the pressure layers used in the calculation is shown in Fig. 23 and 24 respectively. The units are 10^{-6} kj m^{-2} sec^{-1} cb^{-1} and the area covered extends from 28.75N to 88.75N. The computations indicate that in the troposphere the largest contributions to these generations are found in the lowest 30 cb of the atmosphere. The generation of zonal APE is practically a constant in this layer where the contribution slightly exceeds that of the next 40 cb. Significant destruction of eddy APE obviously occurs in the lowest 30 cb probably due to the long wave radiational cooling of warm air masses and the heating (cooling) of cold (warm) air masses by the sensible heat transfer across the earth-atmosphere interface. Destruction of eddy APE decreases with height suggesting that the effects of latent heat release and differential long wave radiational cooling are involved. Clouds in the warm air would lessen the cooling effect of the long wave component and as mentioned earlier, there even could be substantial warming in the layers beneath these clouds. Strong cooling of clear and cold air masses coupled with the release of latent heat in the warm sector would act to lower the net value for destruction. Finally, the layer from 50 to 30 cb does show a positive generation for the eddy component.

Suomi and Shen (1963) calculated a value of 5.8×10^{-4} kj m^{-2} sec^{-1} for the generation of eddy APE in the layer from 100 to 10 cb using Explorer VII

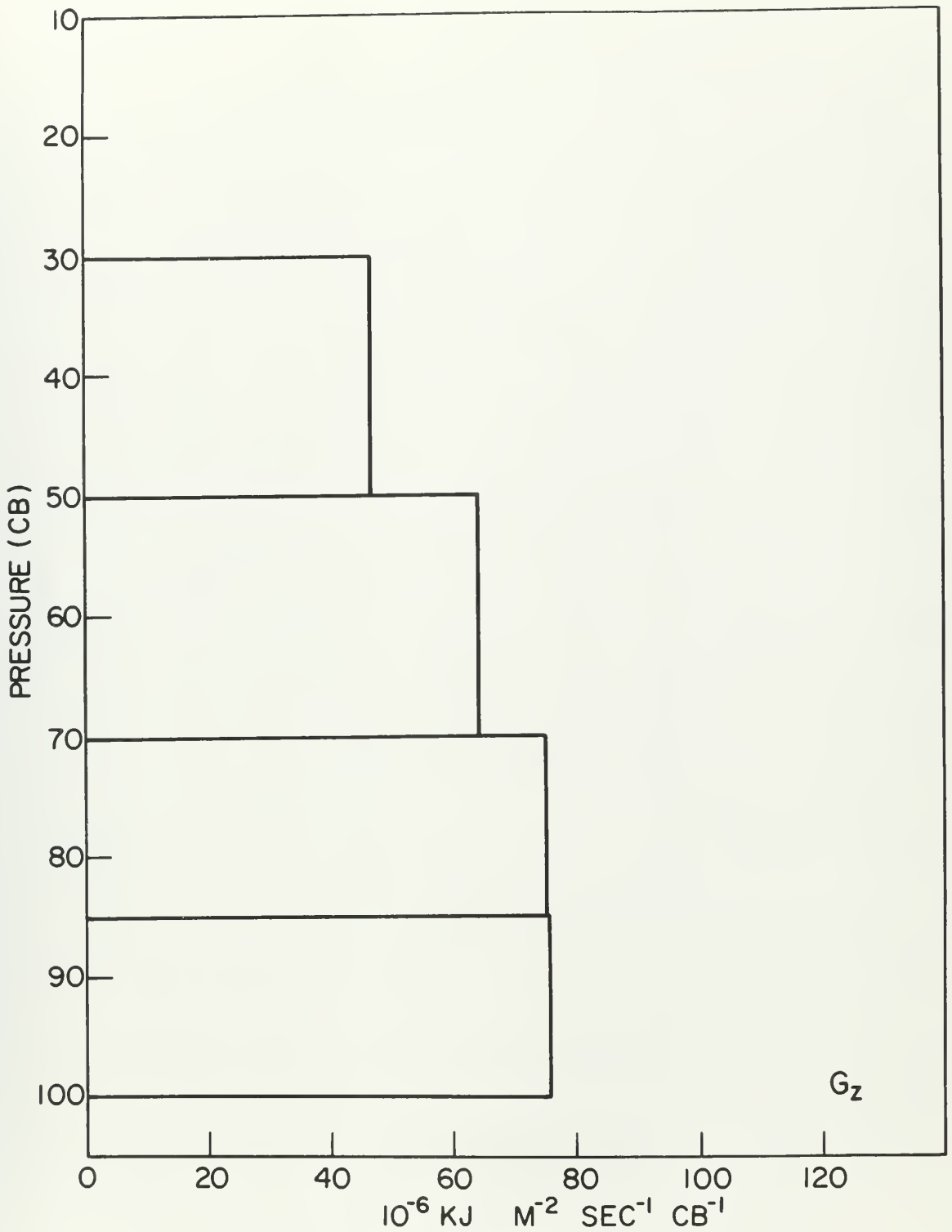

Fig. 23. Monthly average of the generation of zonal APE as a function of pressure layers for March 1963.

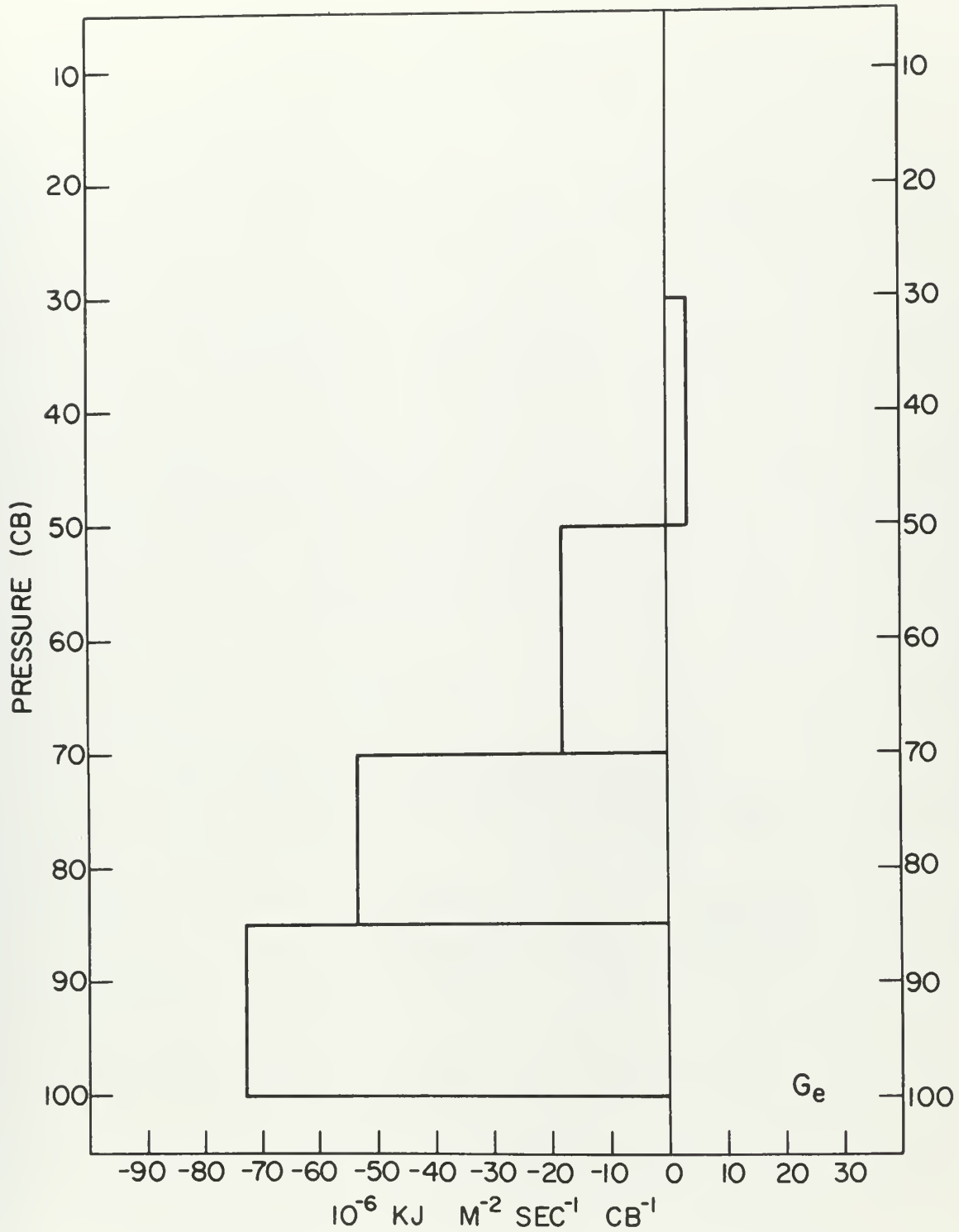

Fig. 24. Monthly average of the generation of eddy APE as a function of pressure layers for March 1963.

radiation data for a portion of the Northern Hemisphere. Corcoran and Horn (1965), using Tiros 2 radiation data and synoptic data from western Europe westward to Japan between 30N and 50N, computed a mean generation of 0.55 x 10^{-4} kj m^{-2} sec^{-1} in the layer from 100 to 50 cb. Johnson (1967) examined 198 radiometersonde flights from thirteen stations in the eastern United States and the Caribbean. He computed an average destruction of eddy APE of - 0.2 x 10^{-4} kj m^{-2} sec^{-1} due to long wave radiation in the layer from 60 to 23 cb. Clearly there is a large variability in the calculations which suggest that they are strongly dependent on time and scale and perhaps method. The standard deviations listed in Table 4 for the contributions from the layers indicate

TABLE 4

LAYER VARIATION OF THE GENERATION OF ZONAL AND EDDY AVAILABLE POTENTIAL ENERGY FOR THE REGION FROM 28.75N TO 88.75N IN THE UNITS 10^{-6} kj m^{-2} sec^{-1} cb^{-1} FOR MARCH 1963

Layer	G_z	Standard Deviation	G_e	Standard Deviation
100 - 85 cb	75.87	62.94	-72.92	30.94
85 - 70 cb	75.54	38.11	-53.42	24.76
70 - 50 cb	64.69	37.37	-17.97	23.57
50 - 30 cb	47.05	35.57	3.43	28.77

that the most variable processes relative to the means are involved with the eddy APE above 70 cb. An examination of the daily values reveals that the generation of eddy APE was negative all of the time in the layer from 100 to 85 cb. Likewise, the same is true for the layer from 85 to 70 cb with the exception of one analysis. Occasional periods of generation existed in the layer

from 70 to 50 cb while the longest such period lasted from 1200 GMT 28 March through 0000 GMT 30 March. Results in the layer from 50 to 30 cb show that during the period from 0000 GMT 10 March through 1200 GMT 23 March, significant generation of eddy APE occurred. A shorter period from 1200 GMT 27 March through 0000 GMT 30 March was also characterized by generation which parallels the results in the layer immediately below. Table 5 lists the contributions

TABLE 5

INDIVIDUAL WAVE CONTRIBUTIONS TO THE GENERATION OF EDDY AVAILABLE POTENTIAL ENERGY IN THE LAYER FROM 50 TO 30 cb IN THE UNITS 10^{-4} kj m^{-2} sec^{-1} FOR THE INDICATED TIMES

	1200 GMT 7 March	1200 GMT 12 March	0000 GMT 26 March	1200 GMT 29 March
Total Generation	-9.7	11.3	-11.0	12.46
Wave 1	-1.9	0.1	0.8	2.7
Wave 2	-1.9	1.7	-4.9	0.8
Wave 3	-2.7	-0.0	1.1	5.7
Wave 4	0.6	3.5	-2.7	-0.9
Wave 5	-0.2	0.7	-2.3	0.8
Wave 6	-2.4	1.8	-1.9	0.6
Wave 7	-1.0	1.7	-0.4	2.4
Wave 8	0.1	1.8	-0.4	-0.1
Wave 9	0.9	0.6	1.5	-0.2
Wave 10	-0.0	-0.6	-1.2	0.3
Wave 11	-1.1	-0.3	-0.3	-0.1
Wave 12	-0.2	0.9	0.2	0.0
Wave 13	0.3	-0.1	-0.2	0.4
Wave 14	-0.1	-0.7	-0.2	-0.0
Wave 15	-0.1	0.2	0.0	-0.1

from the 15 waves in the layer from 50 to 30 cb for four selected times. They were selected on the basis of having the largest magnitude within a period

characterized by either generation or destruction. This magnitude is entered on the first line in the table and is practically the same for the four periods. Underlining has been used in the table to mark the wave component with the largest contribution within each set. Apparently the processes involved in waves 2 through 4 are most important in the generation or destruction of eddy APE in the middle and upper troposphere. This of course would not be true if the remaining waves acted in an opposite sense and were of sufficient magnitude. But in the data displayed, the first nine waves which contain most of the contribution tend to act in the same sense. Why the waves act so from one time to another cannot be answered here. The required relationship between the heating and cooling regions and the temperature patterns to produce either generation or destruction is quite clear. A cloud analysis for this layer might prove useful in explaining the results.

A closer look at Fig. 23 and 24 shows that there is a near balance in the lowest 15 cb between the generation of zonal APE and the destruction of eddy APE. Excluding the lower boundary therefore would not detract from the calculation for the generation of total APE or the intensity of the general circulation. Obviously the intensity of the zonal and eddy components would be misleading if this layer were not included. Of course these results are for one month only and for a limited region. Extensive conclusions should not be recited. But based on these averages, it appears that the diabatic processes at work in the lowest 30 cb of the atmosphere are the dominant factors in generating or destroying available potential energy.

4.7. GENERATION OF EDDY APE BY WAVE NUMBER

Fourier coefficients calculated by harmonic analysis were used to determine the importance of the individual waves in generating or destroying eddy APE. Figure 25 presents the average of the daily values for the layer from 100 to 30 cb in the units of 10^{-5} kj m^{-2} sec^{-1} for the area from 28.75N to 88.75N. With the exception of wave 1, Fig. 25 resembles the January 1963, picture presented by Brown (1964). Whereas he indicates that wave 1 is quite destructive of eddy APE for that January, these results show that the contribution from this wave is not substantial when averaged for the month of March. However, Table 6 which lists the monthly averages along with the standard deviations, shows that wave 1 has large variability. Obviously it is the most important single wave when it comes to substantial generation of eddy APE. Analysis of the daily values for the layer shows that 54% of the time the contribution from wave 1 was positive. In contrast, waves 2 and 3 generated eddy APE only 22% of the time.

The dominant modes involved in destroying eddy APE within the layer are waves 2 through 8. Although the shorter waves appear to have a small role, lack of significant data over much of the hemisphere prevents a meaningful analysis of the importance of these waves. Waves 2 and 3 account for about 50% of the destruction of eddy APE and apparently demonstrate the importance of the land-sea distribution in the Northern Hemisphere in forcing preferred modes. At least for this month, the cooling of warm eddies and the heating of cold eddies due to the scale of the land and ocean contrasts appear to be important effects. Figure 26 through 29 contain the monthly averages of the

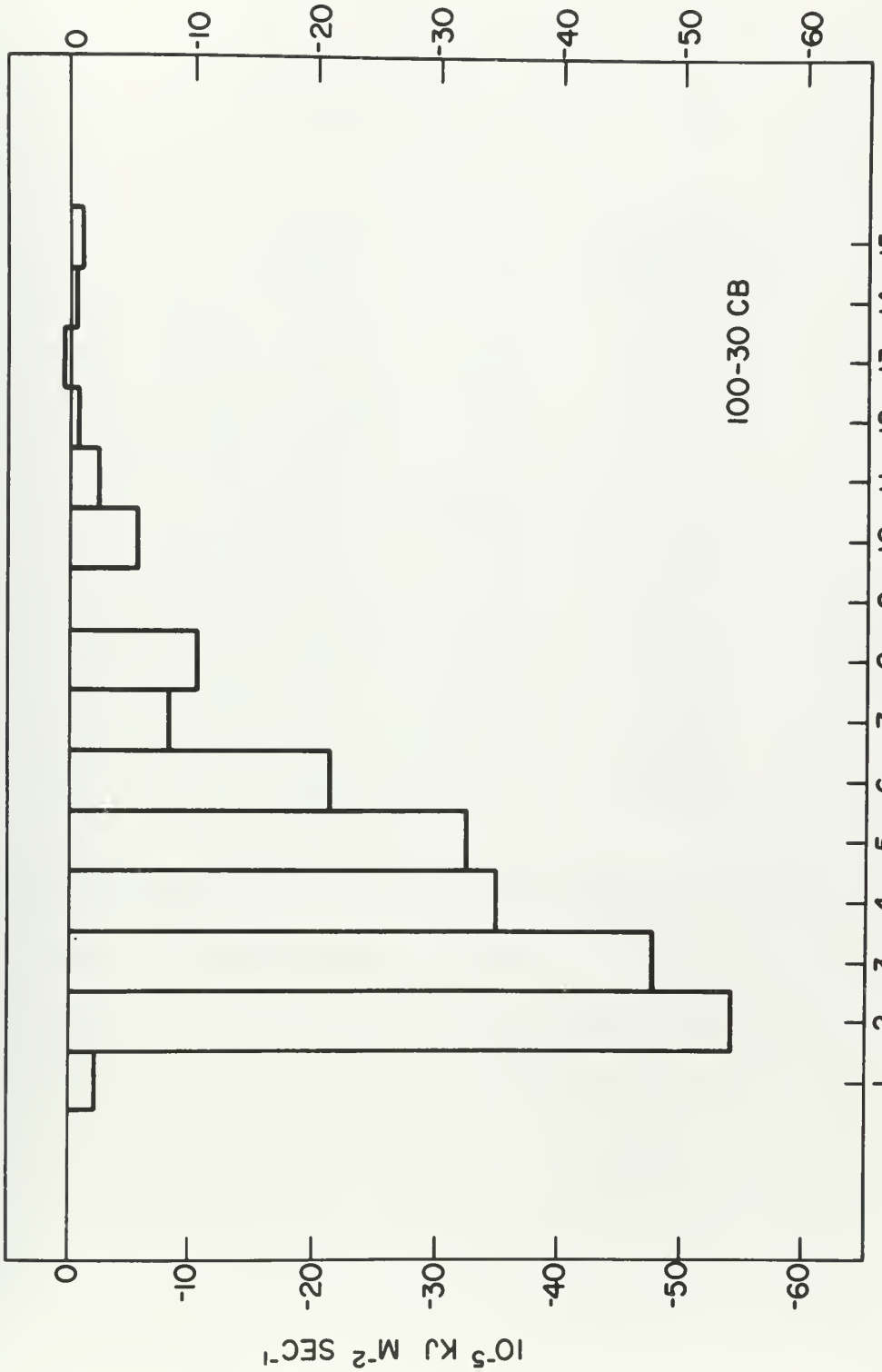

Fig. 25. Monthly average of the individual wave contributions to the generation of eddy APE for the layer from 100 to 30 cb for March 1963.

TABLE 6

HARMONIC ANALYSIS OF THE GENERATION OF EDDY AVAILABLE POTENTIAL ENERGY IN THE LAYER 100 - 30 cb FOR THE REGION 28.75N to 88.75N IN THE UNITS 10^{-4} kj m^{-2} sec^{-1} FOR MARCH 1963

Wave Number	Average	Standard Deviation
1	-0.21	4.00
2	-5.34	6.12
3	-4.77	5.59
4	-3.48	4.90
5	-3.24	3.92
6	-2.13	2.37
7	-0.81	2.74
8	-1.03	1.80
9	-0.00	1.70
10	-0.54	1.44
11	-0.22	0.93
12	-0.05	0.79
13	0.06	0.74
14	-0.03	0.63
15	-0.08	0.49

latitudinal and harmonic analyses for each pressure layer used. Several features stand out in these figures. Waves 2 and 3 are destructive in all the layers while wave 1 and the medium scale waves gradually shift to a generating mode with decreasing pressure. Next, the baroclinic zone associated with the arctic front is pronounced throughout the troposphere while the polar zone shows the modifying effects of latent heat release and cloudiness with decreasing pressure. The magnitude of the generation of eddy APE in the layer from 50 to 30 cb centered at 45N explains why the net result for the layer is characterized by generation.

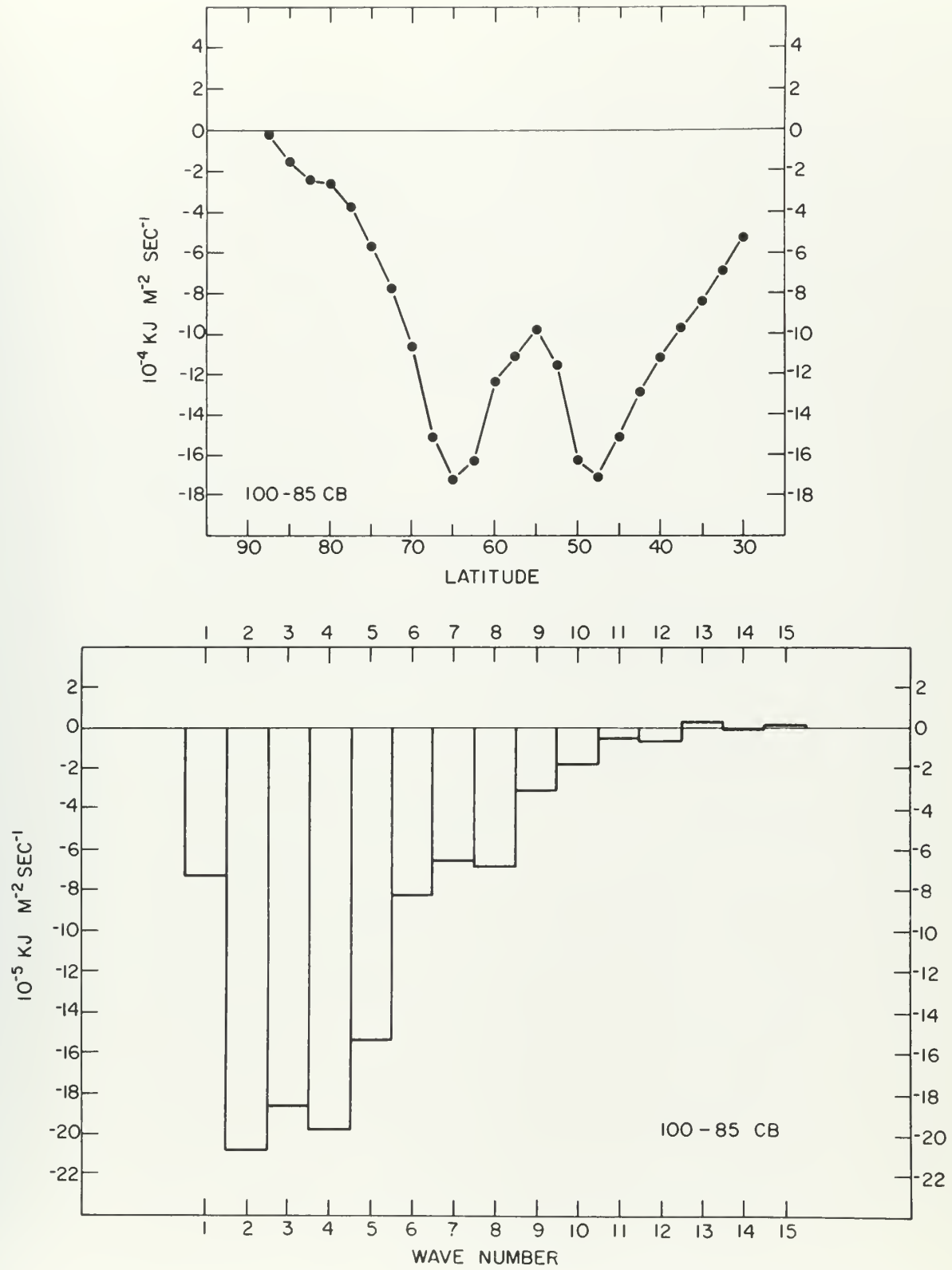

Fig. 26. Monthly averages of the latitudinal variation and the individual wave contributions for the layer from 100 to 85 cb for March 1963.

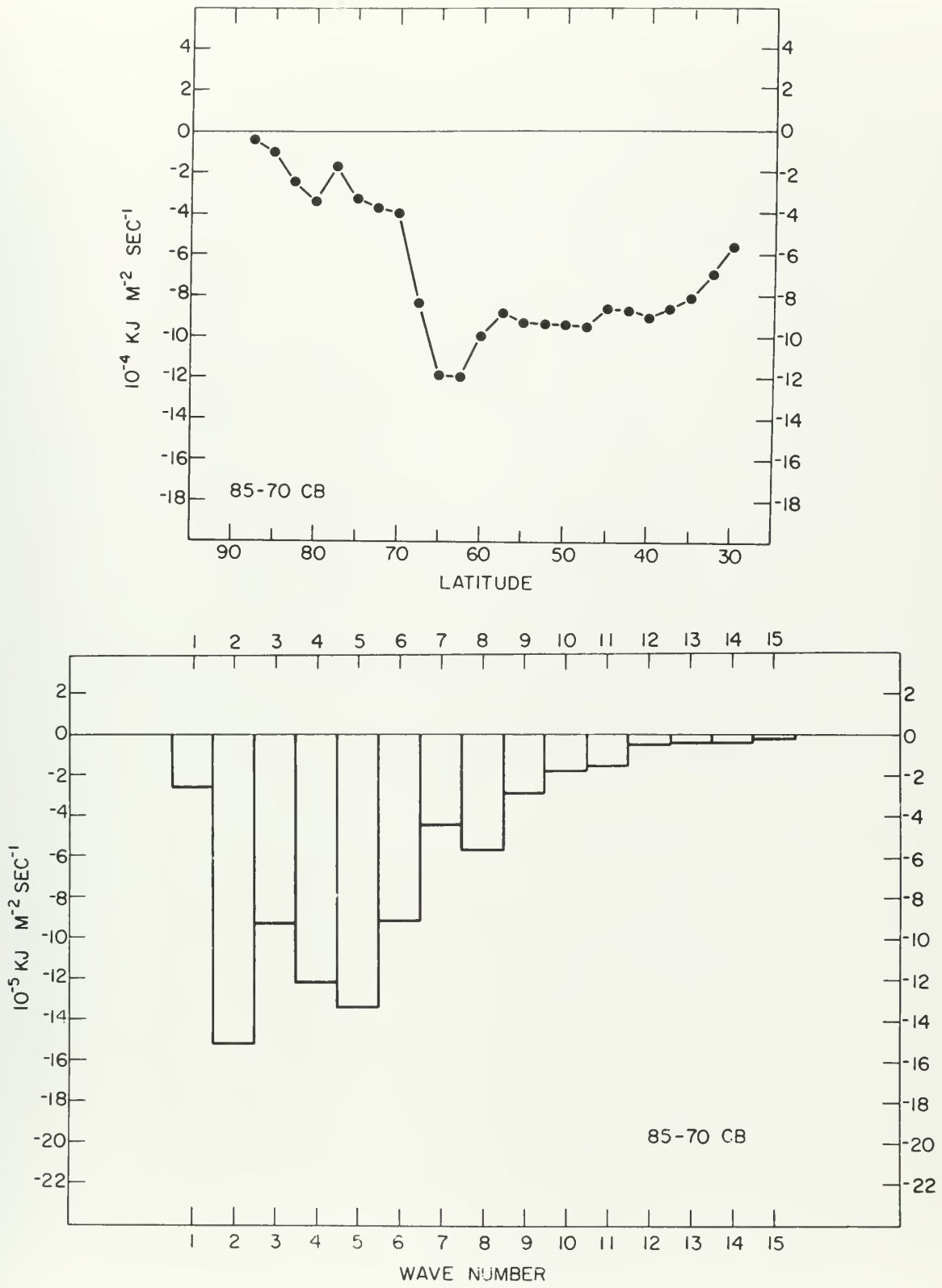

Fig. 27. Same as Fig. 26 but for the layer from 85 to 70 cb.

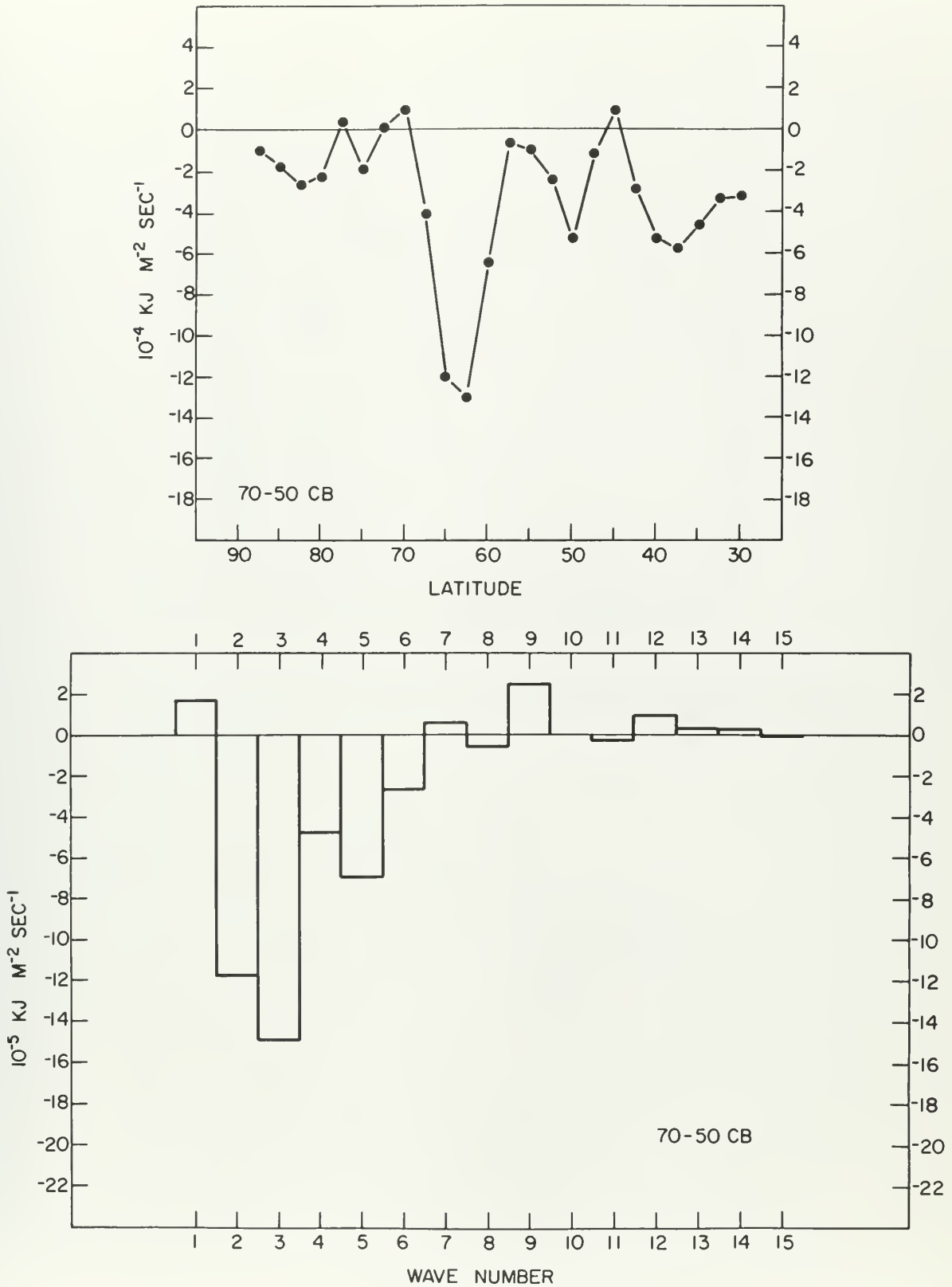

Fig. 28. Same as Fig. 26 but for the layer from 70 to 50 cb.

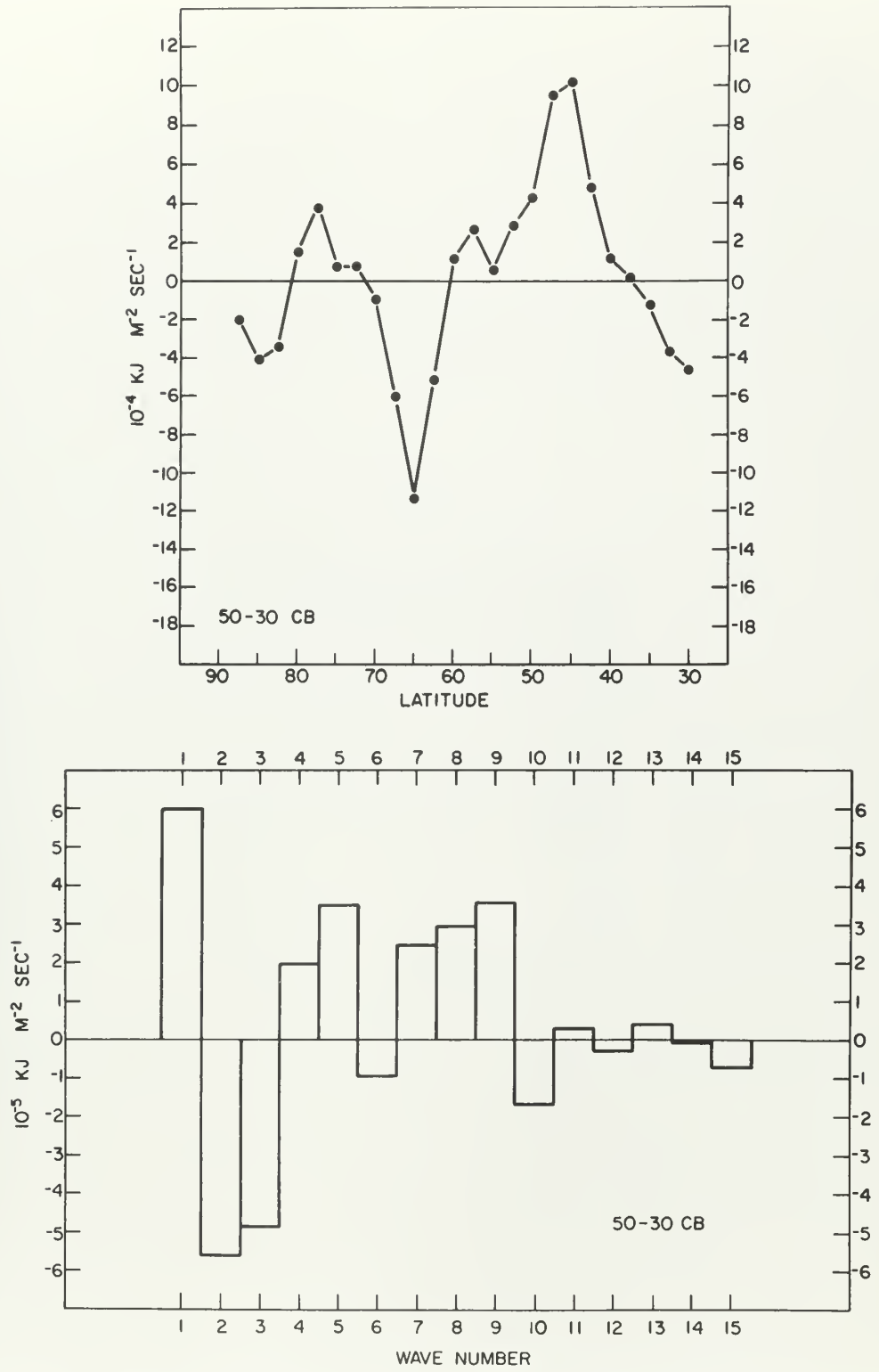

Fig. 29. Same as Fig. 26 but for the layer from 50 to 30 cb.

4.8. THE NET RESULTS OF THE GENERATION OF APE

In a study of this nature, many hours could be spent in exhaustive examination of the results. But the data limitations and the small sample size only justify the highlights presented in this chapter. As mentioned in Section 4.3., a sample period based on different analyses was made available by FNWC. Table 7 lists the results of the generation of APE calculations using the three dif-

TABLE 7

COMPARISONS OF THE GENERATION OF AVAILABLE POTENTIAL ENERGY BASED ON DIFFERENT ANALYSIS SETS FOR 0000 GMT 5 MARCH 1963 FOR THE REGION 18.75N to 88.75N IN THE UNITS 10^{-4} kj m^{-2} sec^{-1}

Analyses	G_z	G_e
SS NMC	9.83	-38.24
NSS NMC	4.49	-30.89
NSS FNWC	19.87	-27.14

ferent data sets. Recall, as shown in Fig. 19, there were not very marked differences between the two NMC sets relative to the mean diabatic processes in the layer from 100 to 30 cb. But the generation computations show how significant the subtle differences are. Zonal generation of APE is more than doubled and slightly more destruction of eddy APE occurs with the statically stable data. The difference between the FNWC and the NMC results relative to the zonal generation is disturbing. For this reason, any detailed investigation of the daily calculations at this time is unwise. It may be that the

average results have a bias but that remains to be determined by performing the calculations on different data sets. With these thoughts in mind, the monthly average of the daily values for the generation of zonal APE is 45 x 10^{-4} kj m^{-2} sec^{-1} with a standard deviation of 20 x 10^{-4} kj m^{-2} sec^{-1}, and for eddy APE is - 22 x 10^{-4} kj m^{-2} sec^{-1} with a standard deviation of 13 x 10^{-4} kj m^{-2} sec^{-1}.

4.9. CALCULATIONS FOR JANUARY 1969

Additional calculations have been made on data for January 1969. Analyses at 100, 85, 70, 50, 40, 30, and 20 cb were provided by FNWC which consist of grid-point values at 3969 locations for each level. The data are complete, vertically consistent, and cover the entire Northern Hemisphere.

Input observational data used by the FNWC objective analysis scheme are collected via a computerized network operated by the U. S. Air Force. Collection centers at High Wycombe, England, and Fuchu, Japan, forward weather data to Tinker Air Force Base, Oklahoma City, Oklahoma. These data are then forwarded to domestic users. Under normal operating conditions, more than 4500 surface observations are available within 3 hr after 0000 GMT and 1200 GMT and about 400 upper-air soundings are reported within 4 hr of these times.

FNWC reruns the upper air analysis using all data received within 10 hr of observation time. These data also include the results of a tropical analysis collected by a computer link to Fleet Weather Central, Pearl Harbor, Hawaii, which consist of winds at 5 deg latitude and longitude intersections. The region covered by these winds extends from 10N to 30N and from 90W westward

to 85E. These updated analyses are the ones which are saved in the historical files. About 500 radiometersondes are used in this final analysis.

Based on the findings of this study, several modifications were made to the model which are: (1) the new calculations were confined to the troposphere, i.e., the layer from 100 to 30 cb; (2) for convenience and economy relative to computer costs, the geostrophic wind was used in place of the stream function wind; (3) based on Gates' (1960) tropospheric data for January and the results shown in Fig. 5, (the dashed line is to the left of the solid line in the troposphere), the static stability parameter was set as a linear function of pressure. An artificial "wall" also was placed in the computation in that the values of the sine and Coriolis parameters at 4N were assigned to all grid points south of that latitude.

Some preliminary results of this new study are shown in Tables 8 through 13. The monthly average of the diabatic processes for the layer from 100 to 30 cb as a function of latitude is listed in Table 8. The transition from mean heating to mean cooling occurs near 50N. Note that the values and sign south of 40N apparently support the criticisms of the NMC analyses relative to the boundary problems. Maximum heating in the layer occurs near 40N while maximum cooling exists near 65N. Although Davis (1963) indicates that the volume between 20N and 70N should undergo net cooling for January, this new calculation shows that for 1969, the net effects of latent heat release, solar insolation, and the transfer of sensible heat across the interface dominated the long wave cooling south of 50N.

Table 9 contains the monthly average of the generation of zonal APE as a

TABLE 8

MONTHLY AVERAGES OF THE DIABATIC PROCESSES IN THE LAYER FROM 100 TO 30 cb AS A FUNCTION OF LATITUDE IN THE UNITS 10^{-2} kj sec^{-1} ton^{-1} FOR JANUARY 1969

Latitude	
5.0	2.4
7.5	2.7
10.0	2.1
12.5	1.0
15.0	0.5
17.5	0.5
20.0	0.3
22.5	0.2
25.0	0.2
27.5	0.2
30.0	0.6
32.5	0.8
35.0	0.9
37.5	1.1
40.0	1.3
42.5	1.4
45.0	1.0
47.5	0.5
50.0	-0.0
52.5	-0.4
55.0	-0.7
57.5	-1.0
60.0	-1.1
62.5	-1.2
65.0	-1.4
67.5	-1.3
70.0	-1.3
72.5	-1.3
75.0	-1.3
77.5	-1.0
80.0	-0.8
82.5	-0.7
85.0	-0.6
87.5	-0.5

TABLE 9

LATITUDINAL VARIATION OF THE GENERATION OF ZONAL AVAILABLE POTENTIAL ENERGY IN THE LAYER 100-30 cb COMPUTED FOR THE RING CENTERED AT THE INDICATED LATITUDE IN UNITS 10^{-4} kj m^{-2} sec^{-1} FOR JANUARY 1969

Latitude	G_z	Standard Deviation
5.0	555.0	575.2
7.5	405.8	293.7
10.0	272.3	155.7
12.5	100.2	96.6
15.0	10.1	65.5
17.5	43.2	59.6
20.0	22.0	54.8
22.5	- 3.7	60.1
25.0	7.6	38.9
27.5	- 5.6	30.8
30.0	18.7	28.1
32.5	13.8	19.8
35.0	0.3	5.7
37.5	-17.4	22.3
40.0	-55.8	50.4
42.5	-89.1	68.2
45.0	-77.3	83.1
47.5	-45.6	98.9
50.0	42.7	123.5
52.5	85.5	163.0
55.0	149.4	157.0
57.5	197.4	144.1
60.0	162.4	172.1
62.5	219.8	137.3
65.0	287.9	152.7
67.5	248.2	184.9
70.0	234.2	184.3
72.5	278.6	170.0
75.0	287.0	192.0
77.5	220.7	206.0
80.0	164.6	265.2
82.5	139.5	280.9
85.0	170.0	320.7
87.5	132.6	461.2

function of latitude bands for the layer from 100 to 30 cb. A comparison with Table 3 shows that the same pattern exists for the comparable bands although January has a wider transition zone and larger values of generation. This is not surprising since the sun's declination places it well south of the equator for January and this month probably represents wintertime extremes for both diabatic processes and temperature distribution in the Northern Hemisphere. The new information in Table 9 is the comparatively weak generation in the tropical latitudes south of 30N which again may be due to the sun's position throughout the month. Results south of 10N are probably unrealistic since there is no reason to expect that a quasi-geostrophic model produces valid computations at low latitudes with their correspondingly low values for the sine.

Table 10 displays the monthly average of the generation of eddy APE as a function of latitude bands for the layer from 100 to 30 cb. Again, a comparison with Table 3 shows a similar pattern with the notable exception that the region near 65N is no longer a maximum during January. The area associated with the polar frontal activity from about 35N to 50N is the maximum zone of destruction of eddy APE for this month. Latitude bands south of 30N do show that the rate of destruction of eddy APE decreases and changes to weak generation south of 20N. (The area in the latitude band centered at 15N is larger by about 1.25 compared to the area in the latitude band centered at 40N.)

Table 11 shows the layer variation of the generation of zonal and eddy APE for two domains. The larger region, from 11.25N to 88.75N, was chosen as being that region in which the quasi-geostrophic theory is reasonably applicable and the other region was selected so as to offer a comparison with March's

TABLE 10

LATITUDINAL VARIATION OF THE GENERATION OF EDDY AVAILABLE POTENTIAL ENERGY IN THE LAYER 100-30 cb COMPUTED FOR THE RING CENTERED AT THE INDICATED LATITUDE IN UNITS 10^{-4} kj m^{-2} sec^{-1} FOR JANUARY 1969

Latitude	G_e	Standard Deviation
5.0	25.5	50.8
7.5	5.1	24.2
10.0	20.8	12.5
12.5	9.2	14.5
15.0	22.9	13.3
17.5	1.0	9.0
20.0	- 5.9	11.2
22.5	- 4.1	15.7
25.0	- 11.4	17.2
27.5	- 15.9	24.5
30.0	- 24.3	22.1
32.5	- 41.7	29.9
35.0	- 60.6	48.1
37.5	- 62.3	53.6
40.0	- 92.1	78.7
42.5	-101.0	60.2
45.0	- 74.2	62.3
47.5	- 84.6	66.7
50.0	- 69.0	58.3
52.5	- 42.2	50.7
55.0	- 18.4	44.9
57.5	- 6.9	39.0
60.0	1.4	41.4
62.5	- 4.6	52.3
65.0	- 8.2	56.6
67.5	- 15.1	48.2
70.0	- 0.8	29.8
72.5	- 0.3	28.1
75.0	- 7.0	35.6
77.5	- 16.5	38.8
80.0	- 16.8	35.2
82.5	- 10.4	23.5
85.0	- 6.6	18.2
87.5	- 2.2	8.3

TABLE 11

LAYER VARIATION OF THE GENERATION OF ZONAL AND EDDY AVAILABLE POTENTIAL ENERGY FOR THE INDICATED REGIONS IN THE UNITS 10^{-6} kj m^{-2} sec^{-1} cb^{-1} FOR JANUARY 1969

Layer	G_z	Standard Deviation	G_e	Standard Deviation
	11.25N - 88.75N			
100 - 85 cb	80.2	34.2	-54.0	25.7
85 - 70 cb	82.3	24.4	-53.5	18.4
70 - 50 cb	75.4	30.6	-32.5	19.5
50 - 40 cb	74.4	46.9	-27.9	20.9
40 - 30 cb	80.0	55.9	-37.0	33.6
	28.75N - 88.75N			
100 - 85 cb	105.9	44.3	-85.5	40.0
85 - 70 cb	105.6	30.9	-79.8	28.6
70 - 50 cb	98.4	34.8	-47.9	28.3
50 - 40 cb	95.4	49.4	-40.4	30.4
40 - 30 cb	101.0	55.2	-49.6	47.5

results. A comparison with Table 4 indicates that aside from the intensity differences, the pattern is the same. For the smaller region, about 44% of the total contribution to the generation of zonal APE occurs in the lowest 30 cb while slightly more than 70% occurs in the lowest 50 cb. Likewise, almost 60% of the contribution to the destruction of eddy APE occurs in the lowest 30 cb and almost 80% occurs in the lowest 50 cb. Values very close to these same percentages apply to the larger domain. Note that there is not a near balance between the zonal and eddy rates in the lowest layer for January. The results also suggest that within the tropics south of 30N, processes responsible for the generation of zonal and eddy APE are less intense at all levels during the winter.

Table 12 contains the contributions from the first fifteen waves to the generation of eddy APE for the two different volumes. In each domain, wave 1 is the most destructive of eddy APE on the average while wave 4 is a secondary maximum. Shorter waves appear to be insignificant but the previous remarks concerning this scale still apply. The standard deviations show that wave 2 displayed considerable variability for the month. Including the tropics diminishes the net destruction of eddy APE at nearly all of the scales presented.

TABLE 12

HARMONIC ANALYSIS OF THE GENERATION OF EDDY AVAILABLE POTENTIAL ENERGY IN THE LAYER 100-30 cb FOR THE INDICATED REGIONS IN THE UNITS 10^{-4} kj m^{-2} sec^{-1} FOR JANUARY 1969

Wave Number	11.25N - 88.75N		28.75N - 88.75N	
	Average	Standard Deviation	Average	Standard Deviation
1	-6.2	5.1	-9.2	8.0
2	-3.6	6.9	-5.1	10.3
3	-3.0	3.2	-4.6	5.1
4	-5.5	4.4	-8.3	6.8
5	-3.3	5.0	-4.5	7.4
6	-2.1	2.4	-2.9	3.2
7	-3.6	3.3	-4.9	4.5
8	-1.3	1.8	-2.0	2.7
9	-0.5	1.4	-0.8	2.0
10	-0.1	1.1	-0.3	1.5
11	-0.2	0.8	-0.3	1.2
12	-0.0	0.5	-0.2	0.7
13	-0.1	0.5	-0.2	0.8
14	0.1	0.5	0.0	0.6
15	0.2	0.4	0.1	0.6

Finally, Table 13 lists the monthly average of the generation of zonal and eddy APE for the different regimes. For the volume between 100 and 30 cb and between 11.25N and 88.75N during January 1969, the average generation of zonal

TABLE 13

MONTHLY AVERAGE OF THE GENERATION OF ZONAL AND EDDY AVAILABLE POTENTIAL ENERGY FOR THE LAYER 100-30 cb BOUNDED BY THE INDICATED LATITUDE CIRCLES IN THE UNITS 10^{-4} kj m^{-2} sec^{-1} FOR JANUARY 1969

11.25N - 88.75N			
G_z	Standard Deviation	G_e	Standard Deviation
54.9	19.6	-29.1	12.0

28.75N - 88.75N			
71.0	22.2	-43.4	17.8

APE was 55 x 10^{-4} kj sec^{-1} m^{-2} with a standard deviation of 20 units while eddy APE was destroyed at a rate of - 29 x 10^{-4} kj sec^{-1} m^{-2} with a standard deviation of 12 units.

CHAPTER 5

SUMMARY AND SUGGESTIONS

5.1. CONCLUSIONS

This study has examined results of the calculations of diabatic processes and the generation of available potential energy. Computations were made over the Northern Hemisphere between 18.75N and 88.75N in the layer from 100 to 10 cb for March 1963. The input data consisted of the grid-point values from the NMC daily objective height analyses at eight levels within this layer. Diabatic processes were calculated using a seven-layer quasi-nondivergent model in which the lower boundary processes and the vertical changes of the total derivative (horizontal) of geostrophic potential vorticity are computed. As a result, for the first time, much better resolution of the vertical structure of the diabatic processes and the generation of APE, based on observational data, is available. The model further includes a more realistic treatment of the lower boundary effects. Specifically, the variable terrain height data due to Berkofsky and Bertoni (1955) and Cressman's (1960) drag coefficients are used to calculate the lower boundary vertical velocities and frictional effects. Also, in accordance with quasi-nondivergent theory, static stability is allowed to vary with pressure.

Values of the calculated diabatic processes south of 30N indicate that the boundary problems associated with the analysis procedure using the NMC octagon produced unreliable results. Also unusable were the computations above 30 cb due to the failure of the model in the high troposphere. Problems arise

in this region because: (1) of the existence of a maximum wind layer which leads to a significant imbalance between the local time change and the horizontal advection terms involving geostrophic potential vorticity, and (2) the value of the static stability parameter becomes much larger here than in the lower troposphere. Vertical summation then propagates the failure throughout the higher layers. Since the product of the square of the Rossby number with the Richardson number must be of order one in quasi-nondivergent theory, the existence of a jet or a very stable region invalidates this relationship and likewise the theory. Thus only the results in 18% of the earth's atmosphere are available for analysis.

Monthly mean values of the diabatic processes in the layer from 100 to 30 cb indicate that the change of surface cover to permanent snow or ice-cover is quite effective in separating the mean heating region from the mean cooling region in the troposphere. For March 1963, this separation occurred at about 53N and extended almost vertically above this latitude throughout the troposphere. The averages for the individual layers reveal the complexities involved when latent heat release, solar absorption, and the transfer of sensible heat from the surface to the atmosphere act to overcome the cooling effect of the long wave radiation component. In particular, although it would seem that the long wave component probably should dominate the layers above 50 cb everywhere, the heating patterns found at 40 cb suggest otherwise. Apparently the existence of regions of high cloudiness is required in order to trap the long wave emission and thus warm the layers beneath the cloud bases.

Using the daily values of the diabatic processes in the four layers from

100 to 30 cb, the daily generation of APE was calculated. For March 1963, the average generation of zonal APE was 45×10^{-4} kj m^{-2} sec^{-1} and eddy APE was destroyed at the rate of -22×10^{-4} kj m^{-2} sec^{-1}. (These values apply to the troposphere which covers only one-half of the Northern Hemisphere's area.) Therefore, heating (cooling) takes place in lower (higher) latitudes and warm (cold) eddies are cooled (heated) everywhere on the average. Tropical latitudes and in fact one-half of the area of the Northern Hemisphere were not included because of the data limitations. It is probably reasonable to conclude that the tropics produce a strong generation of zonal APE. But due to the lack of significant wave structure similar to that found in the middle latitudes, little contribution to the eddy component should be expected on the resolvable scale. Based on this reasoning, for the Northern Hemisphere, the generation of zonal APE is probably larger and the destruction of eddy APE is probably smaller than the values given here.

In the region that was analyzed, on the average most of the generation of zonal APE and the destruction of eddy APE occurred in the lowest 30 cb of the troposphere. Further, in the lowest 15 cb there was a near balance between the zonal and eddy components. This suggests that most of the net production of APE takes place above the boundary layer. Although the net result in the troposphere was destruction of eddy APE, the layer from 50 to 30 cb did show a small average generation for the month. A strong average generation between 40N and 50N in this layer was responsible and this generation was probably due to the baroclinic activity along the polar front. High clouds in the warm sector and strong cooling in the clear and cold regions would be very effective in

generating eddy APE. At the same time, the largest destruction took place throughout the troposphere in the baroclinic zone associated with the arctic front near 65N. Cooling of the warm eddies is probably the key mechanism there.

Harmonic analysis reveals that the waves from 2 through 8 are responsible for the majority of the destruction of eddy APE. Very little energy transformation occurred in the short waves. But since the observational data are not adequately distributed, the exact role of the short waves remains indistinct. Although wave 1 had little contribution in the troposphere on the average, strong periods of both generation and destruction were encountered throughout the month at this scale. It was particularly strong in helping to produce a net positive result in the layer from 50 to 30 cb. Waves 2 and 3 were the dominant modes within the troposphere and indicate that the scale of the land-sea distribution and the thermal contrasts were very significant for this month.

The stated purpose of this investigation was to determine the feasibility of using a multi-layer quasi-nondivergent model to calculate the diabatic processes and the generation of APE. It has been demonstrated that the model is not applicable in the high troposphere and the stratosphere. However, computations indicate that most of the processes which substantially affect the desired information occur within the troposphere itself. Based on these results, there seems to be little doubt that given adequate information relative to the mass-structure of the atmosphere, the model is more than satisfactory in detailing the vertical structure of the diabatic processes and the intensity of the general circulation within the troposphere.

5.2. SUGGESTIONS FOR FUTURE RESEARCH

A very serious problem confronting observational studies is the lack of adequate data on a global basis. The problem is no less serious at the hemispheric level. But it will be some time before this situation improves. At least the available data should be handled in such a way so as to extract the maximum value. It is well within the present capability of numerical analysis to produce results which, although they may not be right everywhere, at least exhibit vertical consistency. In addition, the continued imposition of a lateral boundary well into the area of computational interest makes little sense at this date. In order to avoid the problems encountered by this study, the calculations should be made using analyses which cover a larger area and in fact all of the Northern Hemisphere. The analyses produced at FNWC are ideally suited for this task. Further, numerical analyses should have some way of showing the distribution and amount of input data. Perhaps, packed with the data on the magnetic tape, the number of reports used in the analysis would suffice. Then, knowing the standard distribution of the reports and the average number reporting, a more critical evaluation of the results could be made. And finally, it remains to be determined exactly what constitutes the "best" analysis of the mass-structure of the atmosphere.

The use of the variable lower boundary values at a fixed pressure level was made in this study. Perhaps, as a result, the near balance in the zonal and eddy components for the generation of APE was calculated in this layer. It is true that the number of grid points at which the pressure at terrain height is lower than 85 cb is small. Nevertheless, a comparison utilizing these dia-

batic effects as a function of terrain-height pressure should be made.

Explaining the failure of the model in the high troposphere is based on showing that an imbalance exists among the terms. This imbalance occurs in two ways. The expression for calculating the diabatic processes above the lower boundary, (2.22), can be rewritten as

$$H_p = \frac{p_o}{p}[H_o + \sigma_o p_o \Sigma B\Delta p] \quad . \tag{5.1}$$

It was shown that a significant change occurs in the relationship of the terms in B, i.e., the local and advective changes in the geostrophic potential vorticity, in the high troposphere. This imbalance also affects the relationship between the processes at the lower boundary, H_o, and the integrated effect of B. A serious imbalance at the higher levels of the model is made more so by the fact that the multiplicative factor, p_o/p, increases by an order of magnitude there. Now obviously, if this imbalance could be made smaller, then the calculations might be more reasonable. How to do this is another problem. As can be seen in (2.23), the behavior of the static stability parameter does not affect the calculations of the generation of APE since $H/(\sigma p)$ is involved there.

But suppose that the imbalance of the given terms is real and that neglected processes act as the cancelling agents. Formulation of the model is based on the vorticity and thermodynamic equations. No approximations of any consequence are involved in the thermodynamic equation. The important assumptions enter through the simplified vorticity equation. Since vertical velocities tend to be smaller in a more stable regime, neglecting the vertical advection of horizontal momentum would not appear to be serious near the jet stream.

Wiin-Nielsen (1959a) has shown that when horizontal advection is calculated using a nondivergent wind, absolute vorticity must be replaced by a constant value of the Coriolis parameter in the divergence term. This is done so as to avoid a net production of thermal vorticity. But in a diagnostic investigation, this point is irrelevant. Now it is known that the magnitude of the shear relative vorticity is large near the jet. In fact, regions of negative absolute vorticity have been computed on the anticyclonic side. Assuming that $\partial\omega/\partial p$ remains small so that the advecting wind can still be considered to be horizontally nondivergent, what would be the effect of allowing absolute vorticity to have its full range in the divergence term of (2.1)? From (2.8), it is clear that small values of absolute vorticity could cause computational problems, for example, a value of zero. It is not immediately clear what effect such a change might have. But a lower limit could be placed on the calculated absolute vorticity value and some computations might then be evaluated. However, the system would then be energetically inconsistent. A consistent set of equations allowing the use of absolute vorticity would probably be more complicated.

Perhaps another important and neglected process is frictional dissipation in the free atmosphere as proposed by Kung (1966, 1967), for example. Presuming that the sense of his argument is correct, then this might be quite important in the regions near the jet stream. But if it is, then the invalidity of the quasi-nondivergent theory is merely reemphasized.

It very well may be that no simple theory exists by which the diabatic processes in the higher atmosphere can be determined diagnostically. But by the very nature of the system, the only significant component in these regions

should be long wave radiational cooling. The increasing data being made available through the efforts of the aeronomers may eventually allow computations to be made in this regime. Although the present study implies that most of the important results occur in the troposphere, the inquiry should be expanded as soon as practicable to include the stratosphere and to verify its exact role.

APPENDIX

FINITE DIFFERENCE FORMS OF THE EQUATIONS

A.1. BASIC INFORMATION

The finite difference forms of the equations used in the calculations for the diabatic processes are provided in this appendix. All standard symbols are explained in the list near the beginning of this paper. Figure 30 shows the computational grids required to locate the necessary points. The upper diagram is required only for the vertical differentiation needed in calculating the geostrophic potential vorticity while the lower diagram applies to the horizontal operators. Also, the relevant equation number from the text is given where it is appropriate.

As for the finite differencing scheme itself, consider some f(x) where

$$f(x \pm \Delta x) = f(x) \pm f'(x)\Delta x \pm f''(x) \frac{\Delta x^2}{2} \pm \ldots \quad . \tag{1}$$

Subtracting the two series represented by (1) leads to

$$f'(x) = \frac{f(x + \Delta x) - f(x - \Delta x)}{2\Delta x} + O(\Delta x)^2 \quad , \tag{2}$$

which is a centered difference formula for the first derivative. The order of the remainder, in this case $(\Delta x)^2$, is a measure of the accuracy of the approximation. Usually, the higher the order, the better the approximation is.

Adding the two series in (1) gives the centered difference form for the second derivative,

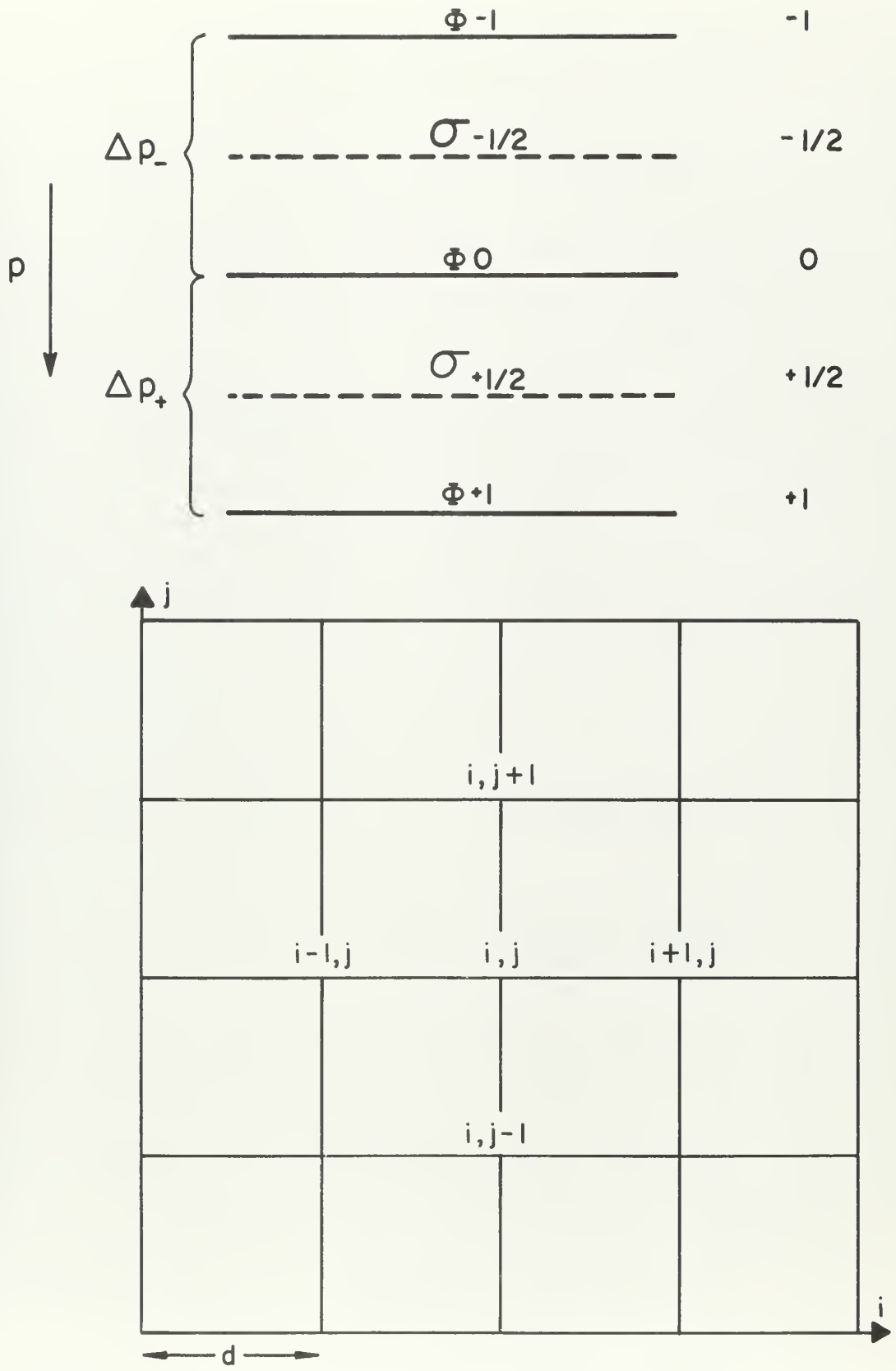

Fig. 30. Vertical and horizontal finite differencing grids.

$$f''(x) = \frac{f(x+\Delta x) - 2f(x) + f(x-\Delta x)}{\Delta x^2} + O(\Delta x)^2 \quad . \tag{3}$$

Since the material presented in this study is diagnostic in nature, computational instability associated with a time-stepping or prediction procedure is not a problem. But since the centered differences have remainders of higher order than either forward or backward differences, they are to be preferred and will be used. Round-off errors due to the physical storage capacity of the computer and truncation errors due to the differencing scheme can be problems. However, nothing can be done about the former and so long as Δx is sufficiently small when compared to the characteristic horizontal scale of the problem, the latter is negligible.

A.2. GEOSTROPHIC POTENTIAL VORTICITY, (2.6)

The geostrophic potential vorticity is calculated using

$$\xi_o = \frac{m^2}{fd^2} \psi^2 \Phi + f + \frac{2\bar{f}}{\Delta p_+ + \Delta p_-} \left[\frac{\Phi_1 - \Phi_o}{\sigma_{\frac{1}{2}} \Delta p_+} - \frac{\Phi_o - \Phi_{-1}}{\sigma_{-\frac{1}{2}} \Delta p_-} \right] \tag{4}$$

where $\psi^2() = ()_{i+1,j} + ()_{i,j+1} + ()_{i-1,j} + ()_{i,j-1} - 4()_{i,j}$.

A.3. LOCAL TIME DERIVATIVE OF GEOSTROPHIC POTENTIAL VORTICITY

Using a centered finite difference over 24 hr, the local time change of the geostrophic potential vorticity is calculated from

$$\frac{\partial \xi}{\partial t} = \frac{\xi_{+12} - \xi_{-12}}{8.64 \times 10^4} \quad . \tag{5}$$

Likewise, all other quantities in (2.8), although capable of being computed at observation time, will be averaged over a 24-hr period using

$$()_t = \frac{\left[()_{-12} + 2()_o + ()_{+12}\right]}{4} \quad .$$

A.4. STREAM FUNCTION, (4.1)

First, rescale (4.1) using

$$\psi = \frac{\bar{f}}{g}\Psi \quad . \tag{6}$$

Then,

$$\nabla^2\psi = \bar{f}\nabla\cdot\frac{\nabla z}{f} \tag{7}$$

or,

$$\nabla^2\psi = 2\bar{f}^2\left[\frac{z_{i+1,j}-z_{i,j}}{(f_{i+1,j}+f_{i,j})} - \frac{z_{i,j}-z_{i-1,j}}{(f_{i,j}+f_{i-1,j})} + \frac{z_{i,j+1}-z_{i,j}}{(f_{i,j+1}+f_{i,j})} - \frac{z_{i,j}-z_{i,j-1}}{(f_{i,j}+f_{i,j-1})}\right] \quad . \tag{8}$$

A.5. HORIZONTAL ADVECTION

Advection using the stream wind is computed using

$$\begin{aligned}(\vec{V}\cdot\nabla\{\}) = \frac{m^2 g}{4d^2\bar{f}^2}\Big[&(\psi_{i+1,j}-\psi_{i-1,j})(\{\}_{i,j+1}-\{\}_{i,j-1}) - \\ &- (\psi_{i,j+1}-\psi_{i,j-1})(\{\}_{i+1,j}-\{\}_{i-1,j})\Big] \quad .\end{aligned} \tag{9}$$

A.6. DEPARTURE VALUE AT THE TERRAIN HEIGHT

Consider a grid point at which the terrain height is related to the heights of two bounding pressure levels such that

$$z_{p_U} > z_o > z_{p_L} \tag{10}$$

Letting D represent the difference between the standard height and the actual height of a pressure level, called the departure value, then the specific temperature anomaly for the bounding layer can be written

$$ST = \frac{D_U - D_L}{Z_{p_U} - Z_{p_L}} \tag{11}$$

Since the anomaly is the mean value for the layer, then

$$D_o = D_U - ST(Z_{p_U} - Z_{p_o}) \quad . \tag{12}$$

But the standard height is determined from

$$Z_{p_o} = z_o - D_o \quad . \tag{13}$$

Therefore, (12) becomes

$$D_o = \frac{D_U - ST(Z_{p_U} - Z_o)}{1 + ST} \quad . \tag{14}$$

A.7. PRESSURE AT TERRAIN HEIGHT

From the results of (14) and knowing Z_{p_o} from (13), using an interpolating polynomial, the pressure at the terrain height is calculated from

$$p_o = \frac{[y(a+by)^2 + u(c+du^2)]}{10} \qquad (15)$$

where

$$a = 724.64$$
$$b = 3.5562$$
$$c = 597.37$$
$$d = 3.1272$$
$$u = \frac{Z_{p_o} - 2.7 \times 10^3}{1.5 \times 10^3}$$

and

$$y = 1 - u \quad .$$

A.8. TEMPERATURE AT TERRAIN HEIGHT

By definition, the specific temperature anomaly is

$$ST = \frac{T - T_p}{T_p} \quad . \qquad (16)$$

Since the standard temperature at a given pressure level is calculated from

$$T_p = 288. - 6.5 \times 10^{-3} \cdot Z_p \quad , \qquad (17)$$

the temperature at terrain height is computed from

$$T_o = (288. - 6.5 \times 10^{-3} \cdot Z_{p_o})(1 + ST) \quad . \tag{18}$$

A.9. GEOSTROPHIC SURFACE WIND

The geostrophic surface wind can be represented by

$$\vec{V}_o = \vec{k} \times \frac{g}{f} (\nabla D)_o \quad . \tag{19}$$

Now the gradient of D at the terrain-height pressure requires the use of (12) but in this case Z_{p_o} is known. Letting the subscript op represent these values at terrain-height pressure, the geostrophic surface wind is determined from

$$V_o = \frac{mg}{2fd} \left[(D_{op,i+1,j} - D_{op,i-1,j})^2 + (D_{op,i,j+1} - D_{op,i,j-1})^2 \right]^{\frac{1}{2}} \quad . \tag{20}$$

A.10. GEOSTROPHIC SURFACE VORTICITY

From the same considerations used to obtain (20), the geostrophic surface vorticity can be computed from

$$\zeta_o = \frac{gm^2}{fd^2} \nabla^2 D_{op} \quad . \tag{21}$$

A.11. FRICTION EFFECTS, (2.15)

Combining (15), (18), (19), and (20), the frictional effects are computed from

$$\left(\frac{\partial F_y}{\partial x} - \frac{\partial F_x}{\partial y}\right)_o = \frac{g^3 m^3 p_{o,i,j}}{2f^2 d^3 \Delta p R T_{o,i,j}} [\,]^{\frac{1}{2}} \nabla^2 D_{op} \quad , \tag{22}$$

where the brackets contain the terms inside the brackets in (20).

A.12. OMEGA IN THE LOWER BOUNDARY, (2.19), (2.20)

The omega due to terrain is calculated using a form similar to (9) except that the geostrophic surface wind is used in place of the stream wind. Calculating the omega due to friction is just a matter of multiplying (22) by $-\Delta p/f$.

A.13. HEATING AT THE LOWER BOUNDARY, (2.17)

Computing the lower boundary heating is straightforward using (15), (18), (19), and the vertical velocities. All the terms are averaged over the 24-hr period since the local time change term is also involved. The averaging is done using the form given in Section A.3.

BIBLIOGRAPHY

Andrews, J. F., 1963: The Weather and Circulation of March 1963—A Marked Reversal from February. Mon. Wea. Rev., 91, No. 6, 309-316.

Berkofsky, L. and E. Bertoni, 1955: Mean Topographic Charts for the Entire Earth. Bull. Amer. Meteor. Soc., 36, No. 7, 350-354.

Brown, J. A., 1964: A Diagnostic Study of Tropospheric Diabatic Heating and the Generation of Available Potential Energy. Tellus, 16, No. 3, 371-387.

Burger, A. P., 1958: Scale Consideration of Planetary Motions of the Atmosphere. Tellus, 10, No. 2, 195-205.

Carstensen, L. P. and G. E. Lawniczak, Jr., 1966: Surface and Tropospheric Analyses. Tech. Note No. 15, Fleet Numerical Weather Central, Monterey, Calif., 15 pp.

Charney, J. G., 1948: On the Scale of Atmospheric Motions. Geofys. Publ., 17, No. 2, 1-17.

Clarke, L. C. and G. E. Lawniczak, Jr., 1962: Hemispheric Solution of the Omega Equation Including Terrain and Surface Frictional Effects. M. S. Thesis, U. S. Naval Postgraduate School, Monterey, Calif., 172 pp.

Corcoran, J. L. and L. H. Horn, 1965: The Role of Synoptic Scale Variations of Infrared Radiation in the Generation of Available Potential Energy. J. Geophy. Res., 70, No. 18, 4521-4527.

Cressman, G. P., 1959: An Operational Objective Analysis System. Mon. Wea. Rev., 87, No. 10, 367-374.

BIBLIOGRAPHY (Continued)

Cressman, G. P., 1960: Improved Terrain Effects in Barotropic Forecasts. Mon. Wea. Rev., 88, No. 9-12, 327-342.

Davis, P. A., 1963: An Analysis of the Atmospheric Heat Budget. J. Atmos. Sci., 20, No. 1, 5-22.

Dickson, R. R. and J. Posey, 1967: Maps of Snow-Cover Probability for the Northern Hemisphere. Mon. Wea. Rev., 95, No. 6, 347-353.

Dutton, J. A. and D. R. Johnson, 1967: The Theory of Available Potential Energy and a Variational Approach to Atmospheric Energetics. Advan. Geophys., 12, 333-436.

Ellsaesser, H. W., 1968: Comparative Test of Wind Laws for Numerical Weather Prediction. Mon. Wea. Rev., 96, No. 5, 277-285.

Gates, W. L., 1960: Static Stability Measures in the Atmosphere. Department of Meteorology, University of California, Los Angeles, p. 9.

Haltiner, G. J., L. C. Clarke, and G. E. Lawniczak, Jr., 1963: Computation of the Large Scale Vertical Velocity. J. Appl. Meteor., 2, No. 2, 242-259.

Haurwitz, B., 1941: Dynamic Meteorology, McGraw Hill, New York, p. 241.

Holl, M. M., J. P. Bibbo, and J. R. Clark, 1963: Linear Transforms for State-Parameter Structure. Tech. Memo. No. 1, Second Edition, Meteorology International, Monterey, Calif., 28 pp.

Holl, M. M., J. P. Bibbo, and J. R. Clark, 1964: The Analysis Cycle for the Mass Structure of the Atmosphere. Quar. Rep. 3, Meteorology International, Monterey, Calif., 13 pp.

BIBLIOGRAPHY (Continued)

Holopainen, E. O., 1967: On the Mean Meridional Circulation and the Flux of Angular Momentum Over the Northern Hemisphere. Tellus, 19, No. 1, 1-13.

Johnson, D. R., 1967: The Role of Terrestrial Radiation in the Generation of Zonal and Eddy Available Potential Energy. Tellus, 19, No. 4, 517-539.

Johnson, D. R. and W. C. Shen, 1968: Profiles of Infrared Irradiance and Cooling Through a Jet Stream. Mon. Wea. Rev., 96, No. 8, 559-572.

Katayama, A., 1966: On the Radiation Budget of the Troposphere Over the Northern Hemisphere (I). J. Meteor. Soc. Japan, 44, No. 6, 381-401.

Katayama, A., 1967a: On the Radiation Budget of the Troposphere Over the Northern Hemisphere (II)—Hemispheric Distribution. J. Meteor. Soc. Japan, 45, No. 1, 1-25.

Katayama, A., 1967b: On the Radiation Budget of the Troposphere Over the Northern Hemisphere (III)—Zonal Cross-Section and Energy Consideration. J. Meteor. Soc. Japan, 45, 26-38.

Kung, E. C., 1966: Kinetic Energy Generation and Dissipation in the Large-Scale Atmospheric Circulation. Mon. Wea. Rev., 94, No. 2, 67-82.

Kung, E. C., 1967: Diurnal and Long-Term Variations of the Kinetic Energy Generation and Dissipation for a Five-Year Period. Mon. Wea. Rev., 95, No. 9, 593-606.

Lettau, H., 1954: A Study of the Mass, Momentum, and Energy Budget of the Atmosphere. Geophys. Bioklimatol., Ser. B, A7, 135-157.

BIBLIOGRAPHY (Continued)

Lettau, H., 1959: Wind Profile, Surface Stress, and Geostrophic Drag Coefficients in the Atmospheric Surface Layer. Advan. Geophys., 6, p. 243.

London, J., 1957: A Study of the Atmospheric Heat Balance. College of Engineering, New York University, p. 44.

Lorenz, E. N., 1955: Available Potential Energy and the Maintenance of the General Circulation. Tellus, 7, No. 2, 157-167.

Lorenz, E. N., 1967: The Nature and Theory of the General Circulation of the Atmosphere. World Meteorological Organization, 161 pp.

Manabe, S., J. Smagorinsky, and R. Strickler, 1965: Simulated Climatology of a General Circulation Model with a Hydrologic Cycle. Mon. Wea. Rev., 93, No. 12, 769-798.

Manabe, S. and J. Smagorinsky, 1967: Simulated Climatology of a General Circulation Model with a Hydrologic Cycle (II)—Analysis of the Tropical Atmosphere. Mon. Wea. Rev., 95, No. 4, 155-169.

Manabe, S. and B. Hunt, 1968: Experiments with a Stratospheric General Circulation Model. Mon. Wea. Rev., 96, No. 8, 477-539.

Oort, A. H., 1964: On Estimates of the Atmospheric Energy Cycle. Mon. Wea. Rev., 92, No. 11, 483-493.

Oort, A. H., 1964a: On the Energetics of the Mean and Eddy Circulations in the Lower Stratosphere. Tellus, 16, No. 4, 309-327.

Perry, J. S., 1967: Long-Wave Energy Processes in the 1963 Sudden Stratospheric Warming. J. Atmos. Sci., 24, No. 5, 539-550.

BIBLIOGRAPHY (Continued)

Phillips, N. A., 1963: Geostrophic Motion. Rev. Geophys., 1, No. 2, 123-176.

Sellers, W. D., 1965: Physical Climatology. The University of Chicago Press, p. 5.

Shuman, F. G., 1957: Predictive Consequences of Certain Physical Inconsistencies in the Geostropic Barotropic Model. Mon. Wea. Rev., 85, No. 7, 229-234.

Smagorinsky, J., S. Manabe, and J. L. Holloway, 1965: Numerical Results From a Nine-Level General Circulation Model of the Atmosphere. Mon. Wea. Rev., 93, No. 12, 727-768.

Suomi, V. E. and W. C. Shen, 1963: Horizontal Variation of Infrared Cooling and the Generation of Eddy Available Potential Energy. J. Atmos. Sci., 20, No. 1, 62-65.

Vernekar, A. D., 1967: On Mean Meridional Circulation in the Atmosphere. Mon. Wea. Rev., 95, No. 11, 705-721.

Wiin-Nielsen, A., 1959a: On Certain Integral Constraints for the Time-Integration of Baroclinic Models. Tellus, 11, No. 1, 45-59.

Wiin-Nielsen, A., 1959b: On Barotropic and Baroclinic Models with Special Emphasis on Ultra-Long Waves. Mon. Wea. Rev., 87, No. 5, 171-183.

Wiin-Nielsen, A. and J. A. Brown, 1960: On Diagnostic Computations of Atmospheric Heat Sources and Sinks and the Generation of Available Potential Energy. Proceedings of the International Symposium on Numerical Weather Prediction in Tokyo, Meteor. Soc. Japan, 593-613.

BIBLIOGRAPHY (Concluded)

Wiin-Nielsen, A., J. A. Brown, and M. Drake, 1963: On Atmospheric Energy Conversions Between the Zonal Flow and the Eddies. Tellus, 15, No. 13, 261-279.

Wiin-Nielsen, A., J. A. Brown, and M. Drake, 1964: Further Studies of Energy Exchange Between the Zonal Flow and the Eddies. Tellus, 16, No. 2, 168-180.

Wiin-Nielsen, A., 1965: On the Propagation of Gravity Waves in a Hydrostatic, Compressible Fluid with Vertical Wind Shear. Tellus, 17, No. 3, 306-320.

Wiin-Nielsen, A., 1967: On the Annual Variation and Spectral Distribution of Atmospheric Energy. Tellus, 19, No. 4, 540-559.

Wiin-Nielsen, A., 1968: On the Intensity of the General Circulation of the Atmosphere. Rev. Geophys., 6, No. 4, 559-579.

thesL319
On a multi-layer analysis of atmospheric
3 2768 002 11118 9
DUDLEY KNOX LIBRARY